

**STUDIES ON ELECTROLUMINESCENCE USING
POWDER AND THIN FILM DEVICES**

S. MURALEEDHARAN PILLAI

THESIS SUBMITTED IN PARTIAL FULFILMENT OF THE
REQUIREMENTS FOR THE AWARD OF THE DEGREE OF
DOCTOR OF PHILOSOPHY


DEPARTMENT OF PHYSICS
UNIVERSITY OF COCHIN
COCHIN 682 022

1984

CERTIFICATE

Certified that the work presented in this thesis is based on the original work done by Mr.S. Muraleedharan Pillai, under my guidance in the Department of Physics, University of Cochin, and has not been included in any other thesis submitted previously for the award of any degree.


Cochin 682 022
27 March 1984


Dr.C.P. Girijavallabhan
Supervising Teacher



DECLARATION

Certified that the work presented in this thesis is based on the original work done by me under the guidance of Dr.C.P.Girijavallabhan, in the Department of Physics, University of Cochin and has not been included in any other thesis submitted previously for the award of any degree.


S. Muraleedharan Pillai

Cochin 682 022
27 March 1984

ACKNOWLEDGEMENTS

The investigations presented in this thesis have been carried out under the guidance and supervision of Dr.C.P.Girijavallabhan, Reader, Department of Physics, University of Cochin during 1979-'84. The author is happy to express his sincere gratitude for the able guidance and competent advice given to him through out this period. The author is indebted to Prof.K.Sathianandan, Head of the Department of Physics, for his encouragement during the progress of this work and for allowing him to use the departmental facilities including those in the Laser Division. He is also grateful to Prof. M.G.Krishna Pillai for extending to him all the facilities available in the Thin Film Division.

Most of the electronic circuits used in the work have been fabricated with the help of Mr.C. Raghavan and the author wishes to express his thanks to him. He also likes to thank Dr.V.P.N. Nampoori for many useful discussions.

The author expresses his sincere thanks to all the research scholars of the Department of Physics, especially to his good friends in the Laser Division and to Mr.Rajeev and Mr. Boben for their help.

Thanks are also due to the technical, administrative and library staff of the Department of Physics and staff of the University Services and Instrumentation Centre of the University of Cochin for the help and co-operation he has received from them.

The author takes this opportunity to thank the Council of Scientific and Industrial Research, New Delhi for awarding him a Research Fellowship.

Finally, he likes to extend his thanks to Mr. K.L. Jose for neatly typing the manuscript.

PREFACE

The subject of electroluminescence has currently acquired great importance because of its potential applications in display systems of a wide variety. A large number of scientists working in commercial, governmental as well as academic institutions all over the world are at present engaged in the intense effort to develop new and efficient phosphor materials and electroluminescent devices. This thesis presents the work carried out by the author in this field during the past few years in the Department of Physics at Cochin University.

The studies discussed here are mostly confined to the development of some new phosphor materials, their uses in powder and thin film electroluminescent devices and to their electrical and spectral characteristics. Care has been taken to bring out the physics involved in all the above aspects of the phenomenon. The major achievements outlined in the thesis are the following:

- 1) Development of an inexpensive high gain PMT preamplifier suitable for low level fluorescence and luminescence studies.

- 2) Introduction of new energy level scheme for the explanation of the experimental findings on the effect of chlorine concentrations in ZnS:Cu,Cl phosphors.

3) Preparation of a highly efficient CaS:Ce phosphor and the observation of Ce \rightarrow Nd energy transfer in CaS:Ce,Nd phosphor.

4) Preparation of CaS:Er, CaS:Sm and CaS:Dy line emitting electroluminescent phosphors and the identification of the sites of Er³⁺ and Sm²⁺ in CaS from a crystal field splitting parameter calculation.

5) Development of a thin film electroluminescent device having MISIM structure using MgF₂ as insulator for the first time.

6) Observation of a dependence of the threshold voltage for the onset light emission on the frequency of excitation and its theoretical explanation in the case of thin film device using MgF₂ layers.

The material presented in the thesis is organised in the form of ten separate but related chapters and one appendix.

The first chapter is divided into two parts and is meant to give an introduction to the phenomenon of electroluminescence. Part A gives a comprehensive review of the powder phosphors together with a brief discussion on the physical mechanism involved in the electroluminescent process. Part B is a review on the thin film electroluminescent devices.

Chapter two presents a concise description of the experimental set up used for these investigations. The method of fabrication of a powder electroluminescent cell is described in some detail, Technique for preparation of various phosphors, the set up for their excitation and the experimental arrangement used for recording the electroluminescent spectra are discussed here at length.

Preparation and properties of a series of phosphors, viz. ZnO:Zn, (2) ZnS:Cu,Mn, (3) ZnS:Cu,Cl, (4) ZnS:Cu,Sm,Cl, and (5) ZnS:Cu,Dy,Cl form the subject of chapter III. The first observation of an ultraviolet band in the electroluminescent spectrum of ZnO:Zn is reported in this chapter. The method for preparing blue emitting ZnS:Cu,Cl phosphor and rare earth doped ZnS:Cu,Sm,Cl; ZnS:Cu,Dy,Cl are outlined. Their respective electroluminescence spectra and probable level transitions are discussed. The report of a detailed investigation on the effect of chlorine concentration on the spectral characteristics of ZnS:Cu,Cl phosphor and a discussion of an energy level scheme which explains all the experimental observations are also given here.

In chapter IV the procedure for preparation of an efficient CaS:Ce EL phosphor is given. Various results obtained from their brightness-voltage-frequency characteristics and the electroluminescence spectrum of the phosphor are reported. The observation of Nd³⁺ emission lines from CaS

host material is reported for the first time in this chapter. The observed quenching of the Ce emission in the presence of Nd ion and the probable Ce \rightarrow Nd non radiative energy transfer process in CaS:Ce,Nd phosphor are also discussed.

Chapter V is a detailed discussion on the emission spectrum of CaS:Er phosphor. The various level transitions giving rise to the nine groups of emission lines in the spectrum are identified and reported. A crystal field splitting parameter calculation is carried out to explain the seven well resolved components of the most intense bands occurring at 550 nm in the emission spectrum of this phosphor. The calculation, also reveals the possible sites for Er³⁺ ion in CaS lattice.

Chapter VI deals with the electroluminescent emission characteristics of CaS:Sm, CaS:Dy and CaS:Mn phosphors. The details of the analysis of the various spectra and the result of the calculations used to identify the lattice site of the samarium luminescent centre are also presented.

Chapter VII gives an account of the various attempts made to fabricate a d.c. powder device using CaS:Ce and ZnS:Cu,Mn powder phosphors.

The techniques adopted for the fabrication of thin film devices are totally different from those used for powder cells. Hence in chapter VIII a comprehensive description of

the various experimental set up used for the fabrication of a thin film electroluminescent device is given. It includes the details of vacuum coating units, design of various evaporation sources, substrate heater, electron beam evaporation system and the quartz film thickness monitor. In addition it contains the details of the chemical vapour deposition of transparent conducting electrode and the etching technique adopted for the selective removal of SnO_2 films.

A detailed account of the technique of deposition of insulating and semiconducting films suitable for electroluminescent devices is given in chapter IX. It also describes the successful fabrication of two thin film electroluminescent devices of MISIM structure viz. $\text{SnO}_2\text{-MgF}_2\text{-ZnS:Mn-MgF}_2\text{-Al}$ and $\text{SnO}_2\text{-Y}_2\text{O}_3\text{-ZnS:Mn-Y}_2\text{O}_3\text{-Al}$. The former was fabricated by the conventional thermal evaporation technique while the latter was accomplished with the help of an electron beam evaporation system. The variation of threshold voltage with excitation frequency, observed in the case of device using MgF_2 insulating layers is explained on the basis of the frequency dependence of the dielectric loss factor of this material.

The concluding chapter provides a summary and evaluation of the investigations presented in the preceding nine chapters. A critical assessment of the major results obtained during the course of these studies is made.

A summary of the electroluminescent properties of the electropolymerised castor oil and liquid paraffin is given as an appendix. EL spectra and nitrogen laser excited fluorescence emission of these materials are discussed along with their other electrical properties.

The references to literature are made at the ends of the respective chapters.

Part of the investigations presented in this thesis has been published/communicated in the form of the following papers.

1. A Simple and Sensitive PMT preamplifier for low level fluorescence and luminescence studies.
S.M.Pillai, C. Raghavan, Sudha C. Kartha and C.P.G.Vallabhan
J. Instr. Soc. of India, Vol.12, No.3, p.7 (1982).
2. Effect of chlorine concentration on the spectral characteristics of electroluminescence in ZnS:Cu,Cl phosphor.
S.M. Pillai and C.P.G. Vallabhan,
Solid State Communication Vol.47, No.11 p.909-11 (1983)
3. Spectral characteristics of EL ZnS:Cu,Sm,Cl and ZnS:Cu,Dy,Cl phosphors.
S.M.Pillai and C.P.G. Vallabhan
Proc. Nuclear Phys. and Solid State Physics
Symp. (BHU, Varanasi) Paper No.SEC 13(1982)

4. A study of electroluminescence spectrum of CaS:Er phosphor.
S.M.Pillai and C.P.G. Vallabhan
J. Phys. C. Solid State Physics (in press)
5. Spectral characteristics of EL emission from CaS:Er phosphor.
S.M. Pillai and C.P.G. Vallabhan
DAE Nuclear Phys. and Solid State Physics Symp.
(Mysore University, Mysore) Paper No.SDD 9(1983)
6. An AC thin film electroluminescent device using double
insulating layers of MgF₂.
S.M. Pillai and C.P.G. Vallabhan
Paper No.CPB-6 presented in the 2nd All India Conference
on thin film state phenomena held at IIT, Madras on
February 1-4, 1984.
7. Electroluminescence of CaS:Sm³⁺ EL phosphors.
S.M.Pillai and C.P.G. Vallabhan (to be published)

CONTENTS

| | Page No. |
|-------------|--|
| | -- |
| Chapter - 1 | GENERAL INTRODUCTION |
| 1.1 | The basic phenomenon .. 1 |
| 1.2 | Importance of II-VI compounds as an EL phosphor .. 3 |
| 1.3 | Activators and co-activators .. 4 |
| 1.4 | Phosphors based on ZnS .. 6 |
| 1.5 | Rare earths as activators .. 8 |
| 1.6 | New phosphor systems .. 9 |
| 1.7 | Mechanism of electroluminescence .. 10 |
| 1.8 | Intrinsic electroluminescence .. 11 |
| 1.9 | Acceleration of the charge carriers .. 13 |
| 1.10 | Collision excitation .. 16 |
| 1.11 | Brightness-voltage characteristics .. 17 |
| 1.12 | Time dependence of electroluminescence .. 18 |
| 1.13 | Injection electroluminescence .. 20 |
| 1.14 | DC powder electroluminescent displays .. 26 |
| 1.15 | Thin film electroluminescence- The present status .. 27 |
| 1.16 | Device physics .. 30 |
| 1.17 | New concepts .. 35 |
| 1.18 | Summary .. 38 |

| | | | | |
|-----------|-----|--|----|-----|
| Chapter - | II | EXPERIMENTAL SET UP | | |
| | 2.1 | Introduction | .. | 44 |
| | 2.2 | Phosphor preparation | .. | 45 |
| | 2.3 | Vacuum furnace | .. | 46 |
| | 2.4 | Test cell | .. | 48 |
| | 2.5 | Excitation sources | .. | 51 |
| | 2.6 | Arrangements for recording the EL emission spectra | .. | 58 |
| | 2.7 | Voltage-brightness measurements | .. | 65 |
| | 2.8 | EL brightness measurements in absolute units | .. | 66 |
| Chapter - | III | ELECTROLUMINESCENCE SPECTRUM IN SOME ZnS BASED PHOSPHORS AND IN SELF ACTIVATED ZnO. | | |
| | 3.1 | Introduction | .. | 74 |
| | 3.2 | Electroluminescence in ZnS:Cu,Cl phosphor and its dependence on chlorine concentration | .. | 75 |
| | 3.3 | Study on ZnS:Mn and ZnS:Cu,Mn,Cl phosphors | .. | 84 |
| | 3.4 | EL spectral study of ZnS:Cu,Sm,Cl and ZnS:Cu,Dy,Cl phosphors | .. | 92 |
| | 3.5 | Electroluminescence in self- activated ZnO | .. | 95 |
| Chapter - | IV | A STUDY ON CaS:Ce AND CaS:Ce,Nd EL PHOSPHORS | | |
| | 4.1 | Introduction | .. | 99 |
| | 4.2 | Phosphor preparation | .. | 103 |

| | | | |
|--------------|--|----|-----|
| 4.3 | Self activated emission of CaS | .. | 105 |
| 4.4 | Experimental results and discussion | .. | 107 |
| 4.5 | Sensitized luminescence and the EL in CaS:Ce,Nd phosphor | .. | 119 |
| 4.6 | Summary | .. | 127 |
| Chapter - V | A STUDY OF ELECTROLUMINESCENCE SPECTRUM OF CaS:Er PHOSPHOR AND ENERGY LEVEL SPLITTING IN Er ³⁺ ION. | | |
| 5.1 | Introduction | .. | 130 |
| 5.2 | Phosphor preparation and study of electroluminescence | .. | 131 |
| 5.3 | Experimental results | .. | 131 |
| 5.4 | Energy level splitting in crystal fields | .. | 133 |
| 5.5 | Theoretical calculation | .. | 139 |
| 5.6 | Conclusions | .. | 147 |
| Chapter - VI | ELECTROLUMINESCENCE IN CaS:Sm, CaS:Dy AND CaS:Mn PHOSPHORS | | |
| 6.1 | Introduction | .. | 149 |
| 6.2 | Phosphor preparation and experi- mental set up | .. | 150 |
| 6.3 | EL of samarium doped calcium sulphide | .. | 150 |
| 6.4 | EL of CaS:Dy | .. | 156 |
| 6.5 | CaS:Mn EL phosphor | .. | 161 |
| 6.6 | Conclusions | .. | 161 |

| | | | |
|----------------|--|----|-----|
| Chapter - VII | A STUDY ON DC POWDER EL DEVICES | | |
| 7.1 | Introduction | .. | 163 |
| 7.2 | DC powder cell fabrication | .. | 164 |
| 7.3 | DC forming of the cell | .. | 166 |
| 7.4 | Structure of a typical cell and its analysis | .. | 167 |
| 7.5 | Preparation of ZnS:Cu,Mn DC PEL cells | .. | 174 |
| 7.6 | Preparation and study of CaS:Ce DC PEL cells | .. | 177 |
| 7.7 | Conclusions | .. | 178 |
| Chapter - VIII | FABRICATION OF THIN FILM EL DEVICES-EXPERIMENTAL SET UP | | |
| 8.1 | Introduction | .. | 183 |
| 8.2 | Vacuum system for the deposition of electrodes | .. | 186 |
| 8.3 | Deposition system for insulator and active layer films | .. | 187 |
| 8.4 | Substrate heater | .. | 190 |
| 8.5 | Thickness measurements | .. | 192 |
| 8.6 | Deposition of transparent conducting electrode of SnO ₂ by spray pyrolysis method | .. | 198 |
| 8.7 | Summary | .. | 202 |
| Chapter - IX | FABRICATION AND STUDY OF AC THIN FILM EL DEVICES OF MgF ₂ AND Y ₂ O ₃ INSULATING LAYERS | | |
| 9.1 | Introduction | .. | 204 |
| 9.2 | Fabrication of MISIM devices | .. | 205 |

| | | | |
|-------------|--|----|-----|
| 9.3 | Results and discussion | .. | 210 |
| 9.4 | Conclusions | .. | 217 |
| Chapter - X | SUMMARY AND CONCLUSIONS | | |
| 10.1 | Summary of the work | .. | 219 |
| 10.2 | Scope for further work | .. | 223 |
| Appendix | ELECTROLUMINESCENCE OF ELECTRO- POLYMERISED CASTOR OIL AND LIQUID PARAFFIN | | |
| 1 | Introduction | .. | 225 |
| 2 | Fabrication of the cells and the electro-polymerisation process | .. | 226 |
| 3 | Conclusion | .. | 239 |

CHAPTER 1

GENERAL INTRODUCTION

PART-A

1.1 The Basic Phenomenon

Emission of light from materials has attracted man from time immemorial. The shining light flashed by fireflies at night, apparently without any harmful heat accompanying it, had remained an enigma for the early man. A substance can be made to emit visible light in a multitude of ways. These include the application of heat, pressure, chemicals, frictional force, high energy radiation etc. Electroluminescence (EL) is the phenomenon of light emission from certain crystals (phosphors) caused by the passage of an electric current. Such electric field induced emission was first observed in SiC crystals by Lossev [1] in 1923. Since then extensive investigations have been carried out by a host of workers on the different aspects of EL in a number of materials [2]. The subject is of great contemporary importance as it finds a variety of potential applications in many high technology areas.

Light emitting devices based on EL have been produced and they find numerous applications as indicators and display units in instruments and systems. In particular EL devices can serve as the information linkage between complex electronic systems and their human users (as a man-machine interface). Hence there is a continued attempt to improve the

performance and efficiency of EL devices. This has resulted in a large number of new EL materials and new configurations for EL devices.

Currently the most prominent EL materials are III-V and II-VI compound semiconductors. The former type is usually known as the LED material since they are widely used in the fabrication of the light emitting diodes (LED) in which the emission is due to the recombination of the injected minority carriers across a p-n junction. These display elements are routinely used in visual alpha-numeric information displays in many hand held and desk electronic calculators, as indicators in a wide variety of electronic instruments, as light modulators etc. These cold emitters have in their emission spectrum bands or lines unlike incandescent sources which usually give a continuous spectrum of visual as well as heat radiation. Light emitting diodes with emission in the near infra red (IR) region are used in fibre optic communication systems [3,4].

Electronic systems are continually increasing in their complexity and in range of applications. This has produced a need for electronic displays of large area, capable of showing complex digital, analogue and graphic information. The LED displays are not quite suitable for the development of such systems due to their high cost and the much higher current density required for their excitation. Even the most efficient devices require a current density

of $0.25\text{A}/\text{cm}^2$ [5]. This will need bulky excitation sources, making battery operation quite difficult.

1.2 Importance of II-VI compounds as an EL phosphor

In the 1950's and early 1960's several thousand papers in the field of EL were published [6]. These deal principally with panels based on powder ZnS and related compounds and with very few exceptions, all devices described were operated under AC excitation. The work during that period has been reviewed and assessed in several books [6,7] and articles [8,9,10]. These studies suggested that EL display panels of low power requirements can be developed with the II-VI compound semiconductors. But it is very difficult to form p-n junction with these materials particularly due to their self compensation effects [11]. The first and the most efficient EL material of this group is ZnS. Electroluminescence in ZnS was discovered by Destriau [12] in 1936. Compounds belonging to this class are comparatively less expensive and have good conversion efficiency. For example Lehmann [13] in 1958 has prepared one optimised ZnS EL device activated with copper and chlorine (ZnS:Cu,Cl) which has an efficiency of 4.5×10^{-2} compared to the value of 1.7×10^{-1} of a 40 W fluorescent white lamp which is the most efficient visible light source available.

Most of the work related to II-VI chalcogenides has been concentrated on the compounds which have relatively larger band gap namely ZnS, ZnSe and CdS. Among these

ZnSe and CdS exhibited some typical semiconductor properties under certain preparation conditions. However, ZnS still stands out as the only material that possesses the most desirable feature in luminescent application, both in cathodoluminescence (CL) and in EL. It is still intrinsically the most efficient phosphor far surpassing GaAs in properties like quantum efficiency (QE) and brightness. Although the defect chemistry and the physical properties of narrow and medium band gap co-valent semiconductors are relatively well known, this cannot be said of wide band gap semiconductors such as ZnS which tend to host various type of recombination centres creating energy levels within their band gaps. The efficiency of luminescence in such phosphors is determined by the nature of the band structure and the various kinetic processes that occur at these centres. These centres interact, and each type of centres plays a significant role in determining the overall efficiency and the emission characteristics of the luminescent materials. Hence for all materials, in particular for this II-VI group of compounds, the procedure adopted for the preparation of the phosphors and the nature and amount of the additives called activators which create these centres are of great significance [11].

1.3 Activators and Co-activators

The activators are certain acceptor type impurities introduced into the pure host crystal lattice to produce luminescence. There are numerous activators that cause

luminescence in these materials as well as certain defect centres that may act as if they were activators. Some of the elements commonly used as activators in II-VI phosphors are copper, silver, aluminium, manganese and various lanthanides. A number of these, copper and silver in particular, may occupy various sites in the crystalline lattice, thereby causing different emission colours and efficiencies. But for many activators to operate properly, it is necessary to incorporate an additional donor impurity usually called as the co-activator. The presence of a co-activator in phosphors may be required to ensure physical incorporation of the activator or to create certain energy levels within the phosphor band structure which aid the luminescence. For example, ZnS with Erbium activator and copper co-activator (Zn:Er,Cu) system, both of these functions are required and apparently performed by the copper co-activator. The copper accomplishes this by performing the two separate and distinct functions, viz. charge compensation and sensitization. When a tripositive ion is substituted for a zinc ion, it creates a charge imbalance that must be compensated by adding a monovalent ion, such as Cu^+ , to the lattice. This is known as the charge compensation. An analogous situation occurs when monovalent copper is present as an activator. In this case, a negative monovalent co-activator such as the halides, typically chlorine, bromine or iodine, is used. Sensitization involves the presence of energy levels within the crystal which transfer exciting energy to certain activators [11,14].

1.4 Phosphors based on ZnS

ZnS:Cu,Cl phosphor is the most extensively studied EL phosphor. As discussed above, it is observed that the properties of the phosphor depend very strongly on the conditions of preparation and on the concentrations of the activator and co-activator present. For example it is found that this phosphor can emit blue, green or red or its combinations [15,16]. In addition, in some cases IR emission at 1.5 and 1.7 μm is observed [17]. There is also a very strong dependence of the emission colour on the excitation frequency and temperature. And it is not at all certain whether these two emission bands are due to two copper levels or due to the modification of the energy levels of the sulphur ions located nearest to the copper ions because of the difference in ionic charge associated with a zinc or copper ion [2]. However, in order to explain the experimental observation G. Curie and D. Curie [18] and Riehl, Schon and Klasen [19] have suggested two different models. In Curie's model (Fig.1.1) it is assumed that the ground state due to Cu^+ ions plays a part in both blue and green centres in ZnS. But the green emission occurs from a transition arising from the donor levels introduced by the oxygen or the co-activator ions. The blue emission is either due to the transition from the conduction band or from an excited level of the luminescent centre which is shallower than the donor levels involved in the green emission. But the Riehl-Schon-Klasen model (Fig.1.2) assumes that the empty low lying (blue) centres will be filled by electrons

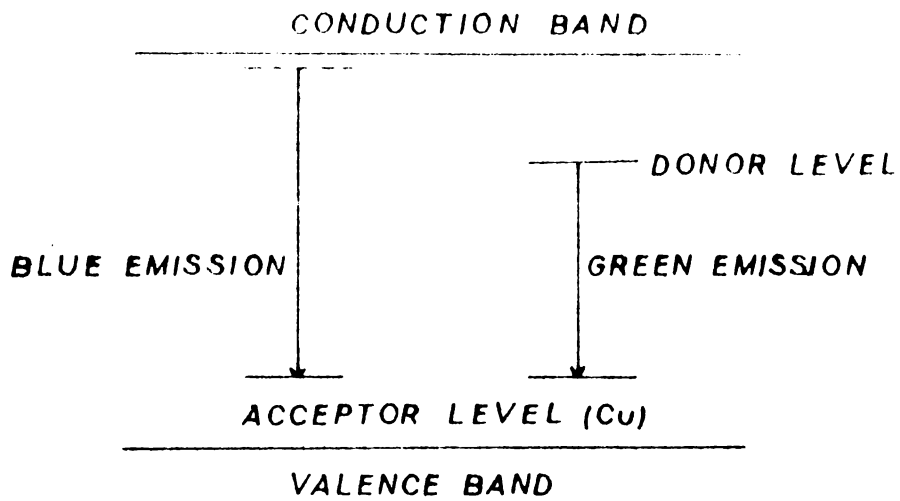


Fig.1.1. The model proposed by G. Curie and D. Curie for blue and green emission centres in ZnS:Cu.

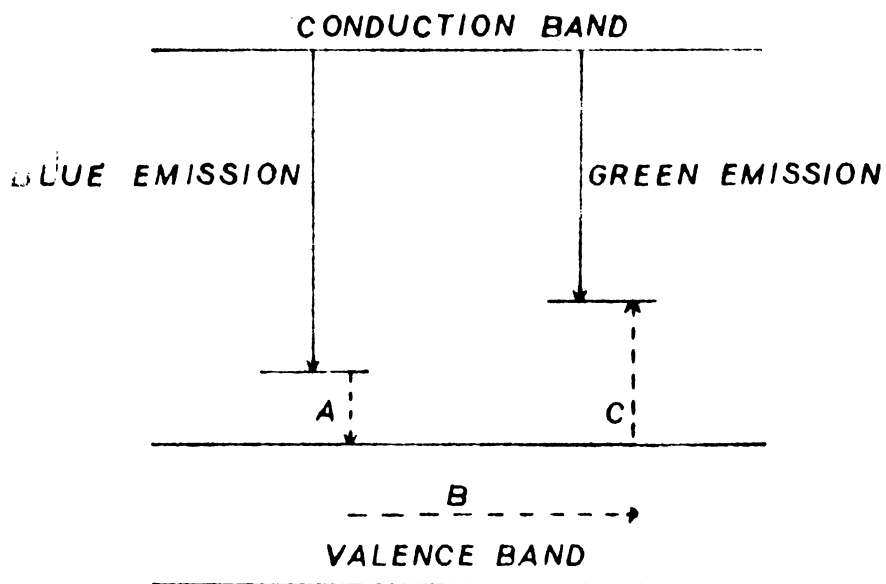


Fig.1.2. Riel-Schön-Klasen scheme. The transport of energy from blue to green centres by hole migration is shown by the arrows A, B and C.

from filled higher (green) centres via the valence band and the emission will be predominantly green if sufficient time and activation energy (temperature) are available.

Both these models explain some of the experimental results but not all. The details of a series of studies which throw more light on the role of Cu centre in ZnS made by the author are presented in Chapter III of the thesis.

At present in ZnS, the activator of practical importance, other than copper, is manganese. ZnS:Mn has a yellow-orange emission. Even though this is one of the earliest EL phosphor systems a complete picture of the physical phenomenon involved in the emission process is not yet well understood. Recently Skolnick et al. [20] have made an attempt to study the light emission mechanism with the aid of the time resolved spectroscopic approach and obtained evidence for the hot carrier impact excitation process in its EL emission. It is found that the emission from ZnS:Cu,Mn is more efficient than the ZnS:Mn phosphor.

1.5 Rare earth as activator

Rare earth (RE) dopants, as activators in luminescent systems (eg. in EL, CL and in photoluminescent (PL) phosphors) are of special importance because of their ability to yield narrow band emissions. It is found that by choosing proper host and rare earth activator, emission in any region covering the UV, visible and near IR regions, can be obtained. RE elements have been used as the activator in ZnS phosphors

by Bryant et al. [21]. Recently laser action has also been reported by Zhong and Bryant [22] in a thin film ZnS:Cu,Nd,Cl cell. One problem regarding this type of activator is that it is quite difficult to introduce them in the ZnS crystal due to smaller cation size of the lattice. So more sophisticated ion implantation technique or sometimes co-evaporation technique has to be adopted for this purpose [21].

1.6 New phosphor systems

Experience in solid state physics in general and EL in particular has shown that cases where theory leads experiment are more of an exception than the rule [23]. So EL researchers are constantly engaged in the synthesis of new and sometimes exotic materials, in addition to the attempts to improve the existing phosphor systems. In their hunt for new materials, they are sometimes guided by the idea that a good CL phosphor may be a good EL phosphor as well. This is because the charge carriers and the luminescent centres involved in the two processes are the same but differs only in the mode of acceleration of the charge carriers.

One such EL phosphor which has gained some importance recently is the ZnO phosphors doped with various activators [24-27]. The most significant achievements in recent times is the conversion of the efficient alkaline earth sulphide phosphors developed by Lehmann [28] into good EL phosphors by Vecht et al. [29]. They have developed a series of band

and line emitting EL phosphors. The notable one is CaS:Ce which has a power efficiency comparable to the established ZnS:Cu,Mn phosphors.

1.7 Mechanism of EL

Three distinct processes are involved in the EL phenomenon:

(1) Excitation of crystals by the applied electric field to an energy state atleast a few electron volts above the ground state. The excited state can be an ordinary conduction state of the crystal, an excited state of an impurity system or a state of high kinetic energy within the conduction or valence band. The excitation process may inject minority charge carriers, field ionize valence electrons or impurities, or accelerate charge carriers within a band to optical energies.

(2) Transport of the excitation energy through the crystals to a region where de-excitation can occur with large probability for radiative transition. The energy transport can be by charge carriers, exciton migration or by resonance transfer.

(3) Radiative-de-excitation. This involves localized states of impurity systems, interband transition or intraband transitions [30].

Various combination of these excitation, energy transport and emission process can occur in actual crystals [31]. Depending on the carrier generation process EL can be classified into two types: (1) Intrinsic EL and, (2) Injection EL.

1.8 Intrinsic EL

High field EL devices based on the II-VI semiconducting compounds generally fall in this group. Curie [18] has suggested a three step process for such an EL emission which is given below:

(1) Transfer of electron from donor levels to the conduction band under the action of the applied electric field and or temperature.

(2) Acceleration of these electrons in the conduction band and the subsequent carrier multiplication or an avalanche effect.

(3) Collision of these electrons with luminescent centres which are thereby excited (ionized) or with the basic crystal lattice itself followed by the production of electron hole pairs.

However, Curie was not specific about the first process and assumed that it is not the important rate determining step. But Piper and Williams have independently considered field acceleration of electrons as the exciting

mechanism in EL. The quantitative treatment by Piper and William [32] differs from that of Curie and considers that the initial production of carriers can influence the EL emission. They have also assumed that the phosphor possesses deep donor levels lying perhaps ~ 0.5 eV below the conduction band.

The effect of the field on the ionization of these donor levels can be explained on the basis of the idea put forward by Frenkel [18]. He has assumed that the field and the phonon mutually assist in producing ionization of the levels. If the depth of the level is ϵ in the absence of the field, the probability of the ionization per second is

$$p = S \exp \left(- \frac{\epsilon}{kT} \right)$$

which is very small if ϵ is large. In the presence of the field E the depth is reduced to

$$\epsilon^* = \epsilon - f(E)$$

and the probability of the ionization becomes

$$p = S \exp \left(- \frac{\epsilon - f(E)}{kT} \right)$$

where $f(E)$ is the apparent change in trap depth due to the applied field. So during first few cycles of the applied

field on an EL cell, the brightness will be very low. Gradually the electrons fall into the traps which at the beginning were empty, and the ionization of the latter by the same process as above soon plays the dominant role in the supply of electrons to the conduction band. This will naturally produce a build up in the EL emission and is actually observed [33].

1.9 Acceleration of the charge carriers

In order to accelerate charge carriers to optical energies, high fields capable of accelerating them to large kinetic energies must exist and also the carriers (holes or electrons) must be injected into or created in this high field region. The latter usually occurs by the field ionisation of shallow donor levels as explained earlier. But here conduction electrons experience an accelerating force as a result of the field and a retarding force resulting from interaction with the lattice phonon. With moderately strong applied field, conduction electrons which experience unusually few collisions with lattice phonon will attain sufficient energy to ionize impurities or valence electrons by inelastic collisions. A typical value of the field intensity is $\sim 10^5$ volts/cm. At a much higher field ($\sim 10^6$ volts/cm) average conduction electrons acquire energy from the field faster than the rate at which energy is lost to the lattice phonons, thereby attaining sufficient energy to ionize impurities or valence electrons by collision.

This may also lead to the conditions for dielectric breakdown [30].

But in order to eliminate the catastrophic consequence of dielectric breakdown Piper and Williams assumed that there occurs inhomogeneous field distribution within the EL crystals, for example, a region where a narrow high field exists in series with an extensive low field region. This will permit operation over a broad range of applied voltages without creation of an unstable breakdown condition. A crystal which is particularly stable against dielectric breakdown is one having non linear characteristics such that the width of high field region as well as the magnitude of the field increases with the applied voltage.

Piper and Williams [34,35] have also assumed that in EL phosphors the acceleration is actually occurring at such a Mott-Schottky exhaustion barrier (Fig.1.3) which arises from the ionization of shallow donor levels. The concentration of deep donor is assumed to be much less than that of shallow donors so that the latter alone determines the potential distribution in the barrier region. Most of the applied potential will appear across the barrier and hence a moderate applied electric field in the barrier region will be sufficient to produce ionization of these deep donors and subsequent acceleration and collision excitation can lead to luminescence. Zalm et al. [36] suggested that the donors responsible for the positive space charge barrier are the

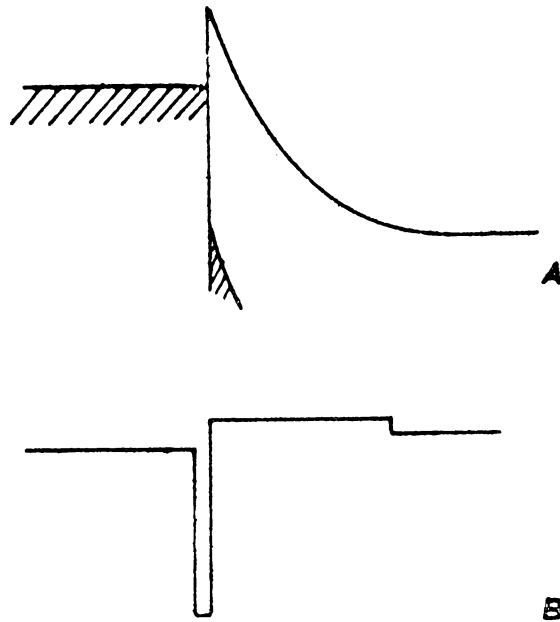


Fig.1.3. Mott-Schottky exhaustion layer (A) potential configuration (B) distribution of electrostatic charge density.

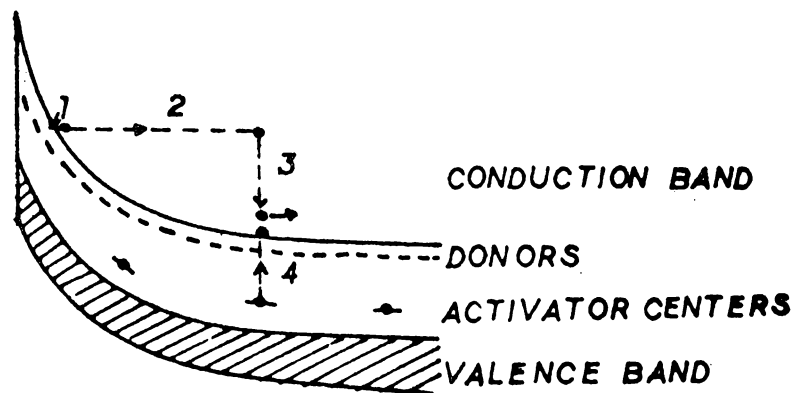


Fig.1.4. Schematic representation of acceleration collision mechanism of electroluminescence. Electrons from traps in the localized high field region are liberated by the action of the field (1) or injected from a contact and then accelerated by the field (2) to acquire kinetic energy above the bottom of the conduction band and collide with activator centres whereby they lose their energy and the activator centre is ionised (4) or excited.

ionized activator centres themselves and that the initial electrons are supplied by a surface layer of Cu_2S .

In the case of Mott-Schottky type barrier an increase in applied voltage increases the breadth of exhaustion region and field intensity increases as the square root of the applied voltage.

An intrinsic layer is another suitable type of barrier. This barrier remains constant in thickness with applied voltage. The field which is independent of position in the barrier varies linearly with applied voltage.

Yet another possibility is a p-n junction biased in the reverse direction. An increase of the applied field in this case increases the width of the depletion region and here the field strength varies as the two third power of the applied voltage [30].

1.10 Collision excitation

The energy of these accelerated electrons is transferred to various activator centres by inelastic collisions and they lose energy by release of further electrons from the centres into the conduction band (Fig.1.4). Both categories of electrons after impact possess some residual motion along the accelerating field direction and will be in the same state they were before getting accelerated.

The other modes of energy transfer relevant to EL emission are the migration of minority charge carriers, exciton and resonance energy transfer processes [30].

1.11 Brightness-voltage characteristics

From the above discussion it can be seen that the carriers which induce emission are generated in a high field region formed within the crystal. It is also known that, depending on the type of barriers involved, the nature of the field producing the acceleration of the carriers varies considerably. This causes the number of carriers generated to produce luminescence and hence the brightness to vary with the type of barrier. In other words we can have an idea about the type of potential barrier involved in the process by studying the average brightness voltage characteristics. Destriau has obtained an empirical relation which relates the brightness (B) and the applied voltage (V) as

$$B = a \exp (-b/V)$$

where a and b are constants. He has later modified this relation to account for the slight curvature of the log B vs $\frac{1}{V}$ plot and wrote

$$B = a V^n \exp (-b/V)$$

The value of n is found to depend on the phosphor used [35].

A number of other empirical relations have also been proposed by various workers and the most popular among them is due to Alfrey, Taylor and Zalm [36,37]. Here the brightness is given by

$$B = B_0 \exp \left[- \left(\frac{V_0}{V} \right)^{\frac{1}{2}} \right]$$

where B_0 and V_0 are parameters which depend on temperature and frequency of the alternating voltage, phosphor type, and on details of the construction of the test cell. The square root term in the relation clearly shows that there involves a Mott-Schottky type barrier for the acceleration of electrons. Over a limited range of voltage this equation may be approximated with a power law. At very low voltages and therefore at very low output the brightness may vary as the 9th or 10th power of the applied voltage. At voltages approaching breakdown of the layer the dependence usually approximates to V^2 or even to a lower power of V . In some cases it is smaller than unity. But Thornton [38] pointed out that since the phosphor contains particles of different sizes, for a given voltage the field experienced by each particle will be different and hence the observed result will be only the average.

1.12 Time dependence of EL

The obvious involvement of transport process, carrier trapping and related effects in EL emission is clear

from the above discussion. So it is quite natural to expect a dependence of the brightness of emission and its spectral contents on the applied frequency of excitation and also on the shape of the wave form.

Generally it is observed that for a sine wave excitation there exist two light peaks (known as brightness waves) per cycle of the applied voltage. The two peaks have different amplitudes [35]. Various workers have observed a phase shift between the brightness peak and the voltage maxima. Destriau [35] has attributed it to the phase shift of the field in the dielectric medium surrounding the phosphor particles. But Zalm [36] has attributed it to the delayed recombination of the accelerated electrons. There occurs a secondary peak for green or blue emitting ZnS:Cu phosphors. These minor peaks are often not well resolved and occur near (and usually before) the instant the applied voltage passes through zero. The detailed characteristics of these peaks were studied by Destriau [40] Thornton [2] and Zalm [39].

Thornton [41] and later Georgobiani and Fok [42] assumed that the brightness wave is a kind of field controlled glow curve since the rate determining factor is the field controlled thermal release of trapped electrons. Thornton developed a model based on reduction of the trap depth by the field. This mechanism facilitated return of the electron to the excitation region, and hence an earlier primary peak, for high voltage and low frequency as well as

for high temperature. Since it is known that trapping of charge carriers plays an important role in the temperature dependence of integrated output, secondary waves, EL build up etc., one can expect its effects on the brightness frequency characteristics also. This is because of some sort of matching (or mismatching) between the field frequency and the trapping time which can affect the release of electrons from the traps and hence the brightness. Such a phenomenon was not observed earlier. But the author has obtained clear evidence for the carrier trapping from the B-f characteristic of the various CaS phosphors and the same is described in detail in Chapter IV of the thesis.

1.13 Injection EL

1.13.1 p-n Junction

Perhaps the simplest type of EL process is that following injection of minority charge carriers, either at an electrode contact or across a p-n junction. At such a junction, in the absence of an applied voltage there is a state of dynamic equilibrium between the competing processes of thermal production and subsequent recombination of electron-hole pairs. Some of recombinations occur with the emission of radiation, which contributes to the normal thermal (black body) radiation of the material. When voltage is applied in the forward direction and additional carriers are injected, this equilibrium is upset and the rate of recombination is increased (Fig.1.5). The resulting emission

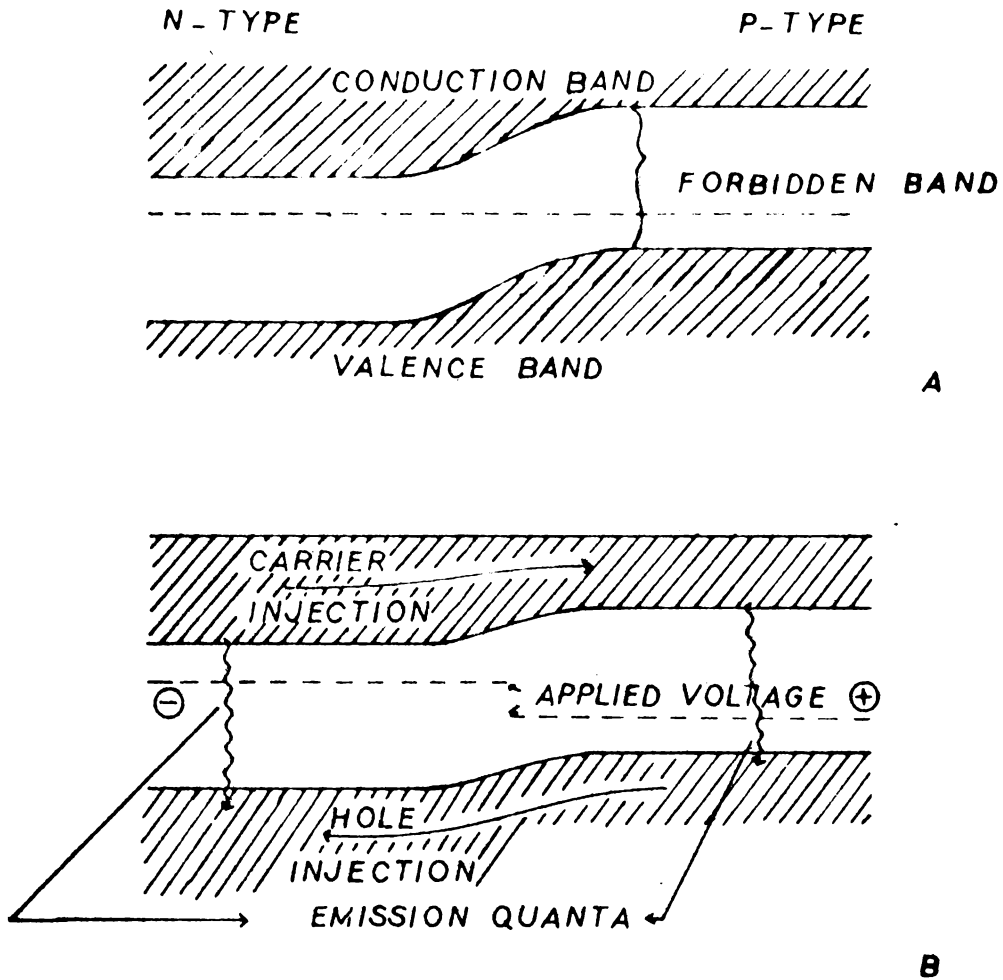


Fig.1.5. Energy level diagram for a p-n junction in the absence of an applied field (A) and for current flow in the forward direction with consequent injection of minority charge carriers (B).

of radiation may be called injection electroluminescence [43,44]. Lossew [1] was first to find such an EL from the rectifying crystals of SiC. Since then this phenomena is observed in a variety of compounds. Reviews of the subject are available in the literature [3,4].

1.13.2 Heterojunction

In order to inject only one particular type of carriers into a luminescent material usually a hetero junction is made use of (Fig.1.6). In this case the source of the injected carriers is a material having a wider band gap with respect to the luminescent region. Then the asymmetry of the barriers seen by electrons and holes assures a high injection efficiency from the layer of the material with wider band gap. Although hetero junctions can be made between completely different materials, the most successful devices are those made from different compositions of miscible alloys having similar lattice constants at the temperature at which they are fabricated, eg. $\text{Al}_{1-x}\text{Ga}_x\text{As}$ with two different values of x on either side of the junction, commonly used in LEDs and diode lasers [45-47].

1.13.3 Schottky barrier

A Schottky barrier usually occurs at the surface of semiconductor in contact with a metal, such a barrier can act as p-n junction. Whenever surface states induce an inversion layer, the surface has the opposite type of

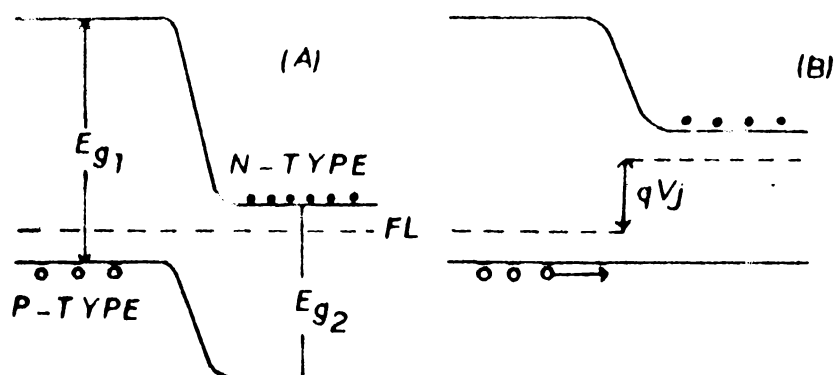


Fig.1.6. Diagram of heterojunction (A) at equilibrium (B) with a forward bias V_j .

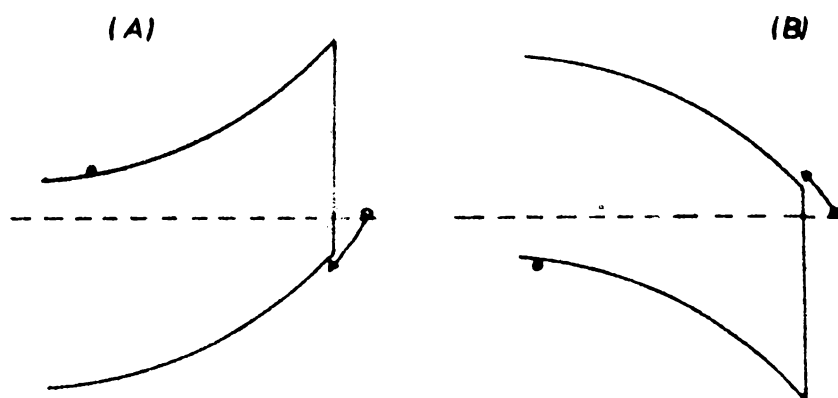


Fig.1.7. Diagram of Schottky barriers to n type (A) and p-type (B) material. The arrows show the minority carrier injection during forward bias.

conductivity compared with the bulk. In effect this is equivalent to a p-n junction immediately below the surface (Fig.1.7). A forward bias tends to flatten the band structure, allowing the injection of minority carriers into the bulk, where they can recombine radiatively just as they would in a p-n junction [43].

1.13.4 MIS structure

When surface charges are insufficient to induce the desired inversion layer, one can induce them by a capacitive coupling to the surface through an insulator. In a metal-insulator-semiconductor (MIS) structure, the surface charge on the semiconductor is determined by the potential applied to the metal [48]. An immediate benefit of the MIS structure is that the phenomenon of band bending can be controlled by the applied voltage (Fig.1.8). Thus an inverse layer can be induced by one polarity, then the carriers accumulated at the surface can be injected by reversing the polarity of the metal electrode. This method has been used to obtain EL in GaAs without p-n junction [49]. **If the insulator is made very thin electrons can also tunnel across the insulator [50].**

Once the minority carriers are injected, a variety of recombination mechanisms are possible. Some of them do not lead to luminescence and thus contribute to the observed low efficiency. These include processes like multiphonon emission, Auger effect and non-radiative trapping by **defects**.

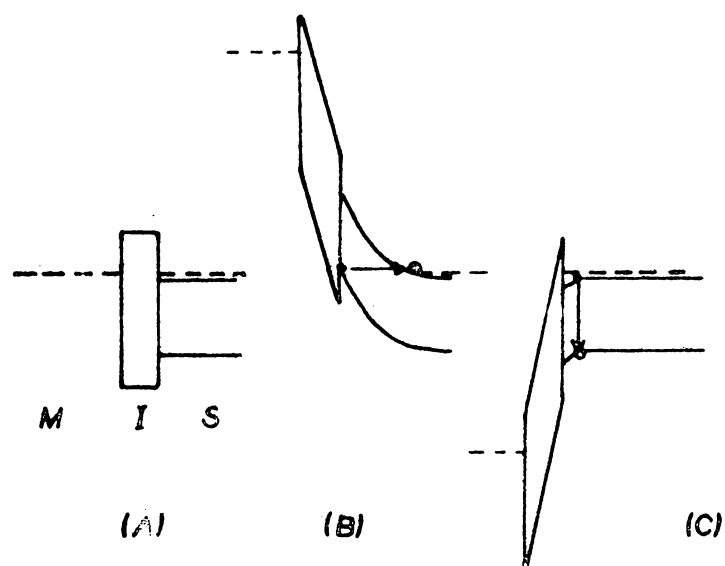


**Fig.1.8. Band structure at MIS junction
 (A) without bias (B) metal
 negatively biased for hole
 generation (C) metal positively
 biased for recombination.**

At present the most successful electroluminescent device prepared from the II-VI compound semiconductor viz. ZnS:Mn is the AC thin film EL device. These cells have a symmetric structure which can be thought of as having two MIS junctions.

1.14 DC Powder EL displays

The renewed interest in the EL of II-VI compounds has resulted in improved devices and their wide application in different display systems. At present nearly 14 different type of EL devices are either available in the market or are in the different stages of development. Among them a promising type of recent origin is the DC powder EL devices. These devices can be operated at very low voltage (~ 50 V). But they are still in the experimental stage eventhough Vecht et al. [10]. have prepared a few good quality Direct Current Powder Electroluminescent (DCPEL) panels using ZnS:Cu,Mn and CaS:Ce phosphors. Television display screens have also been developed based on this technology [52-55]. These devices essentially consist of the phosphor powder coated with a Cu_xS skin [56] and dispersed in a suitable insulator matrix and placed in between a pair of electrodes deposited in a crossed grill fashion. The peculiar nature of these devices is that they have to undergo a current forming process to become luminescent [56]. A detailed account of the structure, the fabrication, the current forming and an analysis of the various characteristics of a DCPEL cell is given in Chapter VII of the thesis.

PART-B1.15 Thin Film Electroluminescence - The Present Status

1.15.1 Introduction

Electroluminescence in phosphors deposited in the form of thin films was first suggested by Halsted and Koller [57] in 1954. They observed a steep nonlinear B-V characteristic in their devices. This property attracted Thornton, a well known display technologist, to this new type of device. Thornton [58] has made such a device but it lasted only for a few hours. Subsequently, a number of workers have entered into this new area. They were successful in developing devices of high brightness (>1000 ft L) and efficiency ($\sim 10^{-4}$) [10,66]. But their poor working life still remained as a serious problem. Most of the early work on thin film EL was centred on thin film devices having the active phosphor layer in between two electrodes. Obviously one of these electrodes should be transparent. In addition to their poor maintenance, preparation of such large area devices was difficult owing to the severe burn out and pin hole problems. Because of this technical constraints a practical and commercially viable display device of this type has not become a reality despite the fact that they can be operated at a relatively low voltage and can have high brightness levels. However, recently, Abdalla et al. [20] have prepared an X-Y matrix display panel of the DC thin film type using a new preparation technique. At

present, such DC thin film EL (DCTFEL) cell structure widely used for the experimental investigation of various luminescent centres in different host materials [21].

1.15.2 AC thin film EL devices

Russ and Kennedy [60] have attributed the failure of the DC cells to the lack of current limiting. So they have prepared an AC thin film EL device of double insulating layer structure. This structure, because of its symmetric nature was able to minimize any slow polarization effect and also offers the required protection by local current limiting. This is possible since the current flowing through the active film (e.g. ZnS:Mn) would charge up the interface with the dielectric and reduce the internal field. The first successful application of this type of current limiting in a practical device was by Soxman and Ketchpel [59]. They have employed an unsymmetrical AC coupled structure to make segmented numeric and X-Y matrix displays. ZnS:Mn is the preferred active material for AC coupled devices. But following the work of Kahng [61] there was also considerable interest in films of ZnS doped with rare earth fluorides such as TbF₃ which produces green luminescence [62]. The studies on Mn doped ZnS films started early in the history of EL. Since 1960, Vlasenko et al. [63-65] have made extensive investigation on ZnS:Mn EL thin films and have published a number of interesting papers. It seemed that all these workers were more

interested in the study of the physics of these devices rather than giving importance for prolonging the life of operation. But the most significant impetus to development in the thin film EL for display applications came, however, with the report of Inoguchi et al. [66] of very high luminance (>1000 fL), coupled with very long life ($>20,000$ hrs) achieved through the use of ZnS:Mn in a symmetrical structure similar to that of Russ and Kennedy but with a layer of Y_2O_3 which has a very high dielectric strength. A very strong non-linearity of luminance vs voltage characteristic of this device was evident and this is quite suitable for application in display systems.

The interest among display technologists was further stimulated by the subsequent report [67] of hysteresis behaviour exhibited by the luminance vs voltage variations for devices with the same structure but made by a slightly different procedure. This report raised the possibility of displays with inherent memory function. An EL display panel, making use of this memory phenomenon with 1248 characters (120×160 mm² area) was reported by the Sharp Group [68] in 1975. From that year to the present, scores of publications have appeared describing the attempts to reproduce or improve the results obtained by the above team. Other commercial manufacturers presently in the market are:

(1) Sigmatron Nova, U.S.A with a 38 mm x 38 mm device of an average brightness of 50 fL [69] and Lohia Corporation.

Finland, which produces a transparent device fabricated by adopting a novel technique known as atomic or alternate layer epitaxy (ALE). This technique was first demonstrated by Suntalo [70]. The films obtained by ALE are reported to have better quality than those prepared by the conventional evaporation technique.

1.16 Device Physics

1.16.1 Non memory

The most important feature of the non-memory EL device is the steep rise of its brightness with voltage and a saturation of the brightness at a high excitation field. (A typical characteristic curve is shown in Fig.1.9)

The analysis of the characteristics involves two components the equivalent circuit aspect and the internal mechanism associated with the active layer. As shown in Fig.1.10 it can be assumed that the device consists of a series capacitance made up of the two dielectric layers and an active layer which has both capacitance and non linear conductance, i.e. at low fields the active layer acts as an insulator but at higher internal fields (in this case 1.5×10^6 V/cm) the breakdown of this layer occurs. This increases the electrical conduction followed by the onset of light emission. The steep rise in brightness reflects the corresponding rise in current density as long as the voltage drop across the ZnS:Mn layer continues to increase. At higher intensity all the charge carriers produced do not recombine and as a

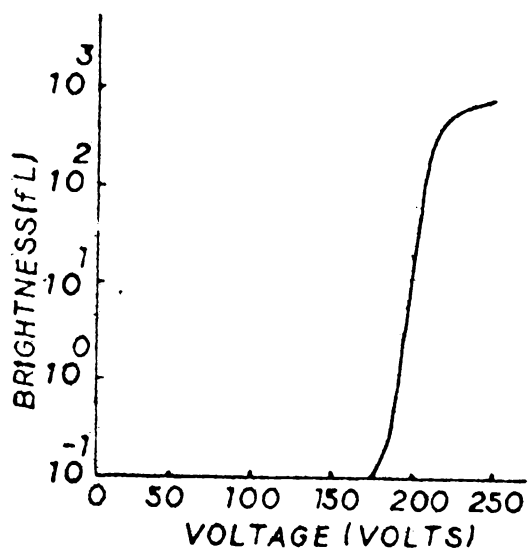


Fig.1.9

Typical B-V characteristic

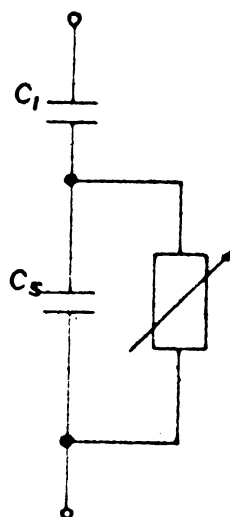


Fig.1.10 (A)

The equivalent circuit

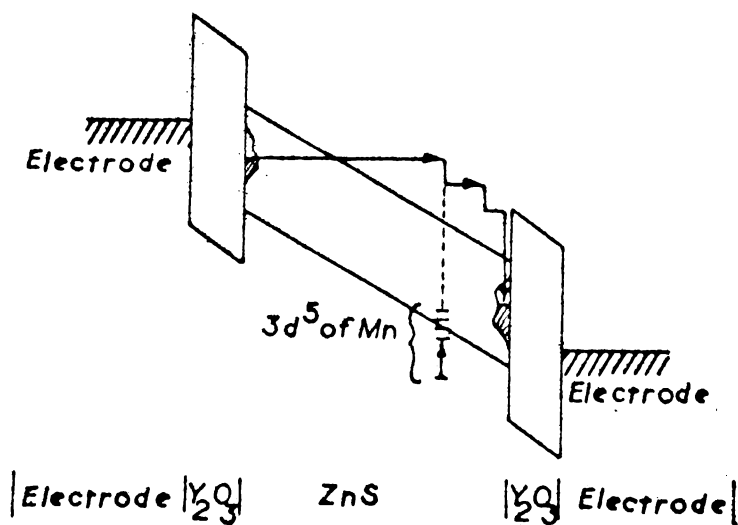


Fig.1.10 (B)

Shows the main features of the field clamping model (1) high field induced tunneling from states near the interface (2) collision excitation of Mn^{++} by electrons accelerated in the high field (3) retrapping near the opposite interface.

result, a surface charge will be formed at the active layer dielectric interface. This will offset the increased external voltage and is known as the field clamping effect [71,72].

The internal efficiency of thin film EL devices depends upon: the field at which current flows, the fraction of electrons at such fields with sufficient energy to produce internal excitation of the activators, the cross action and density of activators and finally on the luminescent probability of the activator. Mn^{2+} , for example, shows a strong concentration quenching, even in PL, at concentrations greater than about 0.5 wt percent in ZnS. It is well known that Mn^{2+} has a more favourable cross section for excitation than the rare earth which is probability related to the difference between d electrons and f electrons, but there are efforts still underway [62] to realize the lumocen concept of Kahng [61] whereby a complex (presumably with large cross section) is impact-excited and then, via. internal coupling, energy is transferred to the activator.

1.16.2 Device Physics-Memory

Yamauchi et al. [67] were the first to report the hysteresis behaviour in the brightness vs applied voltage curve of the thin film EL device with double insulating layer structure. The typical nature of this hysteresis is depicted in Fig.1.11. One practical consequence of this

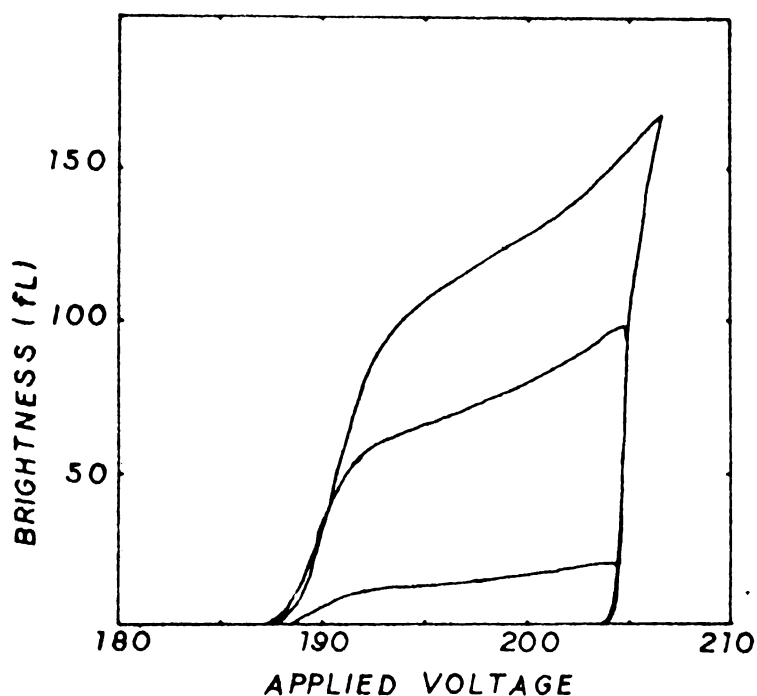


Fig.1.11 (A). Typical B-V characteristic of a hysteretic thin film EL device. The right hand curves are obtained for increasing voltage.

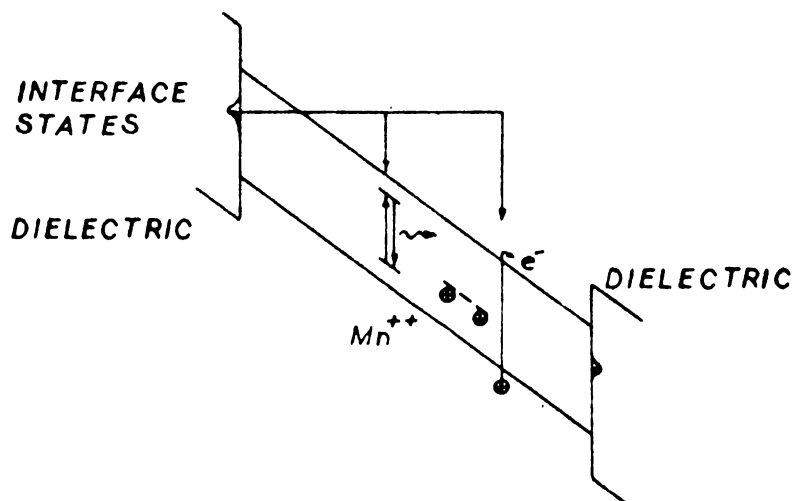


Fig.1.11 (B). Band diagram of an EL memory device illustrating schematically some of the mechanisms involved such as tunnel injection, impact excitation, impact ionization and hole trapping.

characteristics is that in a matrix display all elements can be excited with a steady AC sustaining voltage within the range of hysteresis, at a relatively low frequency. Individual cells can then be switched on or off by transient wave form applied to the X-Y electrodes, and the overall result is a more efficient display system. Additional practical interest in the hysteresis behaviour was generated by the observation that the device could be switched by light [73] and by electron beam [74,75] thus making them suitable for applications like image storage and in high content storage CRT tube displays [75,76]. Another important application of these devices are in the fabrication of image amplifiers [77].

Inoguchi et al. [66] have explained the occurrence of this hysteresis behaviour on the basis of a charge storage and the release of trapped electrons from some deep levels and then subsequent detrapping at the removal of the field. They have also verified the existence of the deep traps from the thermally stimulated current measurement across the active layer.

Howard believes that eventhough the charge storage phenomenon is important in memory behaviour, this by itself cannot produce the observed bistability. So Howard and his colleagues [78-80] proposed a model to explain the observed bistability by incorporating the idea of lattice ionization, electron-hole pair production, electron heating, and the impact excitation luminescence.

There are several key empirical requirements for producing hysteresis behaviour. The active layer films must have good crystallinity, must be thicker than about $0.3 \mu\text{m}$ and should be activated with Mn with a concentration greater than 0.5 wt percent. The former two conditions can be associated with the necessity of inducing enough electron heating to produce ionization. The latter requirement is to form deep traps in order to create and maintain space charge. Essentially the bistability is a consequence of AC coupled negative resistance which arises because of the space charge induced by the trapping of holes following impact ionization of the lattice [71].

1.17 New concepts

The observed maximum efficiency of a high field EL device of the type discussed above is about one percent. Ferd Williams [81] has attributed this low efficiency to the low **effective** temperature of the hot carriers. It is observed that all cathodoluminescent materials will luminescence when placed in contact with hot carriers and CL **efficiency** can be as high as 30 percent. This prompted the idea that if electrons can be accelerated rapidly to optical energies in high field EL devices efficiencies approaching this value might be obtained. To achieve this, **the** functions of acceleration and collision excitation processes may be separately performed in different layers

so that their independent optimization can be achieved more conveniently. The schematic diagram of the proposed structure is shown in Fig.1.12.

In this type of devices, electrons are injected into insulating layers such as SiO or even ZnS at fields such that there is considerable electron heating. The hot electrons so produced can then be injected into a second material where they may produce impact ionization as in CL followed by recombination at donor acceptor activator pairs such as Cu,Cl. One luminescent layer which has been used is $\text{ZnF}_2:\text{Mn}$. This effort has not yet resulted in improved efficiency. However, the work of Hamakawa et al. [82] can be considered as the implementation of the above concept into a practical device.

One of the drawbacks of AC thin film devices is their higher operating voltages. Attempts have been made to reduce the operating voltage by using piezoelectric films as insulator layers. One such device has been reported by Okamoto et al. [83] with PbTiO_3 ($\epsilon \approx 150$). They have prepared devices which can be operated at around 50 V. Another problem is regarding the preparation of devices with reproducible hysteresis behaviour. It is found that when these devices are operated at high brightness, a drifting in voltage of the hysteresis loop accompanied by a change of shape of hysteresis curve occurs [78]. The

ACCELERATOR PHOSPHOR ACCELERATOR
FILM FILM FILM

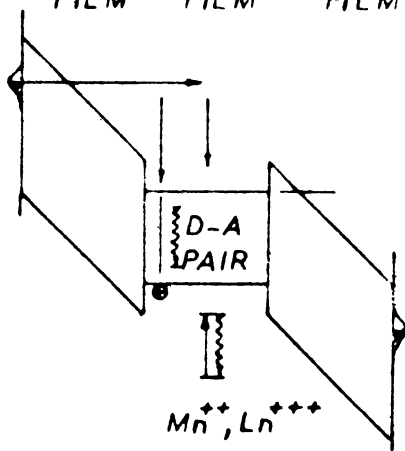


Fig.1.12. Schematic band diagram of the proposed structure to separate acceleration and excitation.

exact reason for the observation of these undesirable qualities are yet to be understood.

1.18 Summary

Part A of the chapter gives a detailed description of the basic phenomenon of electroluminescence together with an account of AC and DC powder EL devices. The fundamental processes associated with EL emission are mentioned. Brief outline of the theoretical concepts are given. Part B presents a concise review of ACFEL devices which are of current importance. Here the latest trends and possibilities in this area are also discussed.

References

1. O.W. Lossew; *Telegrafia i Telefonija* 18(1923)61.
2. H.F. Ivey; *Advances in Electronics and Electron Physics*, Suppl.1, *Electroluminescence and Related Effects* (Academic Press, New York, 1963).
3. A.A. Bergh and P.J. Dean; *Monographs in Electrical and Electronic Engineering, Light Emitting Diodes* (Clarendon Press, Oxford, 1967).
4. F.W. Williams and R. Hall, *International Series in the Science of Solid State Volume 13, Luminescence and the light emitting diode* (Pergamon Press, Oxford, New York, Toronto, Sydney, Paris, Frankfurt, 1978).
5. T. Mishina, W. Quan-kun and K. Takahashi; *J. Appl. Phys.* 59(1981) 5797.
6. H.F. Ivey; *IRE Trans. ED-6* (1959) 203; *J. Electro Chem. Soc.* 108(1961) 590; *Electrochem. Technol.* 1(1963)42.

7. H.K. Henisch; Electroluminescence (Pergamon Press, Oxford, 1962).
8. A.G. Fisher; Luminescence of Inorganic Solids, Ed. P. Goldberg (Academic Press, New York, 1966) 541.
9. F.F. Morhead; Physics and Chemistry of II-VI compounds, Eds. M.S. Aven and A. Prener (North Holland, Amsterdam, 1967) 613.
10. A. Vecht; J. Cryst. Growth, 59(1982) 81.
11. Elliott Schlam; Proc. IEEE, [7]61 (1973) 894.
12. G. Destriau; J. Chem. Phys. 33(1936) 587.
13. W. Lehmann; J. Electrochem. Soc. 105(1958) 585.
14. M. Aven and J.S. Prener, Eds. Physics and Chemistry of II-VI compounds (North Holland, Amsterdam, Netherland, 1967).
15. M.H. Aven and R.M. Potter; J. Electrochem. Soc. 105(1958) 134.
16. H.C. Froelich, J. Electrochem. Soc. 100(1953) 280.
17. G.F. Garlick and M.J. Pampleton; Proc. Phy. Soc. London, B67(1954) 442.
18. D. Curie, Luminescence in Crystals (Methuen and Co. Ltd, London, 1963)
19. P. Zalm, G. Diemer and H.A. Klasens; Philips Research Reports 9(1954) 81.
20. M.S. Skolnick and Paul J. Dean; IEEE Trans. on Electron Devices ED-28[4] (1981) 444.
21. C.C. Yu and F.J. Bryant, Solid St. Comm. 28(1978) 835; G.Z. Zhong and F.J. Bryant, J. Phy. C. Solid St. Physics [4] 13(1980) 797.
22. G.Z. Zhong and F.J. Bryant. Solid St. Comm. 39(1981) 907.

23. Egon E. Loehner; Proc. IEEE [7] 61 (1973).
24. S. Bhushan, M. Saleem and S. Chandra; Pramana 10[1] (1978) 1.
25. L.N. Tripathi, B.R. Chaubey, C.P. Mishra; Phys. Status Solidi A 57(1980) K 137.
26. A. Pfahnl; J. Electrochem. Soc. 110 [5] (1963) 381.
27. S. Bhushan, A.N. Pandey and Balakrishna Rao Kaza; Phys. Stat. Solidi (a) 46(1978) K 123.
28. W. Lehmann; J. Lumin. 5(1972) 87.
29. A. Vecht, M. Waite, M.H. Higtan and R. Ellis; J. Lumin. 24/25 (1981) 917.
30. W.W. Piper and F.E. Williams; Electroluminescence, Solid State Physics Vol. 6, Eds. Frederik Seitz . and David Turnbull (Academic Press Inc., New York, London, 1958)
31. W.W. Piper and F.E. Williams, Phys. Rev. 98(1955) 1809.
32. L. Martin, Solid State Luminescence, Ed. F.E. Williams, Advances in Electronics Vol.5 (Academic Press, New York, 1953) 137.
33. C.H. Haake, J. Appl. Phys. 28(1957) 245.
34. W.W. Piper and F.E. Williams; Brit. J. Appl. Phys. Suppl. 4, S 39 (1955).
35. G. Destriau and H.F. Ivey; Proc. of IRE 10(1955) 1911.
36. P. Zalm, D.G. Diemer and H.A. Klasens; Philips Research Reports 10(1955) 205.
37. G.F. Alfrey and J.B. Taylor; Proc. Phy. Soc. London B 68(1955) 775, Brit. J. Appl. Phys. Suppl. [4] (1955) 44.
38. W.A. Thornton; J. Appl. Phys. 32(1961) 2379.

39. P. Zalm; Philips Research Reports [11] 353 [1956] 417.
40. G. Destriau; Brit. J. Appl. Phys. Suppl. No.4,(1955) 49.
41. W.A. Thornton; Phys. Rev. 102(1956) 38; 103(1956) 1585.
42. A.N. Georgobiani and M.V. Fok; Optics and Spectroscopy 11(1961) 48.
43. J.I. Pankove; Electroluminescence, Topics in Appl. Phys. Vol. 17, Ed. J.I Pankove (Springer-Verlag, Berlin, 1977).
44. D.V. Skobel'tsyn; Ed. Electroluminescence, Proc. of the P.N. Lebedev Physics Institute Vol.50 (Consultants Bureau, New York, London, 1972).
45. H. Kroemer; Proc. IRE 45(1957) 1535.
46. A.G. Fisher; Luminescence of Inorganic Solids, Ed. by P. Goldberg, Academic Press, New York (1966)
47. H. Kressel; J. Electron. mat. 4(1975) 1081.
48. A.S. Grove; Physics and Technology of Semiconductor devices (Wiley and Sons, New York, London, Sydney, Toronto, 1969) 425.
49. C.N. Berglund; Appl. Phys. Lett. 9 (1966) 441.
50. J.I. Pankove and P.E. Norris; RCA Reviews 33(1972) 337.
51. W. Heinke and H.J. Queisser; Phys. Rev. Lett. 33(1974) 33.
52. Hiroshi Kawarada and Nobumasa Obshima; Proc. IEEE [7] 61(1973).
53. M. Yoshiyama; Electron 42(1969) 114.
54. M. Yoshiyama, H. Kawarada and T. Sato; Proc. IEEE Int. Computer Group Conf. (Washington DC, 1970) 261.
55. A. Arin, T. Yoshizawa, K. Awazu, K. Kuruhashi and S. Ibuki; Proc. IEEE Conf. Display Devices (New York. 1970) 52.

56. A. Vecht, N.J. Werring, R. Ellis and P.J.F. Smith;
Proc. IEEE [7] 61(1973) 902.
57. R.E. Halsted and L.R. Koller; Phys. Rev. 93(1954) 349.
58. W.A. Thornton; J. Appl. Phys. 33(1962) 3045.
59. E.J. Soxman and R.D. Ketch Pel; Electroluminescent
Thin Film Research, JANAIR Report 720903(1972).
60. M.J. Russ and D.I. Kennedy; J. Electrochem. Soc.
114(1967) 1066.
61. D. Kahng; Appl. Phys. Lett. 13(1968) 210.
62. J. Benoit, P. Benalloul and B. Blanzat; J. Lumin.
[1,2] 23(1981) 175.
63. N.A. Vlasenko; Opt. Spect. 18(1965) 260.
64. N.A. Vlasenko and A.M. Yaremko; Opt. Spect. 18(1965) 263.
65. N.A. Vlasenko, S.A. Zynio and Yu V. Kopytko; Phys.
Stat. Sol. (a) 29(1975) 671.
66. T. Inoguchi and S. Mito; Electroluminescence,
Topics in Appl. Phys. Vol. 17 Ed. J.I. Pankove
(Springer-Verlag, Berlin, 1977).
67. Y. Yamauchi, H. Kishishita, M. Takeda, T. Inoguchi and
S. Mito; Digest Int. Elect. Dev. Mfg. IEEE
(New York, 1974) p. 352.
68. M. Takeda, Y. Kakihara, M. Yoshida, M. Kawaguchi,
H. Kishi Shita, Y. Yamauchi, T. Inoguchi and
S. Mito, '75 SID Intern. Symp., Sect. 7.8(1975)
69. M.P.R. Panicker, R.J. Bell, S.K.Tiko; SID Inter.
Symp. Digest (1980) 112 and Sigmatron Nova
Display Spec.
70. T. Suntola, J.J. Antson, A. Pakkala and S.Lindfors;
SID Intern. Symp. Digest (1980) 108.

71. W.E. Howard; J. Lumin.24/25 (1981) 835.
72. R. Tornquist; J. Cryst. Growth 59(1982) 399.
73. D.H. Smith; J. of Lumin. 23(1981) 209.
74. W.E. Howard and P.M. Alt; Appl. Phys. Letters, 31 (1977) 399.
75. O. Sahni, P.M. Alt, D.B. Dove, W.E. Howard and D.J. Mc Clure; IEEE trans. Ed-28 [6] (1981) 708.
76. D. Theis; J. Lumin. [1,2] 23(1981) 191.
77. P.K.C. Pillai and Nilonfee Shroff; National Conference on Instrumentation Proc. (1983) 285.
78. W.E. Howard; J. Lumin. [1,2] 23(1981) 155.
79. P.M. Alt, W.E.Howard and O. Sahni; IEEE Trans. ED 26(1979) 1850.
80. W.E. Howard, O. Sahni and P.M. Alt; J. Appl. Phys. [1] 53(1982) 639.
81. Ferd Williams; J. Lumin.23(1981) 1.
82. K. Okamoto and Y. Hamakawa; Appl. Phys. Lett., 35(1978) 508.
83. K. Okamoto, Y. Nasu and Y. Hamakawa; IEEE Trans. ED. 28 [6] (1981) 703.

CHAPTER II

EXPERIMENTAL SET UP

2.1 Introduction

The most important objective of the research activities in the field of electroluminescence is to develop efficient EL phosphor materials suitable for display applications. A detailed study of the physical mechanism responsible for the onset of light emission becomes very relevant in this context. Research in electroluminescence is a meeting ground of two active areas of technologies, viz. phosphors and semiconductors, and hence combines the inherent complexities of both the fields. However, the final objectives are quite challenging and any attempt to achieve the set goals should involve a series of systematic investigations on both experimental and theoretical fronts. Hence extensive trials on the preparation and characterisation of electroluminescent phosphors of different host materials doped with different activators and co-activators become unavoidable before any worthwhile result is obtained.

In the present case in order to carry out such a series of investigations which are in line with the objective as outlined above, a well equipped electroluminescent laboratory has been set up. This consists of a chemical laboratory with facilities to handle high purity materials (usually required during the course of preparation of EL phosphors),

a high temperature vacuum furnace, experimental electroluminescent cells, power supplies to excite the cells, detection and recording set up to study the emission characteristics of the phosphors etc. In this chapter a detailed account of the various systems needed for the experimentation is given. The experimental set up used to record the EL emission spectrum is described with the help of a block diagram, followed by a detailed description of the various sub-systems which include the monochromator, PMT preamplifier, recorder etc. Brief descriptions of the method of measurement of brightness voltage characteristics, lifetimes and the observation of instantaneous brightness wave forms are given. The method used to estimate the EL brightness in absolute units which is a very meaningful parameter in these studies is included at the end of this chapter.

2.2 Phosphor preparation

The electroluminescent phosphors generally consist of a host material doped with an activator and a co-activator. Such phosphors are prepared by two methods: (1) by a slurry-ing technique, and (2) by simultaneous activation. In the former method the activators and co-activators are added in a suitable chemical form to the prefired host material (eg. ZnS) while, in the latter, the dopants are added during the precipitation of the host material [1]. Phosphors for the present investigations are prepared by the slurry-ing technique. To prepare the phosphor, a weighed amount of the

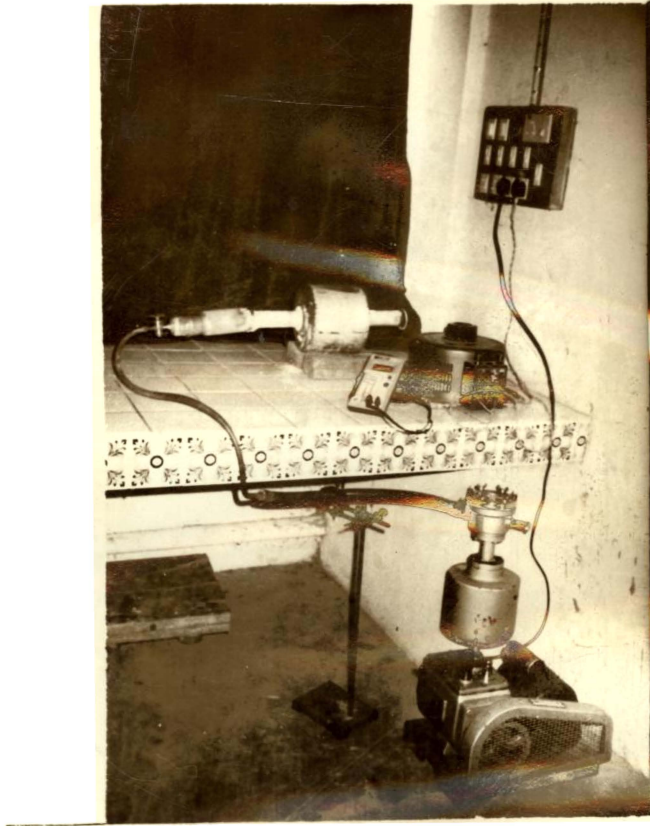
host material is mixed with required weight percentage of activators and co-activators and a slurry is formed in aqueous solution. (The actual materials used for the preparation will be discussed in appropriate sections). The slurry is then slowly heated upto 80°C and dried. The powder thus obtained is then taken in a quartz test-tube with close fitting cap. It is introduced into the high temperature zone of a horizontal furnace which is kept at a high temperature in the range of $800-1200^{\circ}\text{C}$ as required.

To increase the efficiency of the phosphor, the fired sample is sometimes coated with a Cu_2S conducting skin [2]. This is done by slowly heating the fired phosphor samples in a suitable solution containing copper ions. The resulting phosphors are usually black in colour. The coated samples may be washed with $\text{Na}_2\text{S}_2\text{O}_3$ solution or in KCN to reduce the thickness of the Cu_2S coating [3].

2.3 Vacuum furnace

The furnace used for the preparation of the phosphor was constructed with a 5 cm diameter silica tube of length 60 cm. The two ends of the tube were suitably adapted so that it can be evacuated. It is also possible to maintain a suitable atmosphere of the desired gas in the tube. A kanthal wire element of 18 gauge was wound closely over a length of 15 cm at the centre of the tube. The coil covered with fire clay formed the muffle of the furnace. The

A



B

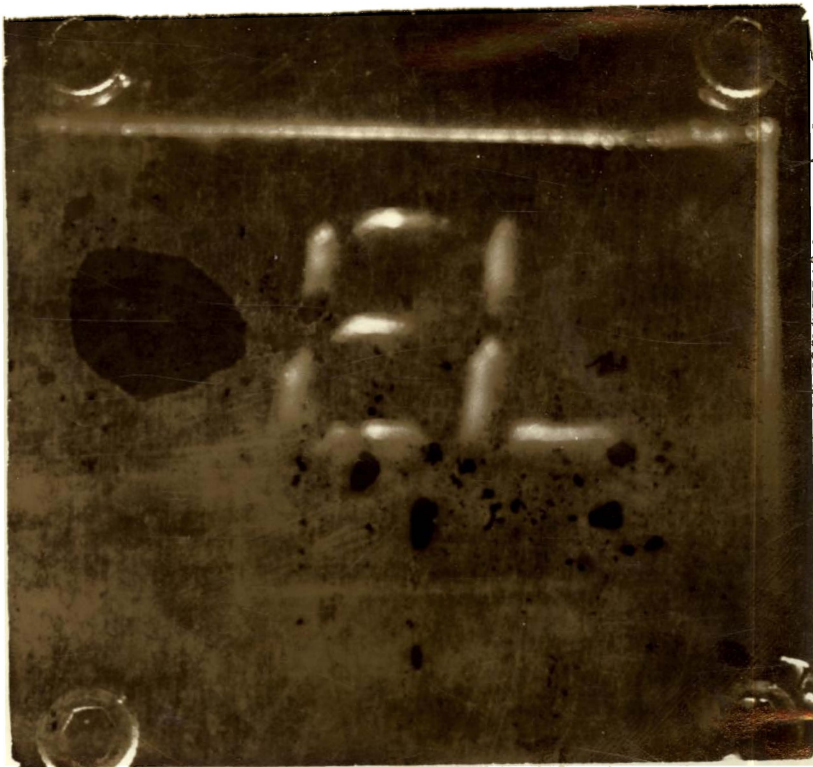


Fig.A. Phosphor firing set up
B. An EL display

external heat insulation was provided by enclosing the muffle in a 25 cm x 20 cm cylindrical MS enclosure filled with silli-minite gravel. The electrical leads were taken through synthanum insulators. The furnace is powered with a 15 A autostat. For an input voltage of 80 V at 1 kw power it can attain a temperature of 1000°C within 90 minutes. The constant temperature zone is of 8 cms in length. It can be evacuated upto 10^{-3} torr. This system is used for preparing different kinds of phosphors studied in the present work.

2.4 Test cell

Electroluminescence is excited by applying an electric field across a thin EL phosphor layer. A simple and widely used electroluminescent cell is the Destrien type EL cell which contains a thin layer of the phosphor powder dispersed in a suitable dielectric sandwiched between two electrodes. For such a cell if E_0 is the mean field applied to the electrodes then the electric field E_1 acting on the phosphor crystals embedded in a medium of dielectric constant k_1 , is given by the Maxwell-Wagner formula [4,5].

$$E_1 = E_0 \left(\frac{3k_2}{2k_2 + k_1 - V(k_1 - k_2)} \right) \quad \dots (2.1)$$

where k_2 is the dielectric constant of the crystals and V is the ratio of the volume of the crystals to the total volume. From this equation it can be seen that for getting high fields

on the crystals, liquids of high dielectric constant are to be used as the dielectric suspension medium. In arriving at the result given in equation (2.1) it has been assumed that the phosphor particles are spherical in shape and are suspended homogeneously. But in practical EL cells both of these conditions are not often satisfied. But attempts made to derive more general relations have resulted in complicated expressions and the results obtained based on these are found to differ very little from that obtained from equation (2.1) [6,7,8].

Depending on the phosphor and the structure of the EL cell, different brightness-voltage relationships have been reported [9,10,11]. But generally it is seen that the logarithm of brightness is a function of the applied voltage, which means that a much higher voltage will increase the brightness of EL emission from the cell. But it is observed that the electrical break down strength of a dielectric in which an electroluminescent phosphor has been incorporated is normally much lower than that of the same material without phosphor particles [12]. So, in order to protect the device from breakdown and to apply a higher field of excitation, a thin insulator of high dielectric constant and of high breakdown strength may be introduced in between one of the electrodes and the phosphor layer. By choosing a material of higher dielectric constant the voltage drop across the insulator layer can be minimised.

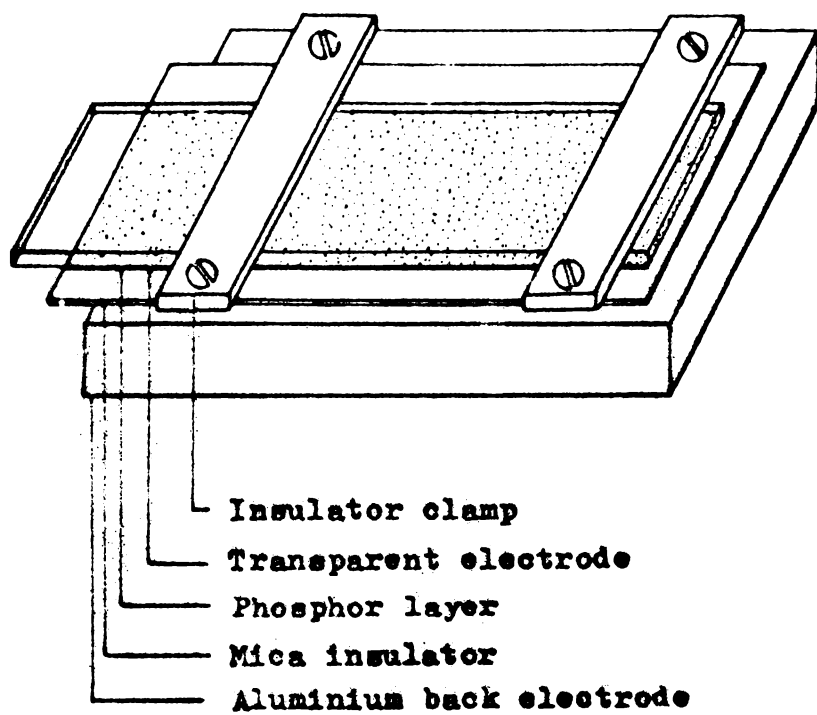


Fig.2.1. Experimental powder XL cell

Considering all these factors a simple experimental EL cell has been constructed as shown in Fig.2.1. It is **essentially** a parallel plate condenser, where an aluminium block acts as one of the electrodes and a transparent conducting glass plate as the other electrode. The thin phosphor layer having appropriate phosphor to binder ratio, and a thin mica sheet form the dielectric. The binder, which is castor oil or silicone oil, eliminates the possibility of glow discharges inside the cell. The conducting glass plate is fastened to the aluminium sheet with the phosphor layer in between, with two insulating clamps. This design is found to be very useful in preparing EL cells for the study of different phosphor samples.

2.5 Excitation sources

From the above discussion on the EL cell structure, it is evident that for the excitation of the phosphors fairly large voltages are to be applied to the cell. A high voltage variable frequency power supply which gives a maximum of 2 KV has been constructed for the purpose. In spite of all the measures taken to avoid the breakdown of the cell, it is found that electrical breakdown of the cells does occur very often during testing. This is mainly due to the breakdown of the mica insulator resulting from its non uniformity in structure and properties. To safeguard the power supply from short circuit during a cell breakdown, protection measures are included in the circuit.

a) High Voltage excitation system

The block diagram of the high voltage excitation is ,source is given below:

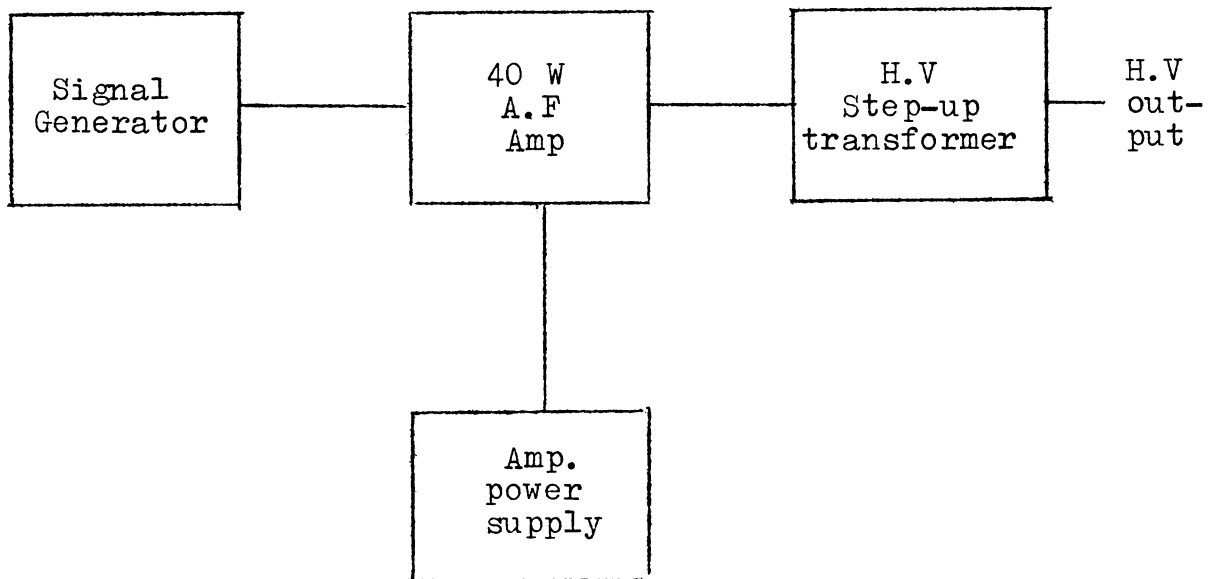


Fig. 2.2

A 1 MHz (Aplab Model No.2004) signal generator having VCO external control has been used to obtain the audio signal at the required frequency.

The low power output from the signal generator is fed to a 40W audio frequency amplifier. The circuit diagram of amplifier is shown in Fig.2.3. In modern amplifier circuits, the coupling transformers used at the output stage are eliminated by the use of complementary pair transistors. This helps to get better output purity at a lower cost. Moreover when these transformers are included in the circuit, a phase shift of the output signal is found to occur at the low and

high frequency cut off regions. This makes the design of feed back circuits quite difficult. Eventhough these drawbacks are eliminated in complementary pair circuits their power handling capacity is very low due to the non availability of suitable high power PNP transistors. This defect is eliminated by using circuits where the complementary pair transistors are used to drive the high power n-p-n output transistors. The circuit mode is then known as quasi-complementary circuit. In this configuration we have all the advantages of the complementary pair circuits in addition to the high power handling capability [13].

The present amplifier makes use of such a quasi-complementary circuit. The transistor TR_1 is a simple signal amplifier. Its output is coupled to the bases of the complementary pair transistors TR_3 and TR_4 . During the positive half cycle of the signal the transistor TR_3 conducts while TR_4 (p-n-p) is turned off. Thus the positive portion of the signal is amplified by transistor TR_5 . During the negative half cycle the transistor TR_4 conducts while TR_3 is turned off. This portion of the signal is amplified by the transistor TR_6 . Both halves of the signals are then fed to the load through the coupling capacitor C_{10} , where the enlarged signal is reconstituted across the load R_L . R_{15} is the feed back resistance. The constant current generator constituted by the transistor TR_2 which is connected to the base of the driver transistors eliminates the drifting of the operating point at high input drive.

It also offers a high impedance to TR_1 . The transistor TR_7 along with the potentiometer R_8 sets and maintain the idling current in the output circuit, despite the temperature changes.

The power supply for the amplifier was constructed using a series regulator. An LED is included in series with zener diode so that the emission from the LED will depend on the current through the zener, and hence will give an indication of the power drawn by the amplifier. The higher the power drawn the smaller is the brightness of the LED. So the glow of the LED indicator gives a rough idea about the load on the amplifier and hence about the power delivered to the cell. This indication is very useful when doing the experiments under dark room conditions.

The amplifier output was used to drive a high voltage transformer wound on an A.F. transformer core. There are 5000 turns in the secondary and for the primary, tappings at 50,100 and 150 turns are provided. This transformer is connected to the amplifier through a 1 ohm, 10 W resistance. A 10 M ohm, 1 W resistance is connected across the output terminals, which will act as a ballast and will protect the system from surge currents which may occur due to the sudden removal of load.

It is to be noticed that the transformer is connected to a 30 V DC terminal through a high capacitance decoupling condenser. So when the amplifier is switched on with the

transformer connected, the condenser charging current passes through the primary of the transformer. This will induce a very large voltage at the secondary and may cause oscillations in the amplifier. These effects can destroy the EL cell. To avoid this, a separate switch has been provided to couple the transformer to the amplifier. This switch is closed only after the system has become stabilized in a few seconds after the power is turned on. The power transistors of this amplifier are fastened to the heat sinks using 'Afcoset' heat sink compound which is a thermally conducting but electrically insulating fluid. No other material is used for the insulation of the transistors from heat sink. The performance of this amplifier is found to be highly satisfactory. Most of the studies reported in this thesis have been made using the above excitation source.

b) High frequency excitation source

The EL cells are to be excited with fast rising square pulses for the measurements of the decay time of EL emissions. It is found that if thin film EL cells and DC powder EL cells are excited using pulses of high frequency and of low duty factor, long lived cells of high brightness can be obtained. Moreover if cells are excited with a wide range of frequencies information regarding the origin of carriers giving rise to the emission can be derived. In view of these additional requirements another high voltage, high frequency amplifier has been constructed.

The circuit of this amplifier is given in Fig.2.4. The square wave output from the signal generator is given as the input to the triode amplifier. The diode connected at the cathode circuit is to provide the necessary grid bias. It is coupled to two 6L6GC amplifier tubes connected in push-pull fashion. Inductance L_1, L_2 and trimming capacitors C_1 and C_2 is adjusted for distortionless output. The amplifier is capable of faithfully amplifying square waves. The rise time of the amplifier is found to be 200 ns. It can give either positive or negative going square pulses.

2.6 Arrangements for recording the EL emission spectra

The setup used for the recording of the EL emission is shown with the aid of a block diagram (Fig.2.5). Here the emission from the EL cell is focussed at the entrance slit of the scanning spectrometer. The beam emerging out of the exit slit of the spectrometer is detected with a high gain photomultiplier tube (PMT). The PMT anode current is amplified with a preamplifier and its output is recorded using a strip chart recorder driven synchronously with the scanning spectrometer. A detailed description of the various subsystems are given below:

2.6.1. Scanning spectrometer

The spectrometer used to analyse the EL emission is a 0.5 M Ebert scanning spectrometer (Jarrel Ash Model 82-000 series).

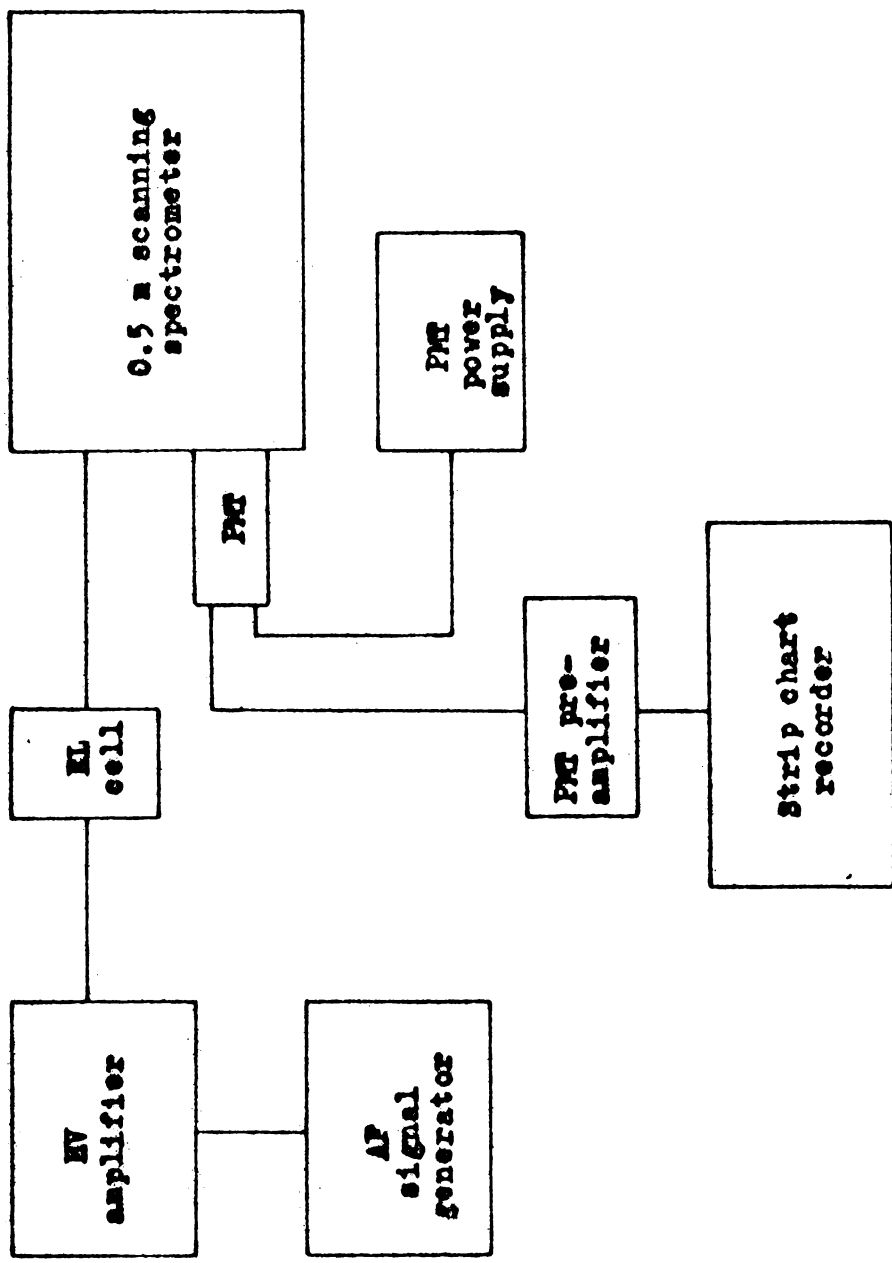


Fig.2.5. Block diagram of the experimental setup used for recording the EL spectrum.

When the emission is focussed at the entrance slit of the spectrometer S_1 , it passes to the 150 mm diameter concave mirror (M) where it is collimated and reflected as a parallel beam to a plane grating G (Fig.2.6). The dispersed light, still parallel but with separate wave lengths diverging, is reflected back to the mirror (M) where it is again reflected and focussed as monochromatic light on the exit slit (S_2). The wave length of monochromatic light emerging at the exit slit is changed by simply rotating the grating about its centre.

The grating is mounted and levelled on a pivot. It is rotated by the action of a lever arm fastened to the lower end of this pivot and driven by a split nut and precision screw. The linkage is designed to provide motion linear with the sine of the angle of rotation, enabling the screw rotation to remain directly proportional to the wave lengths. The grating used has 1180 groves/mm blazed at 500 nm and is driven by a reversible motor [14].

2.6.2. PMT preamplifier

The dispersed light emerging out of the exit slit of the spectrometer is detected with a PMT (EMI 9683 KQB with S-20 cathode). The PMT current induced by this low light flux will be extremely small so that it cannot be measured directly. Such feeble currents are usually measured or recorded with the help of pico-ammeters, electrometers or

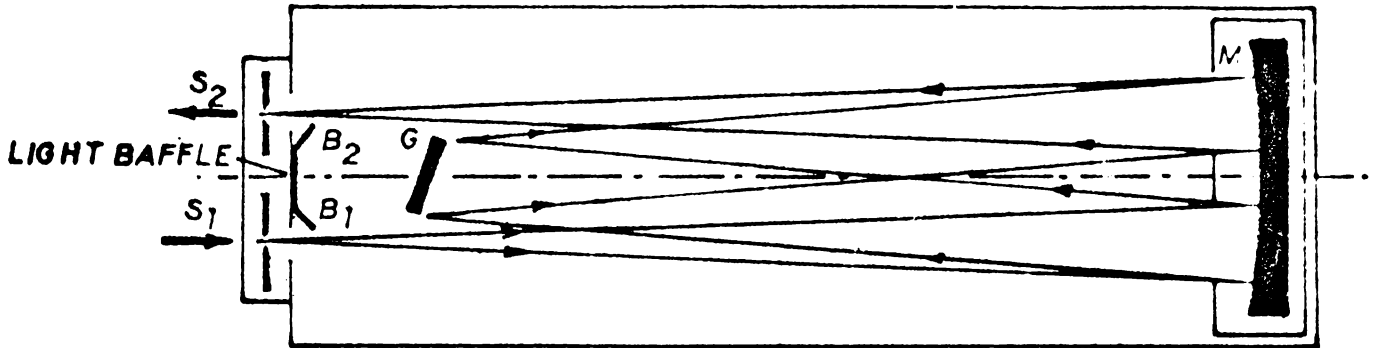


Fig.2.6. The beam paths in the grating spectrometer.

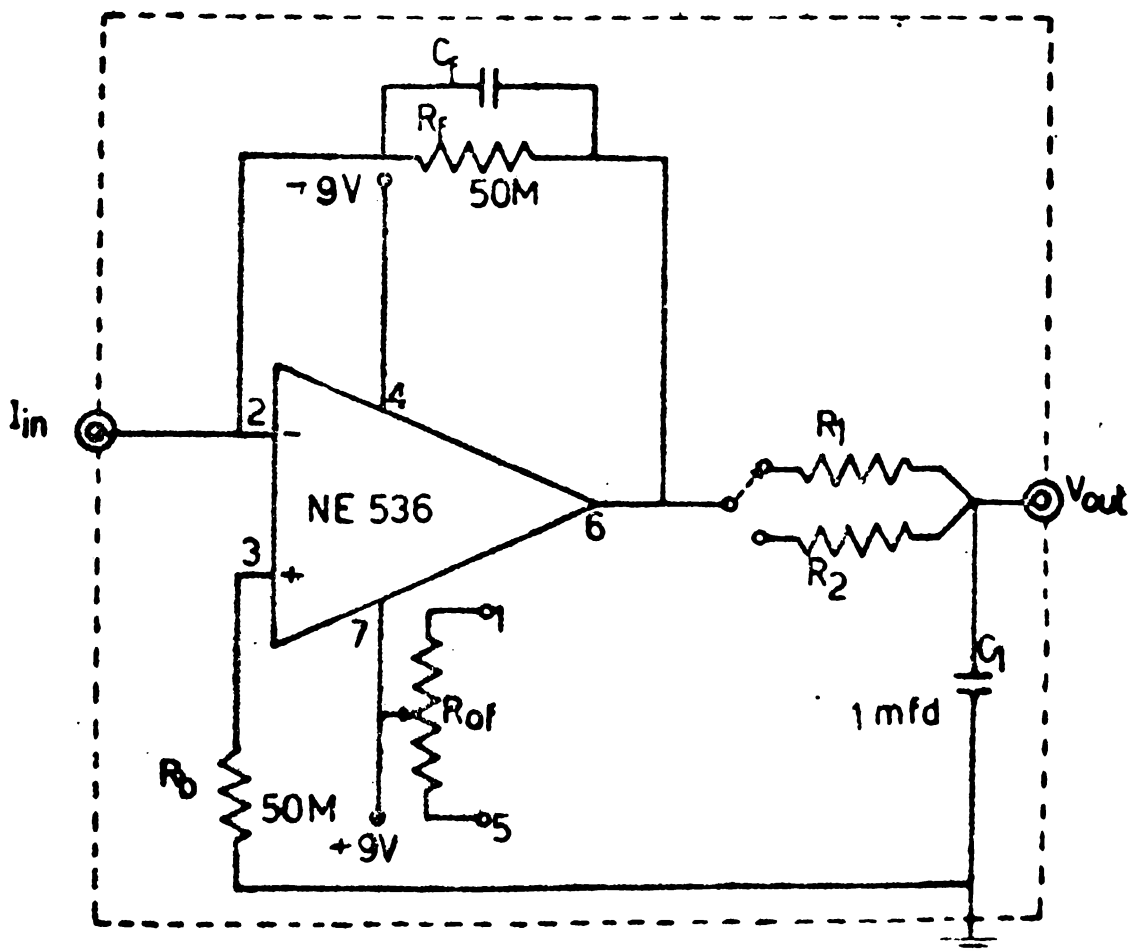


Fig.2.7. Circuit diagram of the PMT preamplifier.

with expensive instruments like lock in amplifiers or Boxcar averager. These expensive and sophisticated systems become imperative in such applications since ordinary amplifiers are unsuitable for the noise free magnification of very small changes produced by these weak light signals in the anode current (which is of the order of a few pico amperes) of PMT. The PMT normally has an output impedance of the order of 10^{12} ohms. So the practical realization of a low noise drift free DC amplifier matching the PMT is a difficult problem. Here the circuit and the constructional details of such an amplifier used for the investigation is presented in detail.

2.6.3. Principle and construction details

The PMT amplifier circuit used here essentially consists of a current to voltage convertor (CVC). When it is included in the anode circuit of a PMT, which can be considered ideally as a current source, then a light flux generating a current I_a flowing through the anode circuit gives an output voltage.

$$V_{\text{out}} = I_a R_f$$

where R_f is the feed back resistance. The input impedance of this amplifier is given by

$$R_{\text{in}} = \frac{R_f}{A_{\text{ol}}}$$

where A_{ol} is the open loop gain of an op. amp [15].

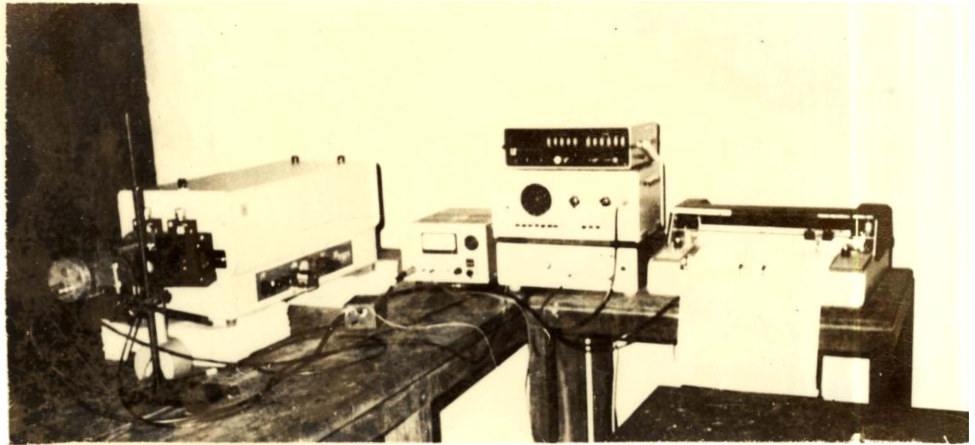
Generally R_{in} is negligible compared with the source impedance offered by the PMT.

In the present circuit as shown in Fig.2.7 an FET input op. amp NE 536 is connected in the current to voltage convertor configuration. Since this integrated circuit has a very large input impedance (10^{14} ohms) it does not load the large resistance R_f (50 M ohms) connected in the feed back circuit. The circuit performance is unaffected by the resistance R_b (50 M ohms) used to compensate for the bias current, since the PMT has an output impedance greater than 10^{12} ohms. The low leakage, low value condensor C_f supresses possible oscillations. The RF filter circuit at the output of the amplifier should have a time constant appropriate with the type of signal to be detected. The circuit was wired on an epoxy board taking care to see that the input terminals of the IC were well isolated to reduce the effect of leakage current. A 7.5 cm x 5 cm x 5 cm MS box with BNC connectors for the input and output terminals, contained the entire assembly along with two 9 V batteries used as the power supply, thus avoiding all possible pick up noise. The system was enclosed in a suitable thermo cool box which provided good thermal isolation thereby helping drift free operation.

2.6.4. Performance evaluation

The input currents for different values of the output voltage were measured with an electrometer and the response was found to be exactly linear. The conversion gain found

A.



B.

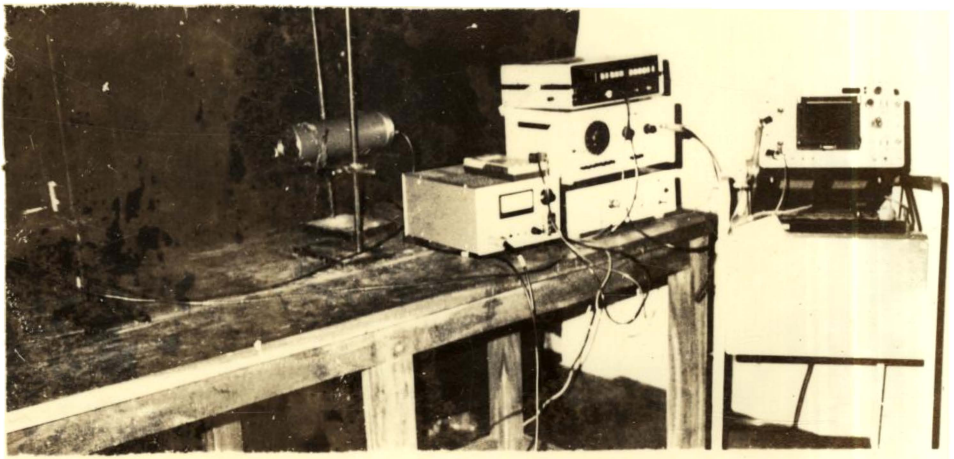


Fig. A. The setup used for the recording of the EL Spectra.

B. The setup used to study the B-V characteristics and the brightness waves

out experimentally from these measurements was identical with the calculated value of 5×10^7 or 1 volt/20 nA. When used along with a 10 mV strip chart recorder the system was capable of measuring clearly a change in the current as low as two pico amperes. The PMT dark current could be compensated by adjusting the off set R_{of} (10 turn pot). The system was found to exhibit a long term drift of the order of 0.3 mV/12 hours which is an indication of good long term stability. All EL emission spectra reported in this thesis are recorded with the help of this preamplifier. The RC time constant used is 0.1 sec,

2.7 Voltage brightness measurements

The voltage brightness characteristics of the EL cells were measured using an EMI 9684 PMT with S-1 cathode along with a highly stabilised power supply. The PMT was kept in front of the EL cell. The PMT current and the voltage across the cells were measured using Digital multimeters of sensitivity 0.1 mV.

The brightness wave form and the decay studies were done by using the PMT in conjunction with a Tektronix 465 Oscilloscope or an Aplab 50 MHz Oscilloscope. For life time measurements the cells were excited using current pulses of a few micro seconds duration. The permanent record of these observations were made by photographing the oscilloscope traces with a Tektronix oscilloscope camera.

2.8 EL brightness measurements in absolute units

In the present study, where a series of investigations on EL phosphors are made, the brightness of the cells are often expressed in arbitrary units. However, a meaningful description of the brightness of the EL cell can be had only by expressing it in terms of absolute units. Usually this is done with a standard lamp in conjunction with interference filters, used to select narrow bands of radiation throughout the range 380-780 nm which covers the entire region where the eye is sensitive. A photomultiplier tube having a spectral response curve closely matching the eye sensitivity curve is used as the detector. In the following section a method by which the EL brightness is measured using the PMT anode sensitivity curve is described.

The anode sensitivity of the PMT is usually expressed in A/lm. This is estimated by measuring the anode current obtained by illuminating the cathode with a standard tungsten lamp kept at 2850°K whose emission spectrum denoted by $I(\lambda)$ is shown in Fig. 2.8. The luminous flux from the same source is by definition

$$F = 680 \int I(\lambda) V(\lambda) d\lambda \text{ lm}$$

where $V(\lambda)$ is the relative response of the human eye [16]. If we are measuring the anode current of the PMT with a cathode response curve of $S(\lambda)$ then the shape of the $I(\lambda)$ curve will

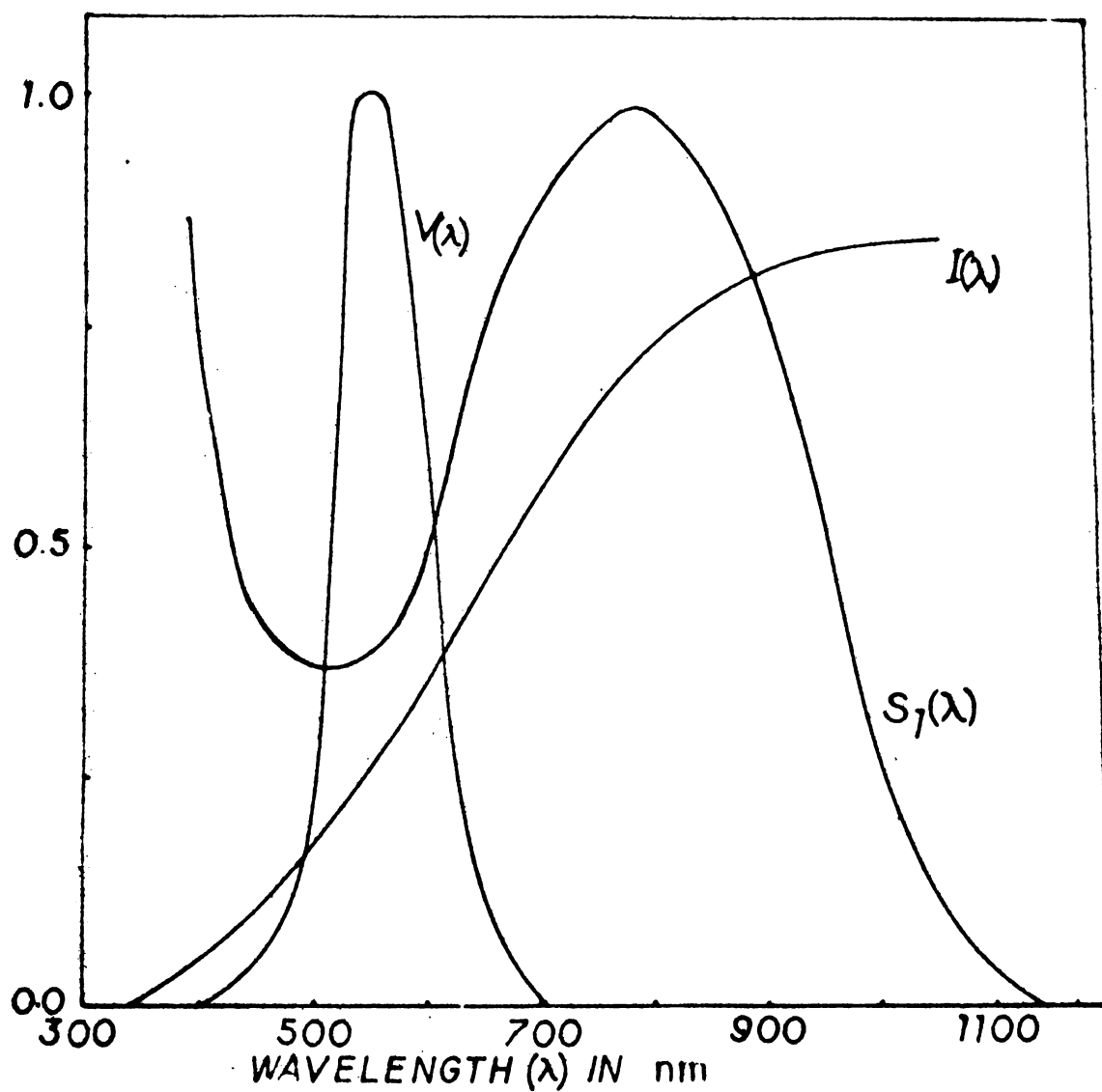


Fig.2.8. Relative response of the human eye $V(\lambda)$, the spectral distribution $I(\lambda)$ of light from a standard tungsten filament lamp and the sensitivity curve $S_1(\lambda)$ of a PMT with S_1 cathode.

be modified as $I(\lambda) S_1(\lambda)$ (Fig.2.9). If we were measuring the anode current of the PMT by illuminating the cathode with this standard lamp suitably attenuated so that the flux incident is 1 lm then measured PMT anode current will correspond to the area under the curve $I(\lambda) S_1(\lambda)$ which will be equal to the anode sensitivity of the PMT at that operating voltage.

But the term, as expressed in the data sheet is meaningless for tubes with spectral response beyond the visible region [17]. So when such a tube is used for actual photometric measurements the specified value is to be corrected for the eye sensitivity. This can be done by plotting the $I(\lambda) S_1(\lambda) V(\lambda)$ curve as shown in Fig.2.9. Then the current corresponding to the area under this curve will be the correct value of the anode sensitivity which should be taken for photometric measurements.

If $E(\lambda)$ is the emission spectra of the source whose brightness is to be measured and is normalised with $I(\lambda) S_1(\lambda)$ curve. The area under this curve will correspond to the measured PMT current. But for the photometric brightness measurement, this value is to be corrected for the visual effectiveness. The area $\int S_1(\lambda) E(\lambda) V(\lambda) d\lambda$ corresponds to this corrected value of the PMT current. From this value the amount of luminous flux incident on the detector can be calculated in lumens.

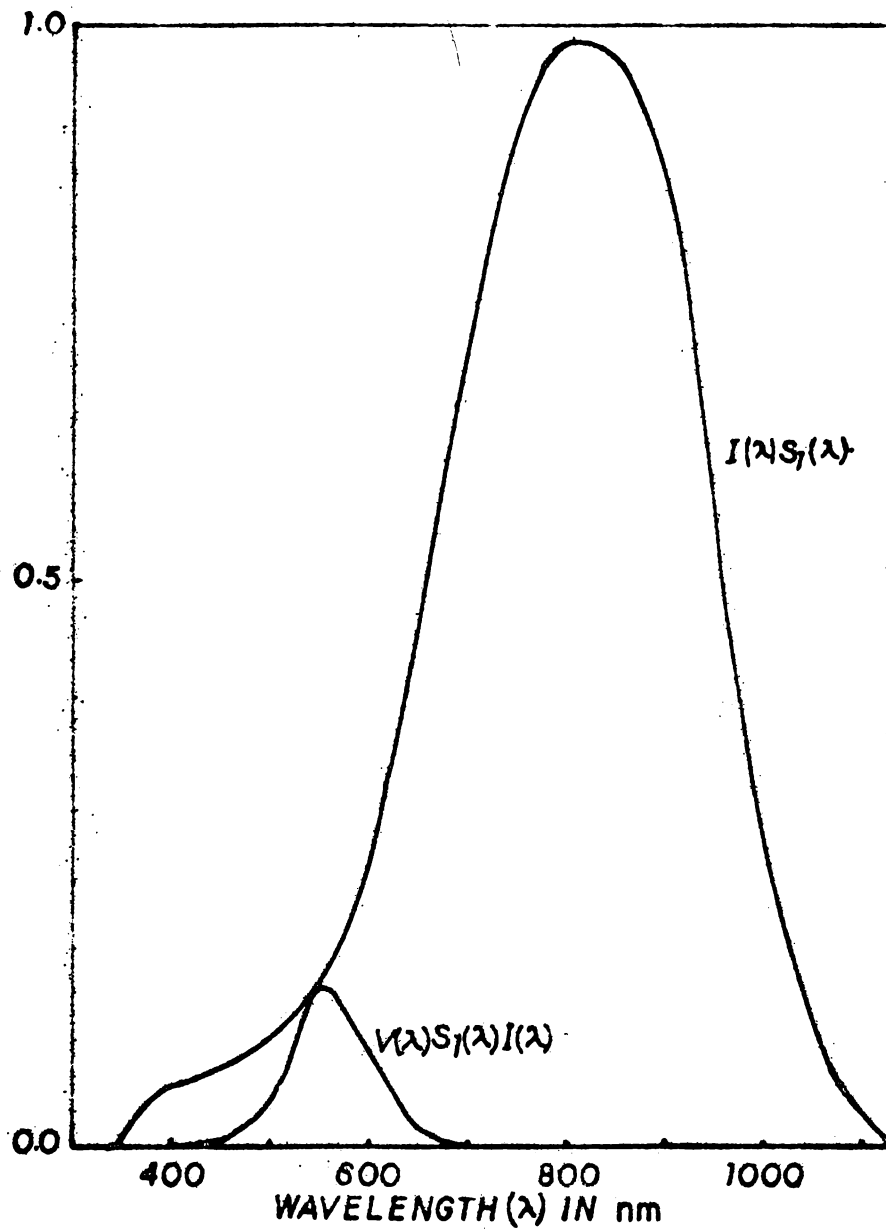


Fig.2.9. $I(\lambda) S_1(\lambda)$ curve is the $I(\lambda)$ curves corrected for the detector response $S_1(\lambda)$. $I(\lambda) S_1(\lambda) V(\lambda)$ curve incorporates the corrections for the detector sensitivity and the relative response of the human eye.

For all practical purpose we can assume that the electroluminescent cell is illuminating uniformly the surface of a hypothetical hemisphere of radius R, where R is the distance between the source and the detector. Then the luminance flux incident per unit area is

$$\frac{I}{2\pi R^2} = I_0$$

where I is the luminance flux emitted by the source. If D_A is the detector area and I_D is the luminance flux measured as described above, then

$$\frac{I}{2\pi R^2} = I_0 = \frac{I_D}{D_A}$$

So

$$I = \frac{2\pi R^2 I_D}{D_A}$$

If 1 sq inch is the emitter area producing a luminous flux I, then the brightness (B) of the detector

$$B = 144 I \text{ foot lamberts (fL)}$$

$$= 144 \cdot \frac{2\pi R^2 I_D}{D_A} \text{ fL}$$

To clarify the method further, the calculation used to measure the brightness of the CaS:Ce EL cell is given in detail below.

The detector used for the measurement is an EMI 9684 PMT with S_1 cathode operating at 1200 volts. At this voltage the anode sensitivity is 2A/lm.

The area under the curve $I(\lambda)S_1(\lambda)$ is found to be 149 sq.cm which correspond to 2A/lm since it is assumed that the standard source is emitting 1 lm. Correcting the $I(\lambda)S_1(\lambda)$ curve for eye response, we get

$$\int I(\lambda)S_1(\lambda)v(\lambda)d\lambda = 6 \text{ sq.cm.}$$

The corrected value of the anode sensitivity value useful for photometric measurement is $\frac{6}{149} \times 2 = 80.5$ mA/lm. The area under the curve $E(\lambda)S_1(\lambda)$ normalised with the $I(\lambda)S_1(\lambda)$ curve at the emission maxima is 3 sq. cm. The area corrected for the eye sensitivity which corresponds to

$\int E(\lambda)S_1(\lambda)v(\lambda)d\lambda = 2.5$ sq. cm. For the measurement the detector is kept at 67 cm away from the source. At maximum brightness the measured PMT anode current is 0.2 mA. But the corrected value of the anode current is

$$\frac{3}{2.5} \times 0.2 \times 10^{-3} = \underline{\underline{0.167 \text{ mA}}}$$

So the incident light flux

$$\begin{aligned} I_D &= \frac{1}{80.5} \times 0.167 \times 10^{-3} \\ &= \underline{\underline{2.075 \times 10^{-3} \text{ lm}}} \end{aligned}$$

The detector area

$$D_A = \underline{\underline{20.41 \text{ sq. cm.}}}$$

The luminance flux emitted by the cell I

$$= \frac{2\pi \times 67^2 \times 2.075 \times 10^{-3}}{20.41}$$

$$= \underline{\underline{2.866 \text{ lm}}}$$

The emitter area is 1 sq. inch

So the brightness of the cell in foot lamberts

$$= 144 \times 2.866$$

$$= \underline{\underline{412.704}}$$

References

1. A. Vecht, N.J. Werring, R. Ellis and P.J.F. Smith;
Brit. J. Appl. Phys (J. Phys. D) 2(1960) 953.
2. A. Vecht and N.J. Werring; J. Phys. D. Appl. Phys.
3(1970) 105.
3. W. Froelich and A.P. Cleiron; J. Electrochem. Soc.
106(1959) 672.
4. K.W. Wagner; Archiv für Elektrotechnik 2(1914) 371.

5. S. Roberts; J. Opt. Soc. Am. 42(1952) 850.
6. W.F. Brown Jr; J. Appl. Phys. 23(1955) 1514.
7. R.S. Smith; J. Appl. Phys. 27(1956) 824.
8. J.A. Reynolds and M.J. Hough; Proc. Phys. Soc. London B 70(1957) 764.
9. Destriau and H.F. Ivey; 43(1955) 1911.
10. W.W. Piper and F.E. Williams; Brit. J. Appl. Phys. Suppl. No.4 (1955) 39.
11. H.F. Ivey; Advances in Electronics and Electron Phys. Suppl. 1 Electroluminescence and Related Effects (Academic Press, New York 1963) 43.
12. H.F. Ivey; Advances in Electronics and Electron Phys. Suppl. 1, Electroluminescence and Related Effects (Academic Press, New York 1963) 122.
13. Derek Cameron; Hand Book of Audio Circuit Design.
14. Jarrel Ash Instruction Manual; Engineering Publication No.82-000/1M RW. 7(1971).
15. A.P. Malvino; Electronic Principles (Tata MacGraw-Hill Publishing Co. Ltd., New Delhi 1976) 531.
16. EMI Photomultipliers (1979).
17. Hewlett Packard Photomultiplier Tube Catalogue (1983).

CHAPTER III

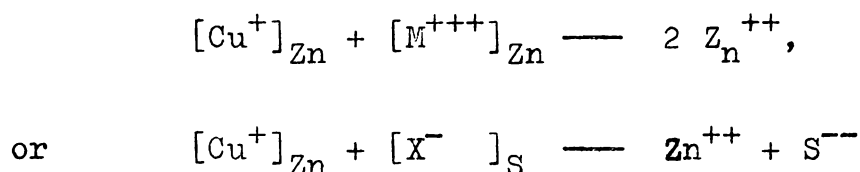
ELECTROLUMINESCENCE IN SOME ZnS BASED PHOSPHORS AND IN SELF ACTIVATED ZnO

3.1 Introduction

ZnS and related compounds form the basis for many photoluminescent and cathodoluminescent phosphors. Also they are the most efficient electroluminescent (EL) phosphor known to date. ZnS exists both in a low temperature cubic (sphalerite or zinc blende) and in a high temperature hexagonal (wurzite) structure. But the actual situation however, is far from simple because the difference in energy of the two structures is small. ZnS in common with SiC exists in many polytypes (at least 10) [10]. Normally, ZnS as the host must be activated with suitable impurities in order to produce luminescence. Photoluminescent emission in ZnS may be activated by a variety of elements [2] which include: Cu, Ag, Au, P, As, Sb, Sn, Pb, Mn, V, Fe, Na, Li, Ga, In, Tl, Se, rare earths and by zinc vacancies in the lattice which are assumed to be responsible for self activated emission [3,4].

The solubility of many of these activator elements (Mn is an exception) in the ZnS lattice is usually limited unless another element called as co-activator is introduced at the same time. The co-activator is usually a halide (Cl, Br, I) or a trivalent ion (Al, Ga, In, etc.) and its action

can be explained on the basis of charge compensation as explained by Kröger [5]. Thus if an ionic model is used for ZnS



Here $[\text{Cu}^+]_{\text{Zn}}$ denotes a Cu^+ ion at a normal Zn lattice site. In this model Mn is divalent and it can substitute directly for Zn and hence does not require any charge compensation.

The effect on the solubility of the activator is not the only action of the co-activator. When it is introduced into the lattice an electron is transferred from the same to an activator atom thus affecting charge compensation. When the phosphor is excited by promoting electrons to the conduction band of the crystal, the co-activator centres can capture these electrons and subsequently release them under thermal action or some other form of stimulation. They, thus, act as electron traps or donors in the same manner as the activators act as hole traps or acceptors. Thus, co-activators can influence many phosphor properties of the material (thermoluminescence, phosphorescence etc.) in addition to electroluminescence [6].

3.2 Electroluminescence in ZnS:Cu,Cl phosphor and its dependence on chlorine concentration

One of the earliest activators used in the preparation of electroluminescent ZnS is copper. In spite of the extensive

investigations made on this phosphor, the exact nature of this activator in ZnS lattice remains obscure. It is observed that the emission colour of such a phosphor depends upon various conditions [6,7]. The properties of these phosphors emitting the three colours viz. blue, green and red have been discussed extensively in the literature. Eventhough the blue- and green-emitting ones are the most efficient and well investigated phosphors, it appears that there are no guiding principles for the preparation of such phosphors with different emission colour, and the various procedures given in this context seem to arise purely from the past experience of the worker involved and from reasons of convenience [6]. Thornton has reported that the emission colour of this kind of phosphors depends on the amount of copper and chlorine present in the sample [8]. Generally, these phosphors show a change in emission colour as the frequency of excitation is changed. Different models have been suggested to explain the occurrence of the two emission bands and their frequency dependence [9,10]. But these models do not furnish a satisfactory explanation for all the observations on these phosphors. Moreover, they do not take into account its red emission also. A ZnS-based EL phosphor (ZnS:Ag,Cu,Cl) giving only the blue emission band which is independent of the excitation frequency has been reported recently [11]. Thus, there exist sufficient reasons for making further investigations on this phosphor directed towards clarifying the various physical processes involved in its EL

emission. Here, the method of preparation and the emission characteristics of a blue emitting ZnS:Cu,Cl phosphor whose emission wavelength remains unaltered for various frequency of excitation are outlined. The spectral characteristics and their dependence on the frequency of the excitation voltage of another set of phosphors obtained by adding an excess amount of chlorine are investigated in detail. The experimental results are explained on the basis of a new energy level scheme consisting of three levels occurring between the valence and conduction bands of ZnS.

For preparing blue emitting EL phosphor a weighed amount of ZnS (luminescent grade) was mixed with cupric acetate solution containing 0.5 wt percent Cu and 5 wt percent NH_4Cl and the mixture was slowly heated and dried. The black powder thus obtained was fired at 1050°C for 90 minutes in a vacuum furnace at 10^{-2} torr. A second set of phosphors was prepared with the same concentration of copper but with varying amounts of chlorine by adding specific quantities of HCl in the primary mixture and firing it in a stagnant sulphur atmosphere at 1050°C . EL properties of these powder samples were studied by preparing a test cell as described in Chapter II. The spectra were recorded with a 0.5 M Jarrel Ash scanning spectrometer having an EMI 9683 KQB PMT with S-20 cathode as detector along with a highly stabilized power supply. An EMI 9684 PMT with S-1 cathode together with a dual beam oscilloscope provided the instantaneous brightness measurements and wave form display.

Figure 3.1 shows the EL spectra of the vacuum fired ZnS:Cu,Cl phosphor recorded at 50Hz and 10KHz excitation frequencies. It can be seen that the emission spectrum consists of a single band with its maxima at 460 nm and the emission wavelength is independent of the frequency of the excitation voltage. Thus, the present ZnS:Cu,Cl phosphor has virtually the same spectral characteristics as those reported in the case of ZnS:Ag,Cu,Cl phosphor [11] even though the former does not contain any silver.

Figure 3.2 is the oscilloscope trace of the EL brightness waves of this phosphor obtained for two different cell configurations under square wave excitation which gives two asymmetric intensity peaks during each cycle. However, the relative position of the higher intensity peak with respect to the exciting voltage depends apparently on the position of the mica sheet within the cell. An analysis of these brightness waves shows that, when the electrode shielded by the mica insulator becomes the cathode, the emission intensity is reduced. This, evidently, is due to the partial blocking of charge carriers from the cathode to the phosphor by the insulator layer [12]. Thus, these asymmetric wave forms displayed here provide a direct evidence for the occurrence of carrier injection from the electrodes into the phosphor material.

Unlike the blue-emitting phosphor, the second set of ZnS:Cu,Cl samples having excess chlorine shows three distinct

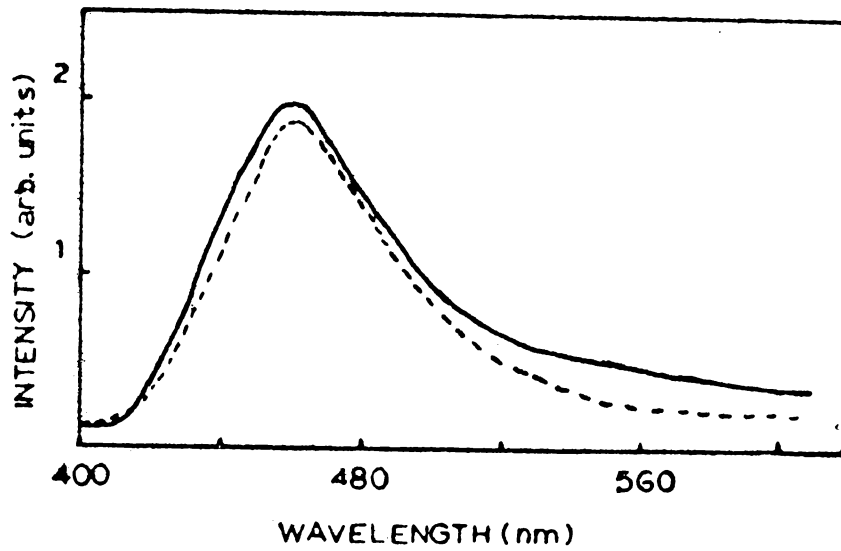


Fig.3.1. The EL spectra of the blue emitting ZnS:Cu,Cl phosphor excited with sine wave voltage at 50 Hz (broken line) and 10 kHz (solid line)

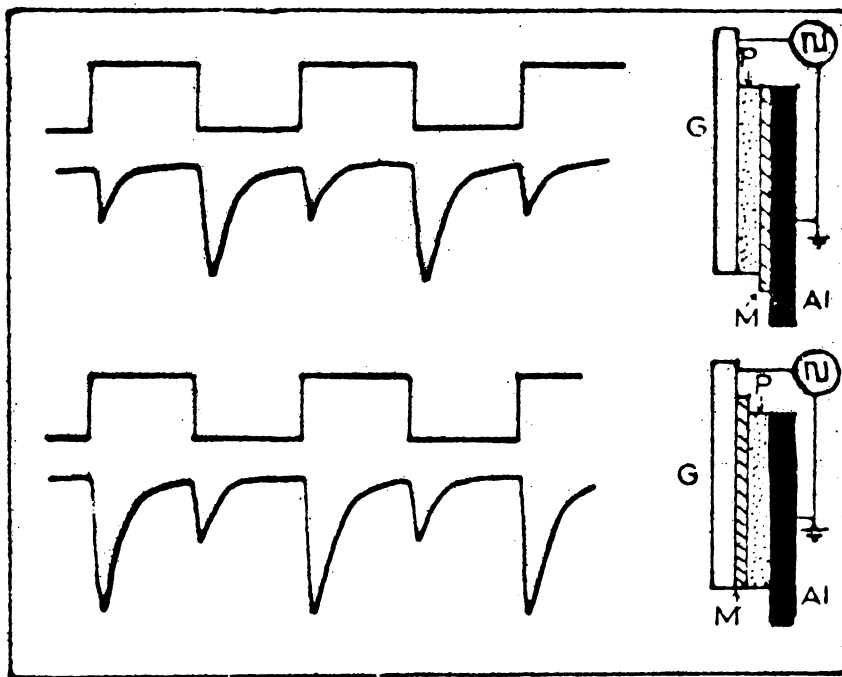


Fig.3.2. EL brightness waves obtained under square wave excitation for two different cell configuration. G- Transparent conducting electrode, M- Mica P- Phosphor layer, Al- Aluminium electrode.

bands in the emission spectrum with the maxima at 460 nm, 520 nm and 640 nm respectively. Figure 3.3 gives the normalised EL spectra recorded in the case of phosphors containing different concentrations of chlorine. It is observed that a higher chlorine content increases the relative intensity of the red band while the blue band is reduced in its intensity. Beyond a certain chlorine concentration the blue band is completely suppressed and only green and red bands are observed.

The above experimental observations can be satisfactorily explained on the basis of an energy level scheme as shown in Fig.3.4. Based on the method of preparation of these phosphors, it is possible to identify three different centres viz. Cu^{2+} , Cu^+ and Cl^- introduced into the ZnS lattice as a result of the firing process [13]. It is evident that the vacuum fired phosphor contains predominantly the Cu^{2+} centres giving rise to the 460 nm transition whose wavelength remains the same for a change in the frequency of the excitation voltage. The addition of dilute HCl to the mixture converts a portion of the cupric salt into cuprous chloride thus producing Cu^+ and Cl^- ions. The relative concentration of Cu^{2+} , Cu^+ and Cl^- centres should depend entirely on the amount of chlorine added in the form of HCl in the initial mixture. So the relative intensities of the green and the red band should increase as the chlorine concentration is increased and the blue emission should be completely suppressed

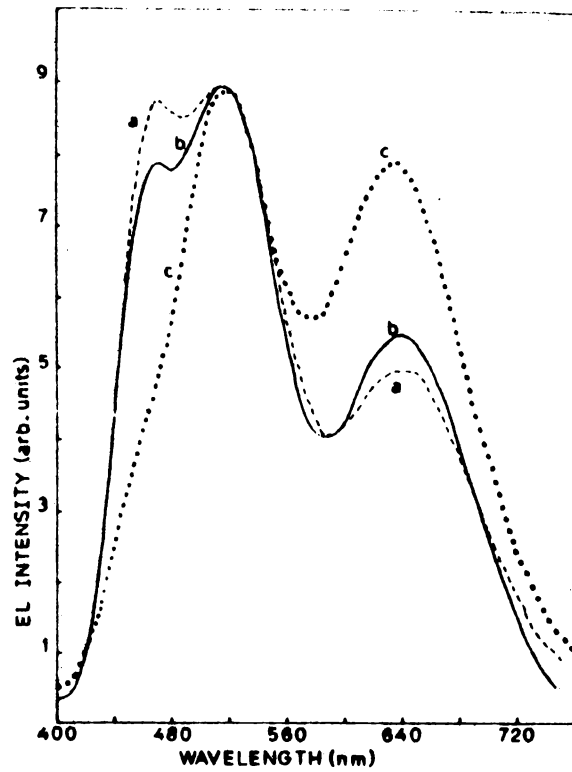


Fig.3.3. Normalized EL emission spectra recorded at 2.5 kHz for three phosphor samples a,b,c containing chlorine in the ratio 1:2:5 in the prefired mixture.

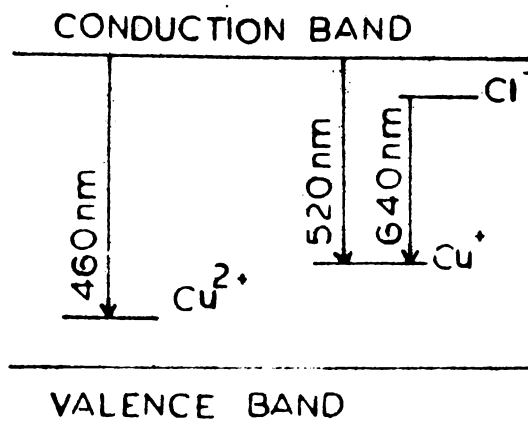


Fig.3.4. The proposed energy level scheme for ZnS:Cu,Cl phosphor giving blue, green and red EL emission.

at a sufficiently high concentration of HCl. This, in fact, is observed experimentally (Fig.3.3), Curve C.

Detailed measurements show that the brightness versus excitation voltage obeys the customary exponential relation, $\log B \propto \frac{1}{\sqrt{V}}$ indicating the occurrence of acceleration collision mechanism involved in the EL emission. But it is to be noted that the relative intensities of the various bands in the emission spectrum remain unaltered for any change in the excitation voltage. In this phosphor the initial electrons required for the acceleration and collision excitation of the luminescent centres arise mainly from the field ionisation of the chlorine (donor) levels which are equivalent to deep traps. These electrons are either raised to the conduction band or recombine with a nearby Cu^+ centre giving rise to red emission. The green band can be attributed to the recombination of Cu^+ centres with the conduction band electrons. According to the present energy level scheme the red band should show the smallest rate of increase of intensity with the increase of frequency of excitation voltage since it, evidently, arises from donor acceptor recombination which, relatively, is a slow process [9,14]. Such an effect does, indeed, take place as can be seen from Fig.3.5. Here an increase in the frequency of excitation clearly increases the intensity of the blue and the green bands, but the red band is virtually unaffected indicating saturation. On the basis of the present energy level

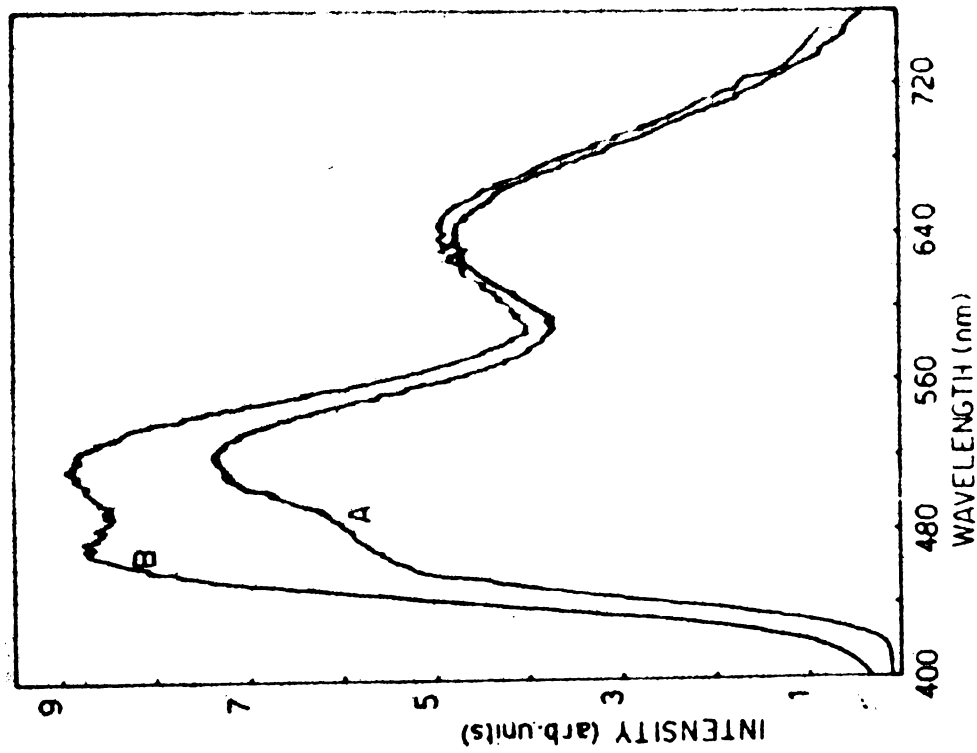


Fig.3.5. The EL spectra recorded for the sample (ZnS:Cu,Cl) at two different excitation frequencies (A) 1 kHz (B) 2.5 kHz.

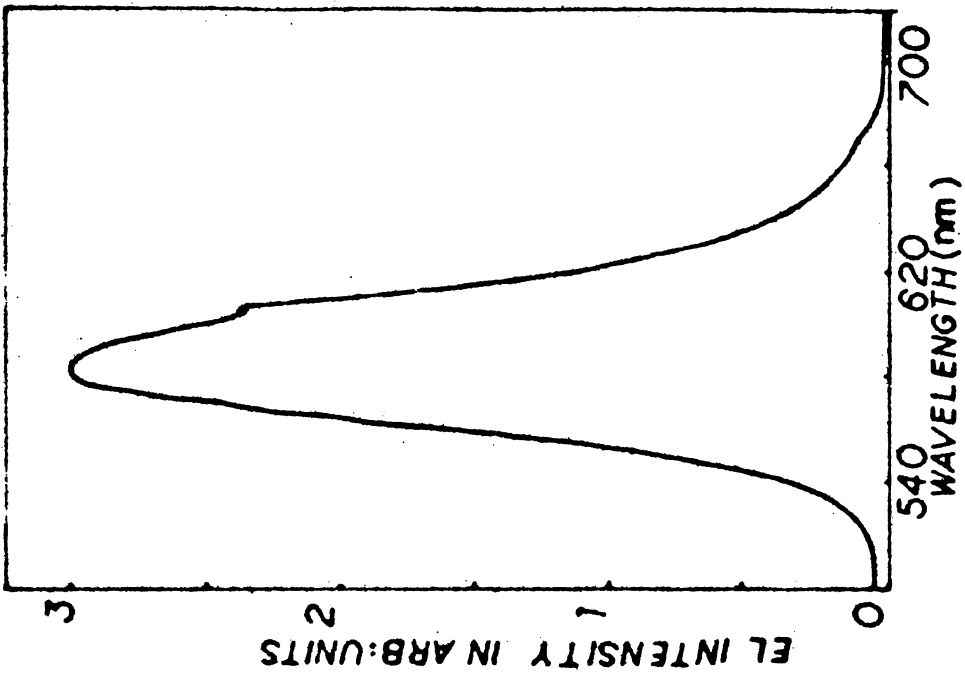


Fig.3.6. EL emission spectrum of ZnS:Cu, Mn, Cl EL phosphor

scheme the position of the Cl^- donor level can be calculated and is found to be 0.46 eV below the bottom of the conduction band. This is in good agreement with the result obtained from thermoluminescence experiments [15].

In conclusion, the experimental results show that addition of excess chlorine in the form of HCl in the pre-fired mixture gives green and red EL emission from ZnS:Cu,Cl phosphor apparently due to the creation of additional Cu^+ and Cl^- centres, the concentration of which is strongly dependent on the amount of excess chlorine added. A detailed study of the EL emission characteristics indicates the occurrence of three different energy levels attributed to Cu^{2+} , Cu^+ and Cl^- centres in ZnS.

3.3 Study on ZnS:Mn and ZnS:Cu,Mn,Cl phosphors

The only activator of practical importance other than Cu is Manganese. If sufficient amount of Mn (a few percent) is introduced into a conventional ZnS:Cu phosphor, the emission due to Cu is suppressed completely and instead

an yellowish orange emission due to Mn appears. ZnS:Mn phosphors are found to be less efficient. The higher efficiency of ZnS:Cu,Mn phosphors is attributed to sensitization of Mn centres by quantum mechanical resonance transfer of energy from Cu centres [16]. This conclusion does not seem to be very definite, however, since Ag, In and Ga are equally or more effective in sensitising photoluminescence from Mn

but are ineffective in the case of EL [16]. The observation that ZnS:Cu,Mn is superior to ZnS:Cu for DC excitation and that no secondary peak similar to that for ZnS:Cu is normally noted in its output wave-form favours the idea of direct excitation of Mn centres or sensitization by the lattice (electron-hole pair) rather than sensitization by Cu in this phosphor [17]. A recent investigation based on the study of time resolved spectrum of DC EL powder cells by Skolnick [18] also supports this assumption. In practice, Cu in ZnS:Cu,Mn provides inclusions of Cu_2S which is highly conducting. It is generally found that compared to emission from ZnS:Cu the yellow emission of these ZnS:Cu,Mn phosphors increases less significantly with the exciting voltage or its frequency.

The preparation and study of manganese doped EL phosphors are of special importance since these are used in the preparation of commercial DC powder EL displays [19] and in DC thin film devices [20]. High-field EL devices of high brightness and long life employing the double insulating layer structure make use of ZnS:Mn active layers [14]. Hence to fabricate such devices it becomes necessary to master the technique of preparation and study of this type of phosphors. In this section the details of the preparation and their various properties studied are presented. A detailed description of the thin film EL devices prepared using this phosphor will be discussed in Chapter IX.

The ZnS:Cu,Mn,Cl phosphor samples were prepared by mixing a weighed amount of ZnS (luminescent grade) cupric acetate (0.5 wt percent Cu), Manganese acetate (1 wt percent Mn) and 5 wt percent NH_4Cl . A slurry of this mixture was formed in aqueous solution and was then slowly dried. The black powder thus formed was taken in a quartz test tube with a close fitting cap and introduced into the high temperature zone of a vacuum furnace which was then evacuated to 10^{-2} torr. The samples were then fired at 1000°C for 90 minutes. For preparing ZnS:Mn, the same procedure was adopted but the slurry contained only ZnS and Manganese acetate.

The phosphor samples thus prepared showed good Mechanoluminescence (ML). A slight pressure on this sample gives very good ML emission. Of the two samples ZnS:Cu,Mn,Cl is found to give better ML.

The EL cell prepared with this phosphor gives bright yellow orange emission. The emission spectra of the sample are shown in Fig.3.6. The emission maxima are found to occur at 585 nm. This is attributed to the ${}^4\text{T}_1 - {}^6\text{A}_1$ transition in the Mn^{2+} ions [18]. The ZnS:Mn and ZnS:Cu,Mn,Cl phosphor shows same emission spectrum. It is found that the ZnS:Mn cell when excited shows bright intense emission spots while the ZnS:Cu,Mn,Cl cell has uniform emission and higher efficiency. It is to be noted that the emission spectrum does not have any blue or green band even though it is prepared

with the same amount of copper as in blue emitting phosphors. It is also observed that the wavelength of the emission maxima is independent of the excitation frequency.

Another noticeable property of the phosphor is that the average brightness of the cell increases very rapidly with increase in applied voltage. But at higher voltages the rate of increase is lower. In order to derive some information regarding the carrier generation and recombination mechanisms involved in the emission process usually the brightness voltage (B-V) characteristics of the cells are studied [6]. For the present phosphors it is observed that a plot of $\log B$ versus $\frac{1}{V}$ curve is a straight line Fig.3.7. This implies that

$B = a \exp(-b/V)$, where B is the brightness, V the voltage applied, and a and b are constants.

Such an expression for the dependence of brightness on voltage can be derived if we assume that the luminescent centres are excited by the collisions of the accelerated electrons [9,21]

Suppose an electron with charge 'e' traverses a path x in the direction of the field E, it acquires a kinetic energy

$$E_{kin} = e Ex$$

If W is the energy for an accelerated electron to excite or ionize a luminescent centre in collision, the path x must

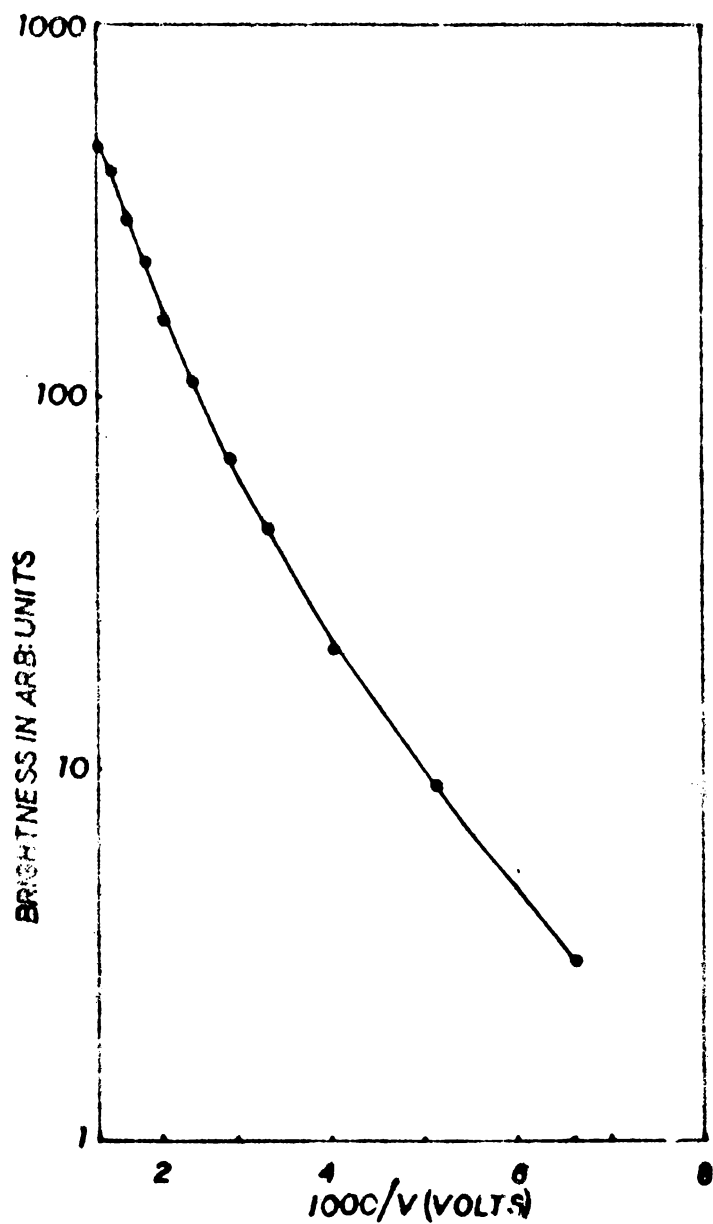


Fig.3.7. $\log B$ vs $\frac{1}{V}$ plot for a ZnS:Cu,Mn,Cl powder EL cell.

be great enough so that

$$E_{\text{kin}} > W;$$

$$\text{i.e. } x > 1 \text{ with } W = e E l = h \nu$$

where ν is the frequency of the emitted light. If \bar{x} denotes the mean free path for the accelerated electrons, the fraction of electrons with pathlength greater than l is

$$f = \exp\left(-\frac{l}{\bar{x}}\right)$$

The brightness B is proportional to the fraction f , then

$$B \propto \exp\left(-\frac{b}{E}\right)$$

where

$$b = \frac{W}{e\bar{x}}$$

So

$$B = a \exp\left(-\frac{b}{E}\right)$$

But the field E inside the crystal will not be exactly proportional to the applied voltage. So the formula cannot be exact for all types of phosphors [9].

Fig.3.8 shows the brightness waves of the present ZnS:Cu,Mn,Cl phosphor. From the figure it can be seen that the emission maxima are not in phase with the applied voltage maxima, and the two peaks are not identical but one is slightly higher than the other.

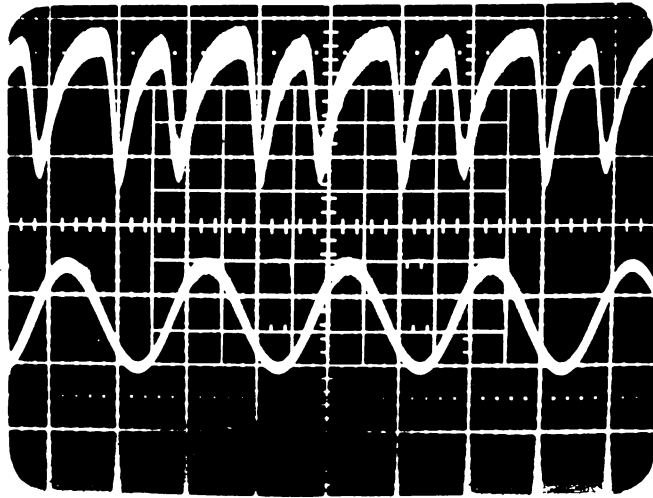


Fig. 3.8. The brightness waves of a ZnS:Cu,Mn,Cl EL cell.

According to Destriau [21] the observed phase change is due to the fact that the field acting on the crystals is out of phase with the field in the insulator.

If a voltage is applied to the cell, within the cell, the field experienced by the phosphor particles will be out of phase with the field in the insulator around the crystal, the former leading the latter by an angle ψ such that [21]

$$\tan \psi = \frac{2}{k_1 \rho f}$$

where k_1 is the dielectric constant of the crystals, ρ is their specific resistance and f is the frequency. But the field in the insulator also lags with respect to the potential applied to the EL cell by an angle γ such that

$$\tan \gamma = \frac{2k_2 \rho f}{4\frac{b}{a} + k_1 \rho^2 f^2 (k_2 + k_1 \frac{b}{a})}$$

where k_2 is the dielectric constant of the insulator, a is the thickness of the phosphor layer and b is the thickness of the insulating layer. Thus

$$\varphi = \psi - \gamma, \text{ and}$$

$$\tan \varphi = \frac{\tan \psi}{1 + kx}$$

$$\text{with } k = \frac{k_2}{k_1} \text{ and } x = a/b$$

Thus the total phase change ϕ becomes zero only if there is no insulator ($b=0$, i.e. electrodes in contact with the crystal) and it increases upto ψ when a/b is decreased to very small values.

The asymmetry in the brightness waves results from the asymmetric structure of the EL cell due to the introduction of the mica insulator.

The maximum brightness of the cell under prolonged operating condition is as much as 1000 fL when estimated by the method described in chapter II. This is indicative of the high efficiency of the phosphor developed and used in the cells.

In conclusion it is found that the ZnS:Cu,Mn,Cl and ZnS:In phosphor prepared in the laboratory have their emission maxima at 585 nm. No emission from Cu is observed for the ZnS:Cu,Mn,Cl phosphor. The $\log B$ vs $\frac{1}{V}$ plot for the cell is a straight line. The maximum brightness level upto which the experimental cell can be operated without breakdown is as high as 1000 fL.

3.4 EL spectral study of ZnS:Cu,Sm,Cl and ZnS:Cu,Dy,Cl phosphors

Sensitised luminescence from ZnS phosphors activated with rare earth ions has been subjected to a series of investigations by earlier workers [22]. But the recent development of efficient electroluminescent devices which

emit the three basic colours (blue, green and red) [23] and the observation of lasing phenomena in ZnS:Cu,Nd,Cl thin film direct current electroluminescent devices [24] have renewed the interest in rare earth activated ZnS phosphors. But no such phosphors of the latter type doped with rare earth ions other than Nd have been subjected to detailed investigations inspite of their great technological importance. This prompted to study the spectral characteristics of two such new phosphors viz. ZnS:Cu,Sm,Cl and ZnS:Cu,Dy,Cl. The results of the investigations made on these samples are presented in this section.

The phosphors were prepared as follows. A weighed quantity of luminescent grade ZnS was mixed with 0.5 wt. percent Cu in the form of cupric acetate (Analar grade), 1 wt. percent rare earth chloride (99.9 percent) and 5 wt. percent NH_4Cl (Analar grade) and the mixture was fired at 1050°C under vacuum in a quartz test tube for 90 minutes. In this case the EL cell was prepared by dispersing the phosphor powder in DC 704 silicone oil.

The emission spectrum of ZnS:Cu,Sm,Cl shows two bands, one at 570 nm and the other at 620 nm, the former being more pronounced Fig.3.9, curve B. The emission of ZnS:Cu,Cl is completely suppressed. These observed emission bands are evidently due to the transition ${}^4\text{G}_{5/2} \longrightarrow {}^6\text{H}_{5/2}$ and ${}^4\text{G}_{5/2} \longrightarrow {}^6\text{H}_{7/2}$ in Sm^{3+} .

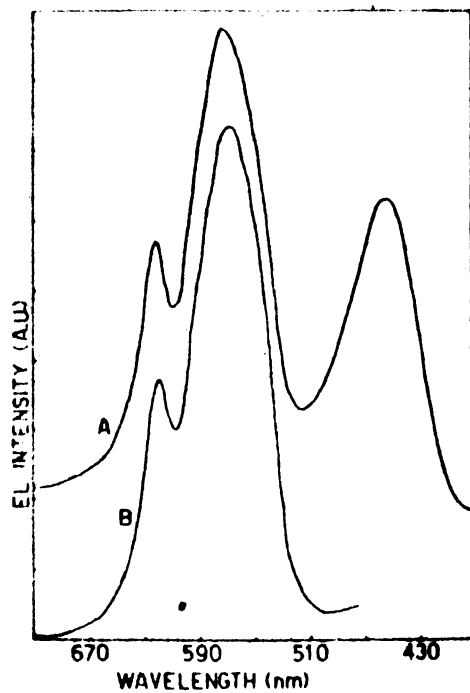


Fig.3.9. Curve (A) EL spectrum of ZnS:Cu,Dy,Cl and curve (B) EL spectrum of ZnS:Cu,Sm,Cl.

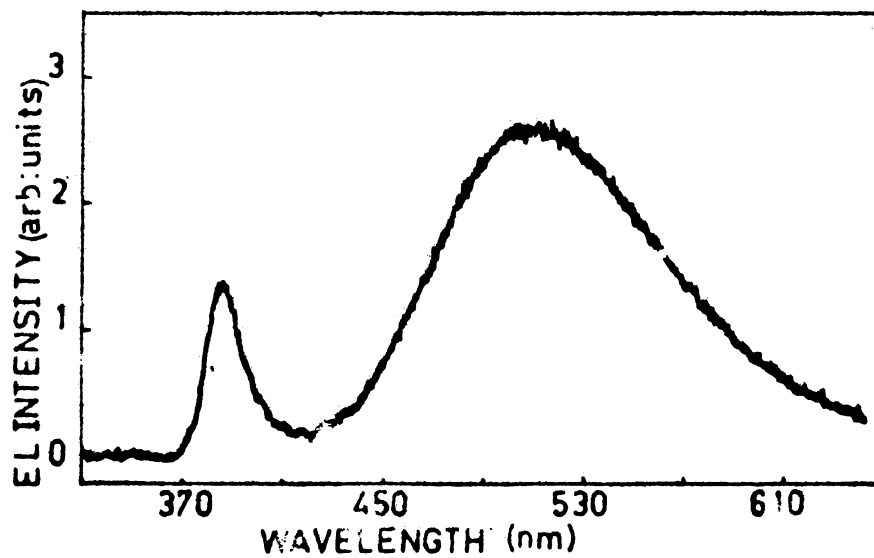
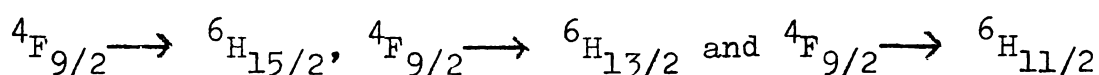


Fig.3 10. EL spectrum of self activated ZnO.

The spectrum of ZnS:Cu,Dy,Cl phosphor consists of three bands in the regions 450 nm, 570 nm and 620 nm corresponding to the respective transitions:



in Dy^{3+} (Fig.3.-9, curve A). Following the arguments of Anderson et al. [22] it can be concluded that these emissions are due to the resonance energy transfer from blue centres in ZnS:Cu,Cl to the rare earth ions. Eventhough the 450 nm band in the ZnS:Cu,Dy,Cl lies in the emission region of ZnS:Cu,Cl it can be attributed to the rare earth ions, since ZnS:Cu,Sm,Cl with the same concentration of Cu and Cl gave no such emission band. Also,an emission band in this region is found to occur in PL spectrum of CaF_2 doped with Dy [25] which support this argument. However, definite conclusions regarding the origin of these bands can be derived only by studying. the dependence of emission characteristics on the sensitizer concentration, the time resolved emission spectra and the decay characteristics of the emission.

3.5 Electroluminescence in self activated ZnO

ZnO is one of the earliest and well known luminescent materials. Its luminescent properties under ultra violet excitation [26] and cathode ray irradiation [27] are well studied. Recently this substance has gained importance as an EL material as well. Previous workers in this field have studied the spectral distribution of the EL emission in the

visible region only [28]. But its photoluminescent and cathodoluminescent spectra suggest the possibility of the occurrence of an ultraviolet band in its EL emission spectrum also. Suppression of this emission by self absorption and re-emission in the optical region will certainly enhance its optical emission efficiency as discussed and demonstrated by Shrader [27] and Nicoll [29,30]

The phosphor was prepared by firing pure ZnO powder in air at 950°C for one hour in a muffle furnace.

The emission spectrum of the self activated ZnO consists of two bands as shown in Fig.3.10. This is in close agreement with the cathodoluminescent spectrum of ZnO[Zn] [27]. The ultraviolet band has its maximum at 385 nm and the other broad band in the visible region has its maximum at 510 nm. The latter is the well known bluish green band of self activated ZnO. The UV emission at 385 nm is observed here for the first time in the EL spectrum of ZnO. The Zn⁺ centres formed during firing process have been suggested as the cause for this band in the visible region [28]. The 385 nm band corresponds to an energy gap of 3.2 eV which is exactly the band gap of ZnO. Hence it is obvious that this ultraviolet band arises from a band to band transition involving the conduction and valence bands of ZnO. From these studies it can also be concluded that the self activation centres, probably the Zn⁺ levels, responsible for the 510 nm band are situated ~ 0.8 eV above the valence band.

References

1. L.W. Strock and V.A. Brophy; Am. Minerologist 40(1955) 94.
2. S. Roths Child; Solid State Physics in Electronics and Telecommunications, Vol.4, Eds. M.De'sirant and J.L. Michiels (Academic Press, New York, 1960) 705.
3. J.S. Prener and F.E. Williams; J. Chem. Phys. 25(1956)361.
4. F.A. Kroger and H.J.Vink; J. Chem. Phys. 22(1954) 250.
5. F.A. Kroger and J.E.Hellingman; J. Electrochem. Soc. 93(1948) 156, 95(1949) 68.
6. Henry F. Ivey; Advances in Electronics and Electron Physics, Suppl, 1.Electroluminescence and Related Effects (Academic Press, New York, 1963).
7. H.C. Froleich; J. Electrochem. Soc. 100(1953) 280.
8. W.A. Thornton; J. Electrochem. Soc. 107(1960) 895.
9. D. Curie; Luminescence in Crystals (Mathuen, London,1963).
10. P.Zalm, G. Diemir and H.A. Klasens; Philips Research Reports 9(1954) 81.
11. Y. Nakanishi, H. Yamishita and G. Shimaska; J. Appl. Phys. 20(1981) 2261.
12. W.J. Harper; J. Electronics 109(1962) 103.
13. M. Godlewski, W.E. Lamb and B.C. Covenett; J. Phys. C. Solid State Physics 15(1982) 3925.
14. J.I. Pankove; Topic in Applied Physics, Vol.17 Electroluminescence (Springer Verlag, NY, 1977)

15. M.S. Waite; J. Luminescence 24/25 (1981) 921.
16. H.C. Froelich; J. Opt. Soc. Am. 43(1953) 320.
17. D.A. Cusano and F.E. Williams; J. Phys. Radium
17(1956) 742.
18. M.S. Skolnick; J. Phys. D. Appl. Phys. 14(1981) 301.
19. A. Vecht, N.J. Werring, R. Ellis and P.J.F. Smith;
Proc. IEEE [7] Vol.61(1973) 902.
20. M.I. Abdalla, J. Thomas, A. Brenac and J.P. Noblane
IEEE Trans. on Electron Devices ED-28[6](1981) 694.
21. G. Destriau and H.F. Ivey; Proc. IRE 43(1955) 1911.
22. W.W. Anderson, S.Razi and D.J. Walsh; J.Chem. Phys.
43(1965) 1153.
23. J. Benoit, B.P. Benalloul and B. Blankzat; J. Lumin.
23(1980) 175.
24. G.Z. Zhong and F.J. Bryant, Solid State Commun.
37(1981) 907.
25. A. Sivaram, H. Jagannath, D. Ramachandra Rao and Putcha
Venkateswarlu, J. Phys. Chem. Solids 40(1979)1007.
26. D.C. Reynolds; Optical Properties of Solids, Ed. S. Nudelman
and S.S. Mitra, Optical Physics and Engineering Series
Ed. William L. Wolfe (Plenum Press, NY, 1969) 271.
27. R.E. Shruder and H.W. Leverenz; J. Opt. Soc. Am. 37(1947) 939.
28. K. Kumar and S.G. Prakash; Indian J. Phys. 54A(1980) 264.
29. F.H. Nicoll; Opt. Soc. Am. 38(1948) 417.
30. H.W. Leverntz; An Introduction to Luminescence of Solids
(John Wiley and Sons, New York 1950).

CHAPTER IV

A STUDY OF CaS:Ce and CaS:Ce,Nd EL PHOSPHOR



4.1 Introduction

Alkaline earth sulphides are known for a long time as excellent and versatile phosphor host materials [1] but very little progress has been made on these compounds compared to the vast amount of work done on other phosphor materials like ZnS. This is essentially due to their reported poor reproducibility in the preparation and the questionable chemical stability. Their bad reputation as poor CL and PL phosphors, in fact, hindered their development as a good EL phosphor as well. Wachtel [2] has prepared EL CaS:Cu, Eu phosphor powders with red emission arising from Eu centres. The absence of blue Cu emission is attributed to energy transfer from Cu to Eu centres. The excitation seems to be from a kind of contact electroluminescence [3] resulting from the agglomerate of particles and is relatively weak and depends greatly on the physical state of the material.

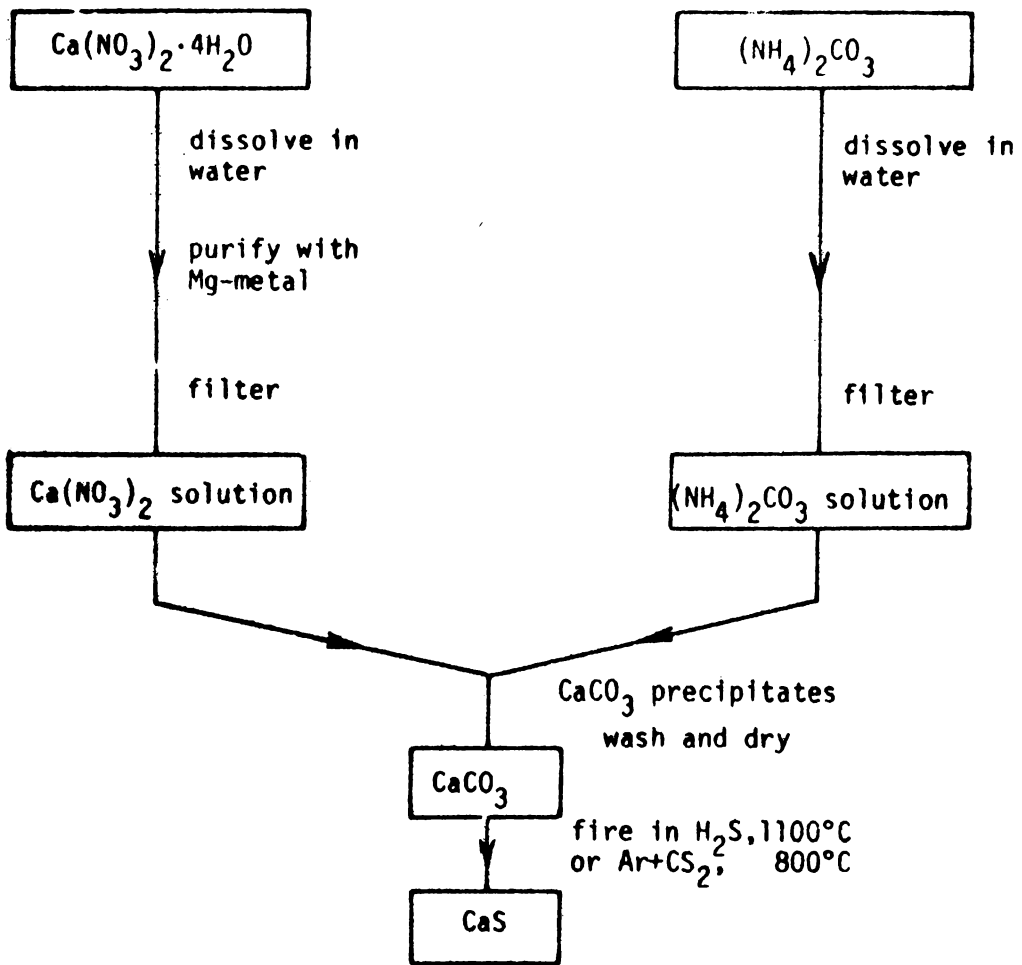
This group of phosphors commonly called Lenard phosphors consisting of MgS, CaS, SrS and BaS crystallises in NaCl structure. The most important member of the group is CaS which has a band gap of 4.8 eV. This makes it a suitable host for the preparation of blue or green emitting

phosphors. The interest in this long neglected class of phosphors was revived by the classic work of Lehmann [4]. He has prepared about, 31 different phosphors from CaS alone by adopting a carbonate process for the preparation of pure CaS which is shown schematically in Table-1. These phosphors are superior to all other phosphor systems and are easily adaptable to the existing application techniques. Efficient phosphors of this kind which can emit in visible U.V. and I.R. regions can be easily prepared. They are relatively burn resistant and have efficiency comparable with the best ZnS phosphors. Moreover they have fast recombination time ($\sim 10^{-7}$ sec.) and show little current saturation at enhanced current densities.

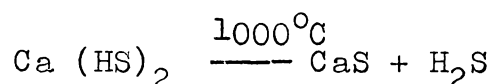
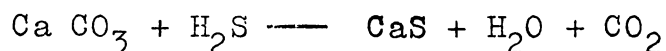
The excellent properties of these alkaline earth . CL phosphors prompted many workers to study their EL properties as well. Laud and Kulkarni have prepared a series of SrS:Cu [5,6], BaS:Cu [7] and rare earth doped alkaline earth sulphides [8,9]. Rastogi and Mor have tried (Ca,Ba)S:Cu,Nd [10], $\text{Ca}_x\text{Sr}_{1-x}\text{S}:\text{Cu},\text{Nd}$ [11], CaS:Nd,Cu [12] etc.

But the most striking advancement in converting these CL materials into efficient EL phosphors was made by Vecht et al. [13]. They have prepared high efficiency EL phosphors of rare earth sulphides which have emission spectrum as reported by Lehmann for his CL phosphors. These workers prepared the phosphors from the respective

TABLE I
PREPARATION SCHEMA OF PURE CaS, "CARBONATE PROCESS"



carbonates and from hydrosulphides by the following reaction.



The latter process is reported to have yielded phosphors with low oxide contamination and low particle size distribution. The CaS:Ce phosphors prepared by them have efficiency greater than 5×10^{-4} W/W approaching the value of 10^{-3} W/W reported for ZnS:Cu,Mn phosphors. These samples did not show any tendency to saturate at high brightness levels.

The present chapter and the subsequent two chapters describe the details of preparation and the various investigations made on a set of CaS based phosphors. This chapter gives the details of the method adopted for the preparation of a highly efficient CaS:Ce phosphor and its EL spectra, B-V characteristics and the frequency dependence of brightness. A brief note on the EL spectra of CaS obtained without any intentional doping and that of CaS:Ce containing different concentrations of cerium are given. An attempt has been made to identify the ionization state of the Ce luminescent centres. A brief discussion of the various energy transfer process occurring in luminescent solids is given followed by the description of the EL properties of the CaS:Ce,Nd phosphor, the Ce emission quenching and the probable Ce \longrightarrow Nd resonant radiationless energy transfer process.

4.2 Phosphor preparation

The starting material used for the preparation of the various phosphors is commercially available high purity CaS (Riedel). This is a white powder giving a slight pinkish after glow under UV excitation. For the preparation of the CaS:Ce phosphor, to a weighed amount of CaS, a known weight percentage of $\text{Na}_2\text{S}_2\text{O}_3$ and ammonium ceric sulphate were added. A slurry of this mixture was then prepared in aqueous solution. The slurry was then slowly heated and dried. This gave a solid mass which was crushed and mixed with equal amount of sulphur and introduced into the high temperature zone of a horizontal furnace kept at 1050°C . The container used was a quartz test tube fitted with a close fitting cap. One end of the furnace was closed while the other end was fitted with a small bore stopper to allow the gases evolved during the solid state reactions to escape. The firing was done at 1050°C for 90 minutes. The product obtained after the firing process was found to have a yellow tinge which is found to depend on the amount of cerium salt added. The samples were then tested for their EL emission. It showed spotty bright green emission. A portion of the sample was then coated with Cu_2S over layer. This was achieved by treating the fired phosphor sample in an aqueous cupric acetate solution. The resulting powder was black in colour. The sample was then tested for its EL performance. It showed good EL emission and was several times brighter than the uncoated phosphor.

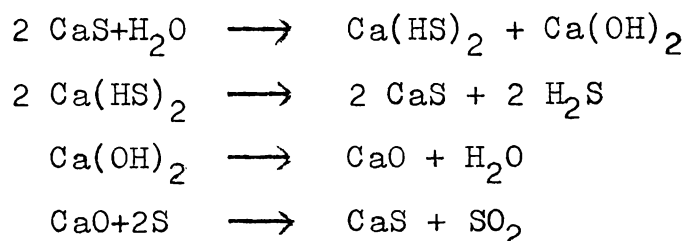
In order to determine the optimum quantity of flux, activator concentration and the best condition for the deposition of Cu_xS over coating on the phosphor particles, a series of phosphor samples were prepared and tested for performance. To find out the most suitable flux quantity six phosphor samples were prepared from the prefired mixture containing equal amounts of CaS and Cerium salt but with 0, 2.5, 5, 10, 20 and 40 wt. percent of $\text{Na}_2\text{S}_2\text{O}_3$. EL cells were then fabricated with these samples. It was found that there is no strong dependence of the emission efficiency on the flux content but a flux amount of about 5 wt percent is sufficient. It is seen that the addition of flux has increased the emission efficiency.

Another set of phosphor samples was prepared containing varying amount of Ce. but all of which contained fixed amount of flux. Phosphors containing .001, .01, .1, .5, 2, 3 and 5 wt percent of Ce in the prefired mixture were tried. It is found that the phosphors containing cerium concentration in the range 1-5 wt percent showed almost the same emission efficiency. In order to find out the next parameter viz. the condition for the copper sulphide coating, a phosphor sample containing 2.5 wt percent Ce and 5 wt percent $\text{Na}_2\text{S}_2\text{O}_3$ in the pre fired mixture was treated with fixed volume of solution having different concentrations of cupric acetate. From these trials the optimum values of the various phosphor constituents were found out empirically.

It is found that a second firing process of the copper coated phosphors increased the brightness level substantially. Phosphor samples which can be excited to a brightness level of 500 fL have been prepared. It is felt that with some more trials phosphors which can have brightness level much higher than this value can be produced by this method.

4.3 Self activated emission of CaS

In order to make sure that the emission is due to the cerium impurity a phosphor sample containing 5 wt percent $\text{Na}_2\text{S}_2\text{O}_3$ and equal amount of sulphur (99.9 percent) but with no cerium salt was prepared. The resulted powder showed an yellow orange after glow under UV irradiation. The EL spectrum of the sample is shown in Fig.4.1 curve A. The possibility of Na to become an active luminescent centre is ruled out since prefired mixture containing about 50 percent $\text{Na}_2\text{S}_2\text{O}_3$ also showed this emission; otherwise at such higher concentration it should have disappeared due to the concentration quenching effect. The slurry preparation and the subsequent firing process in sulphur atmosphere bring about the following chemical reaction:



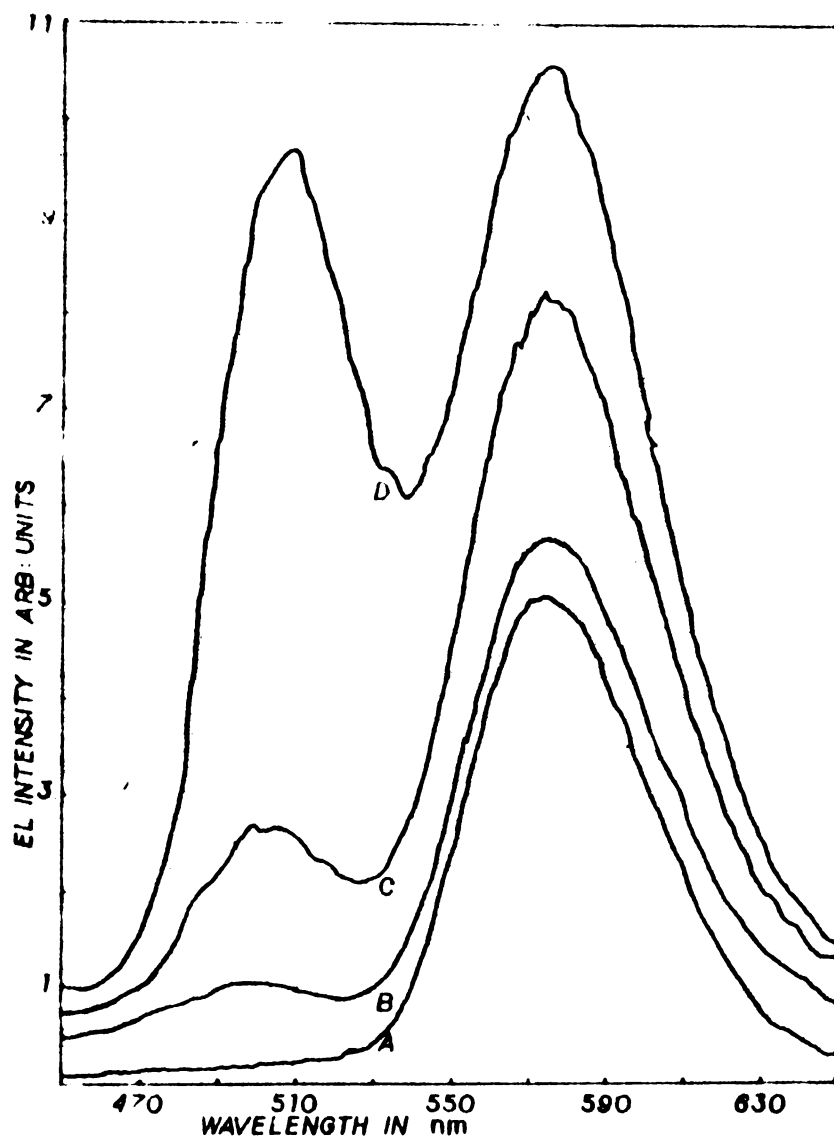


Fig.4.1. Curve A is the EL spectra of self activated CaS. B, C and D are the EL spectra of CaS:Ce phosphors containing 0.001, 0.01 and 0.1 wt percent of Ce in the pre-fired mixture

It can be seen that the reaction in the last step need not be complete since it is a solid state reaction and will leave traces of CaO which will, in effect, act as impurity centres in the CaS lattice as Ca^{2+} and O^{--} and give rise to the emission band which is denoted here as the self activated emission. This, however, is only a speculation since no detailed investigation on this phosphor was carried out due to its poor emission efficiency.

The EL emission spectra of the various phosphors were recorded with the set up described in detail in Chapter II. The experimental cell was fabricated with castor oil as the dielectric. The details of the set up used for the B-V and B-f characteristics are also given in Chapter II.

4.4 Experimental results and discussion

The EL emission spectra of the phosphors prepared without any intentional doping and of those having .001, .01, 0.1, 1.0 and 3.0 wt percent of Ce are shown in Fig. 4.1. The emission spectra of the first four samples were recorded under the same condition. These spectra are the superposition of emission due to self activated CaS and that of CaS:Ce, occurring respectively at 510 nm and 570 nm. It can be seen that as the Ce concentration is increased the intensity of the green band also increases. So it can be concluded that this band is due to the Ce activator. The emission intensity of the phosphor was so large that at cerium concentration of

1.0 and 3.0 wt percent the spectra were recorded at a much reduced gain (Fig.4.2). In this condition the contribution due to the self activated emission in the recording is negligible. So the two bands occurring at 510 nm and at 570 nm can be attributed to cerium alone. Such a pair of emission bands was recorded by Vecht et al. and Lehmann at a slightly shifted wave length of 524 nm and 585 nm respectively. The emission spectrum of the CaS:Ce obtained after the second firing process is shown in Fig. 4.3. It can be seen that the two bands almost merge together. This is apparently due to broadening of the two bands. The reason for this band broadening is as follows.

The magnitude of the lattice parameter of a phosphor particle increases with decrease in its size, and the energy band gap with a larger lattice parameter is narrower than that of a phosphor with a small lattice parameter [14,15]. The lattice parameter and the wavelength of light emission can be related empirically as

$$a = k \ln \lambda + a_0, \quad a \text{ being the magnitude of the}$$

lattice parameter, λ the wave length k and a_0 are constants. The reason why phosphors with large particle size have a small lattice parameter can be considered as follows:

A phosphor with less distortion can grow to large particle size, while a phosphor with more distortion cannot grow to a large particle size, since much energy is needed

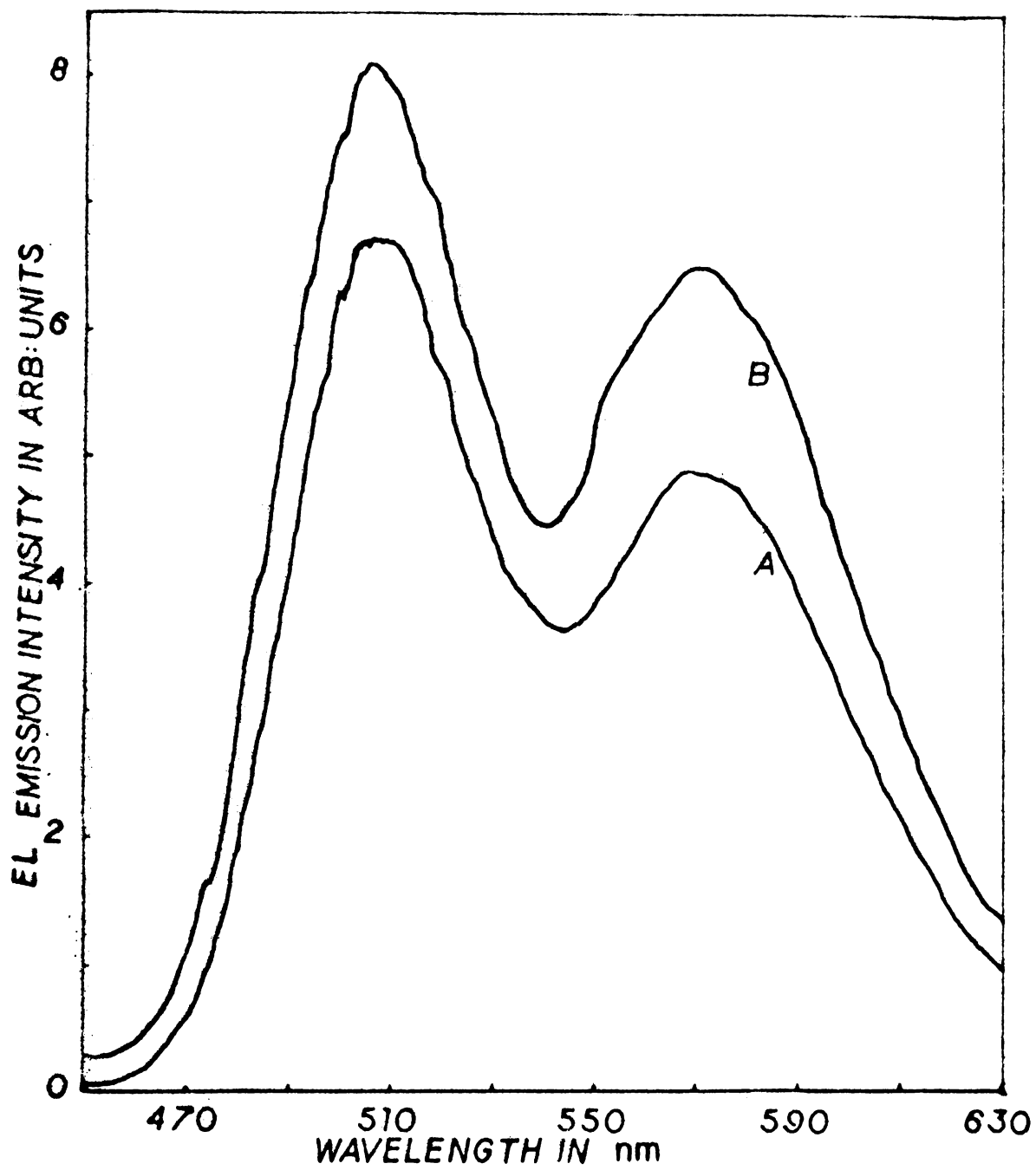


Fig.4.2. EL spectra of the CaS:Ce containing 1 wt percent and 3 wt percent Ce in the pre-fired mixture.

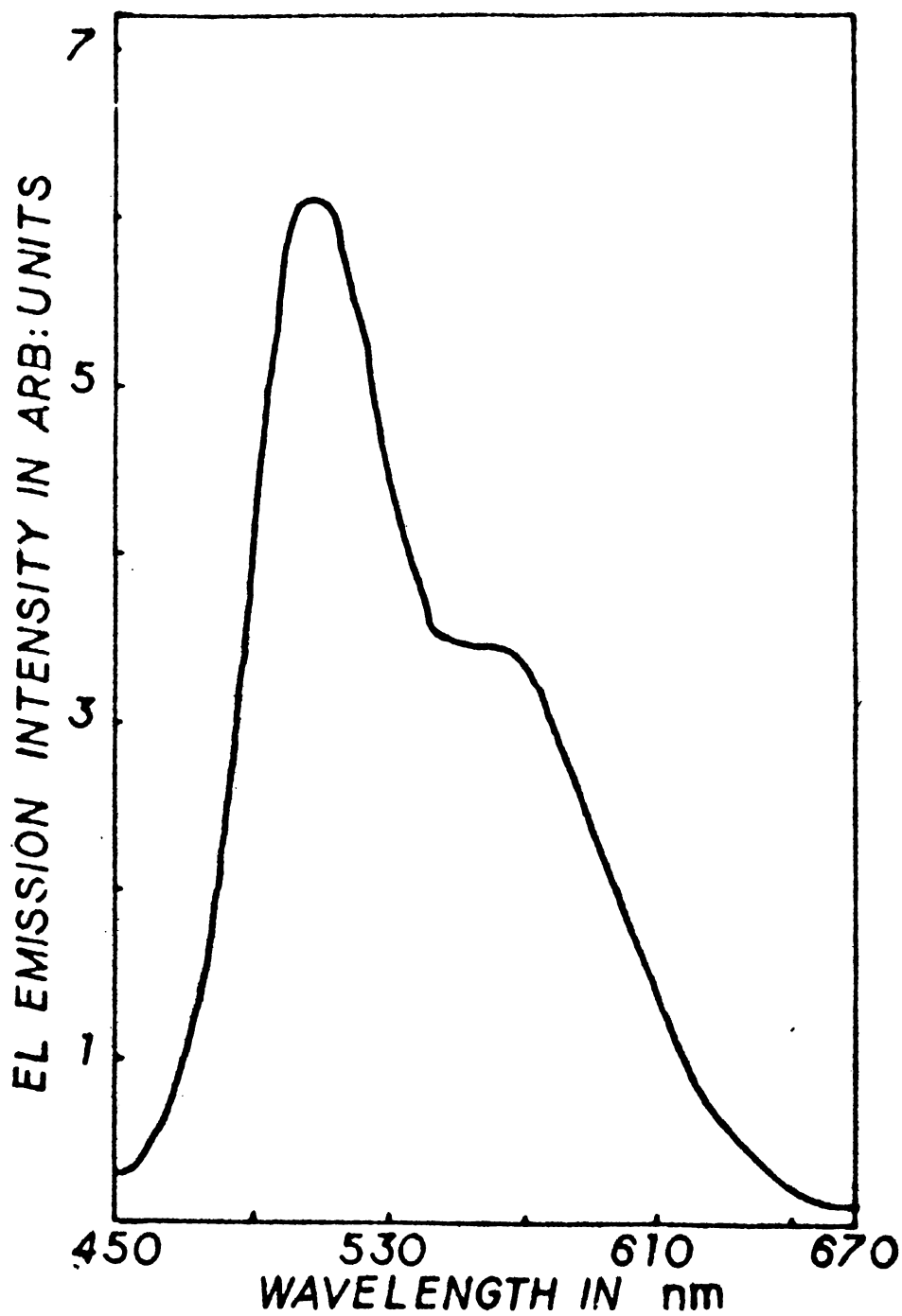


Fig.4.3. EL spectrum of CaS:Ce obtained after the second firing process.

to maintain a lattice with distortion during growth [16,17]. So the broadening of the bands can be attributed to the distribution of the particle size existing in the phosphor which might take place during the second firing process.

These two emission bands are attributed to the 5d-4f transition in the Ce ion by Lehmann but is more accurately assigned by Asano et al. [18] as due to the ${}^2T_{2g} \rightarrow {}^2F_{5/2}$ and ${}^2T_{2g} \rightarrow {}^2F_{7/2}$ in Ce^{3+} ion. These workers assumed that the Ce ion is entering the CaS lattice as the triply ionized Ce^{3+} ion. But it will, however, be more justifiable if these emissions are attributed to doubly ionized Ce^{2+} ion due to the following reasons.

Eventhough the spectra of RE^{2+} and RE^{3+} ion are associated with two types of transition f-f and f-d i.e. transition between terms of f configuration or between the terms of the f configuration and terms of mixed $f^{k-1}d$ configuration, they differ sharply. In the RE^{3+} spectra the f-d transition (in absorption and luminescence) occur in UV region and do not overlap the f-f transition, whereas in the case of RE^{2+} the f-d and f-f transitions lie close to each other and overlap. The RE^{3+} spectra originating basically from f-f transition are line spectra, and they consist of a large number of narrow and weak lines. The RE^{2+} spectra (f-d transition) are broad, high intensity bands in absorption and in luminescence.

In the case of rare earths it is established that transitions onto the levels of mixed $4f^{k-1} 5d$ configuration and also onto the $4f^{k-1} 6s$ and $4f^{k-1} 6p$ levels give rise to broad intense absorption bands. This is due to the fact that the said transition occurs between states with dissimilar electron configuration and therefore are parity allowed. So in these transitions the oscillator strength are of the order of $10^{-2} - 10^{-5}$ which is 3-4 orders higher than those for the forbidden f-f transition. The effective absorption cross section is about $5 - 10^{-1} \text{ cm}^{-2}$. Since these transitions involve 'd' electrons, unshielded against interaction with the lattice, greater splitting of the levels due to the crystal field effects can give rise to greater halfwidth of the emission lines. Moreover the band positions will be different for different host crystals [19]. In this case i.e. in CaS:Ce, the cerium emission is in the green region but it is bluish green in SrS and yellow in CaO which strongly supports that the emission involves a 5d state.

A plot of the Log B versus log V for the CaS:Ce is found to be a straight line (shown in Fig.4.4) which implies that

$$B = b v^n$$

which is a special case of the Destriau relation. This type of characteristic arises when the carrier acceleration is occurring at a Mott-Schottky type barrier [20].

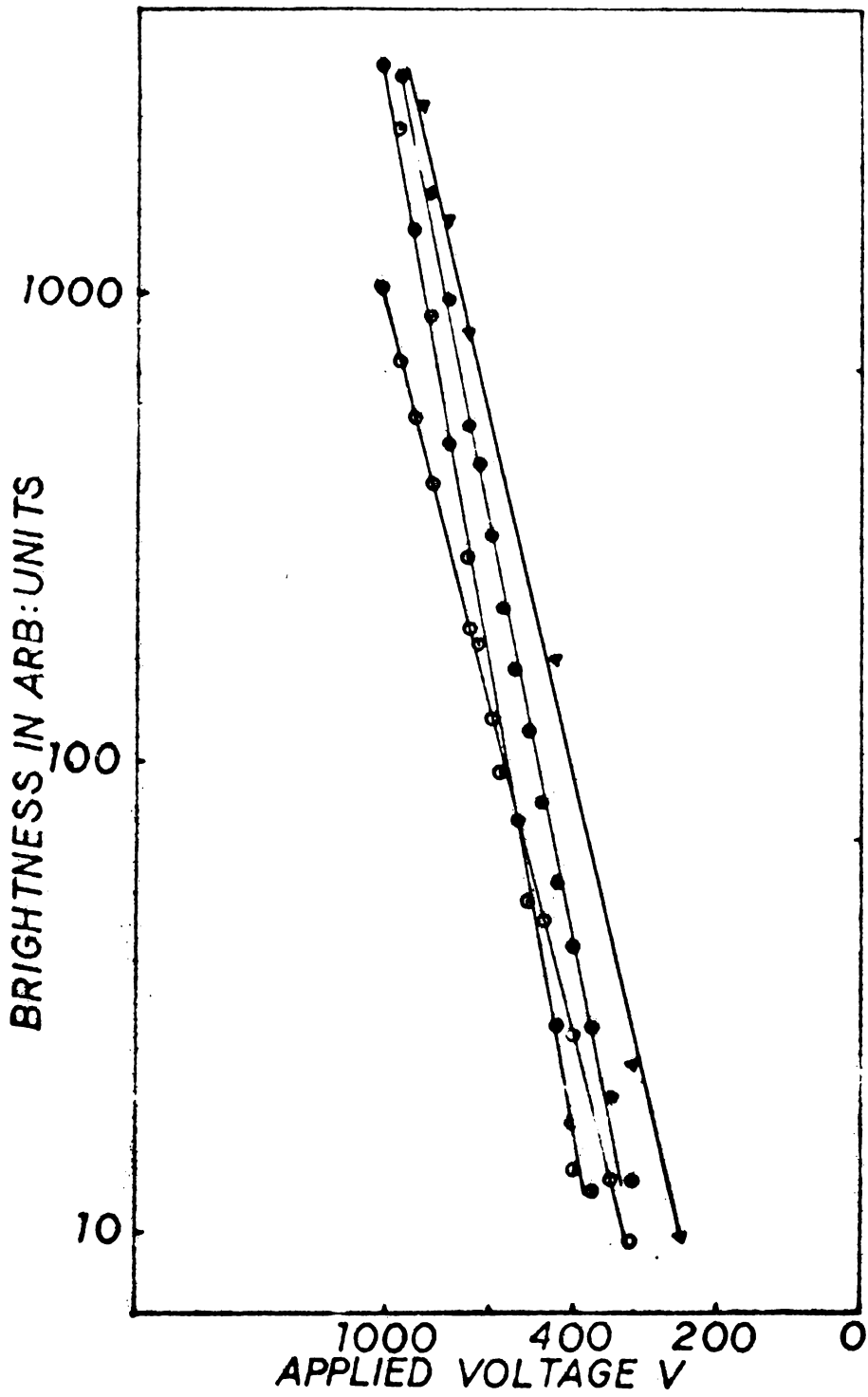


Fig.4.4. log B vs log V plot of a CaS:Ce EL phosphor.

The brightness wave of the phosphor under AC excitation is shown in Fig.4.5. It consists of two brightness peaks in each cycle of excitation but slightly asymmetric in amplitude. The width of these peaks are small compared to that observed in the case of ZnS:Cu,Mn,Cl. This is due to the shorter lifetime of the luminescent centres causing this emission. The decay time of this phosphor with a sharp rising square voltage pulse is 10 μ sec. The slight asymmetry in the peaks can be attributed to the asymmetric structure of the cell. Another notable feature is the absence of any d.c. component in the emission as compared to the ZnS:Mn which indicates the absence of any slow recombination mechanism. Destriau has attributed the observed phase change as due to the phase change occurring in the dielectric [20]. But Zalm [21] has ruled out this possibility and has attributed it to the spatial separation of the charge carriers and the delayed nature of the recombination.

A notable feature of this phosphor is its brightness (B) frequency (f) characteristics. A typical plot of B vs f plot is shown in Fig.4.6. It is seen that for a fixed voltage as the frequency is increased from 50 Hz the brightness **increases** upto 1 KHz and then decreases and attains a minimum value at 3 KHz and again increases with increase in frequency.

At first it was thought that this peculiar nature is due to the resonance absorption of power by the cell at

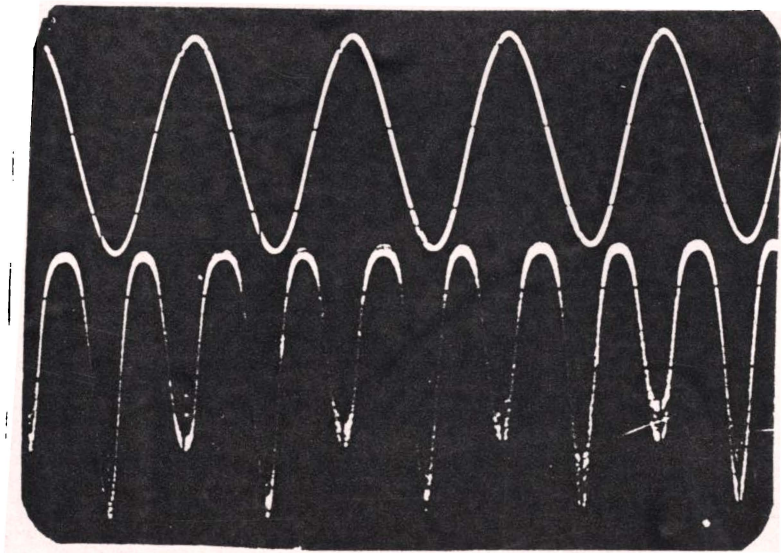


Fig.4.5. The brightness waves of a CaS:Ce EL cell.

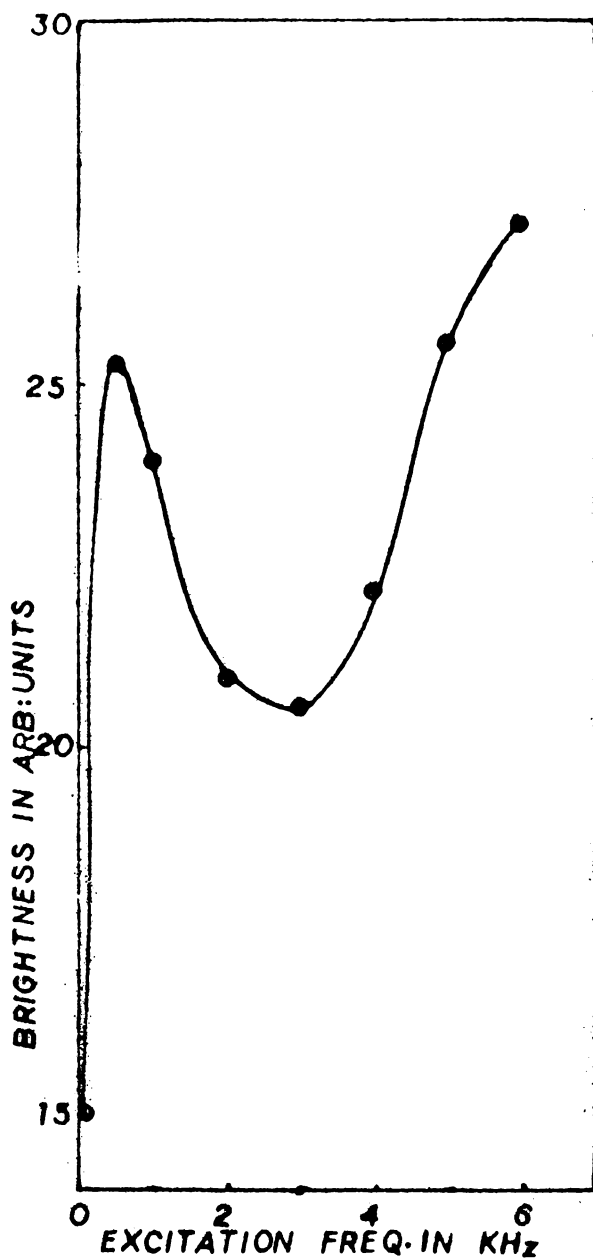


Fig. 4.6

B-f plot of the CaS:Ce EL phosphor

1 KHz and hence this increase in brightness. This was checked by using cells with different CaS phosphors. The experiment was also repeated by changing the thickness of the mica sheet used in the cell and the dielectric liquid. But the same characteristics were obtained in all cases. So it is attributed to the CaS phosphor.

According to the model suggested by Zalm [21] the electrons released from the luminescent centres during one half **cycle** of the applied voltage are swept away by the field. They can return to the luminescent centres only after the field has been reversed. In the meantime they may get trapped in the low field regions. Thornton [22] has shown that many of the effects of frequency and temperature on EL brightness of ZnS phosphors can be explained by considering the return of the electrons to the excitation region to be controlled by their thermal and field release from such traps. The number of electrons which are successful in returning to the excitation region is a function of the release rate (which depends on voltage and temperature) and also on the time available (frequency). The return is facilitated if the driving voltage is higher and time interval is sufficient (low frequencies).

When an EL cell is excited with a sinusoidal voltage for each cycle of excitation there occur two brightness peaks. The mean brightness measured will depend on the number of such brightness peaks occurring per cycle. As the frequency

is increased the number of such peaks and hence the mean brightness will increase linearly.

The anomalous behaviour of the B-f characteristics observed in the present case can be explained by adopting the model suggested by Zalm [21] which assumes that, during the application of the field, the charge carriers are generated and are spatially separated from the recombination centre. On removal of the field they recombine with the luminescent centres giving EL emission. Naturally, the intensity will depend on the number of carriers recombining with the luminescent centre in a half cycle. Now let us suppose that for a particular frequency of excitation, during one half cycle a certain number of charge carriers have been generated and are displaced from the recombination centres. If there are a few trap levels which can trap some of these electrons, and if their detrapping time is such that before the field gets reversed all of these trapped carriers are released and have recombined with the centres. In this condition the occurrence of the trap levels will not affect the brightness. But now consider the case at a higher frequency with period comparable to the detrapping time of the levels. In this case all the trapped electrons will not be detrapped to combine with recombination centres and hence the brightness will not increase as before. As the frequency is further increased the number of electrons remaining in the trap increases thereby causing a reduction in the observed intensity. This process

can continue upto a frequency at which the whole of the trap levels remain filled, since at this frequency the field variations are so rapid that it cannot be followed by the trapped carriers. Beyond this frequency the phosphor will act as though there are no traps. If we increase the frequency the brightness also will increase linearly with the frequency. Hence when such trapping processes occur one can expect that as the frequency is increased initially the brightness increases and attains a maximum value and then gets reduced. On increasing the frequency still further, the brightness goes on decreasing and attains a minimum value and then it starts increasing linearly. This type of a behaviour is observed in the present case.

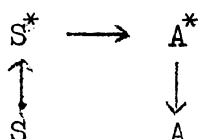
4.5 Sensitized luminescence and the EL in CaS:Ce,Nd phosphor

If two or more number of activators are introduced into a crystal, then an interaction between these ions can take place and its effect can be observed in the emission characteristics of the system. The absorption spectrum will be a simple superposition of the absorption spectra of the individual ions. But the emission spectra may be a superposition of the individual emission spectra, but other effects can also occur as noted below.

(1) The luminescence spectral intensity of one ion can gain in strength at the expense (of the diminishing intensity) of the other. (2) An ion not luminescent at a given

concentration in a given crystal becomes luminescent in the presence of another ion when introduced in a different crystal. (3) If luminescence is not observed for an ion at a particular excitation frequency it may be excited by introducing another ion having a strong absorption for that particular excitation. (4) In some cases the luminescence of one ion is intensified with the complete quenching of the other.

These changes in luminescence of one ion in the presence of another are due to transfer of excitation energy from one to the other [19,23]. Luminescence of ions excited as a result of the energy transfer from another ion excited in the absorption band is termed sensitized luminescence and proceeds conformable to the scheme.



Here S is the sensitizer (energy donor) and is the activator (energy acceptor); Asterisks denote their excited states.

In the case of the phenomenon of sensitized luminescence the energy absorbed in the absorption band of one ion (sensitizer) can be re-emitted in the emission band of the other ion (activator). The transfer of energy from sensitizer to activator is accomplished through the following

main types of transfer mechanism: (1) emission-reabsorption (2) resonance radiationless, and (3) non-resonance radiationless. These are explained below:

(1) The emission-reabsorption type of the energy transfer (cascade luminescence) implies emission of light by single ion (primary luminescence) and its absorption (reabsorption) and emission (secondary luminescence) by the other ion. Both ions behave as independent systems, and do not interact directly. A condition necessary for this method of transfer to manifest itself is the closeness of the **emission** energy of one ion to the absorption energy of the other. The pattern of the ion energy levels must have two close matching levels. In this type of energy transfer in the luminescence spectrum of the ion sensitizer, only the intensity of the line absorbed by the activator diminishes and the other line intensities remain unchanged.

(2) The resonance radiationless mechanism of the energy transfer is effected between interacting ions behaving like a single system. A condition necessary for this mechanism of transfer is that there should be a coincidence or a close match between energy level pairs of the ion sensitizer and the ion activator. An essential difference is that the transition between the levels of the sensitizer is not necessarily emissive, whereas the activator absorption corresponding to the pair of levels close to the **first** one may be of a very low intensity. Then the emission of the

activator does not necessarily occur as a result of transition between the pair of levels to which the energy of the sensitizer is transferred.

Here the energy transfer is resulting from dipole-dipole or dipole-quadrupole interaction between ions and the energy transfer probability depends upon the type of interaction. With dipole-dipole interaction the probability of transfer is proportional to r^{-6} (where r is the mean distance between interacting ions, which, in this case, should not exceed 30 \AA) and with dipole-quadrupole interaction to r^{-8} (not more than $10\text{-}12 \text{ \AA}$). Here the process of luminescence is of an additive nature, and a reduced duration and decreased quantum yield of the luminescence of the sensitizer (partial or complete quenching) are compensated by a longer duration and greater quantum yield of the activator luminescence.

With interaction of ions the intensity of the entire luminescence spectrum of the sensitizer decreases. Because of short critical distance between the sensitizer and the activator ions, the effectiveness of the sensitization does not depend either on the size or on the shape of the sample.

(3) The non resonance radiationless mechanism leads to the transfer of energy between the ions in the event of substantial non-concurrence of distances between the levels of an ion transferring the energy (upper) and the levels of an ion receiving the energy (lower). The difference between

these energies goes either to the lattice in the form of a phonon or to a third ion which has a pair of levels supplementing this difference.

Among the three types of energy transfer process the most important and most prevalent type is the resonant radiationless energy transfer process. This type of sensitized luminescence involving such a process can be used to excite luminescent centres in crystals and phosphors which are, otherwise, not possible to be excited directly at a particular excitation frequency. This technique is widely used to excite RE^{3+} doped laser crystals where the luminescent ions contain weak narrow absorption lines associated with the forbidden f-f transition. This is achieved by adding another RE^{3+} impurity ion which has an absorption at the excitation wavelength giving rise to resonance excitation of the transition of interest.

One of the rare earth activator which failed to produce luminescence in CaS is Nd in Lehmann's work [4]. But Nd^{3+} is an important lasing medium. It has the disadvantage that the sharp f-f Nd absorption lines are difficult to pump. The Ce-Nd energy transfer process has been made use of extensively to pump the Nd ion in glass or crystalline media in which cerium, neodymium and Lanthanum (an optically inactive dilutant) are soluble. Recently Brewer and Nicol [24] have reported such a phenomenon in Lanthanum sodium sulphate. An efficient fast red phosphor of $LaS:Ce,Nd$

which employs this Ce \longrightarrow Nd energy transfer mechanism has been reported [25]. Rastogi and Mor [12] have prepared a CaS:Cu,Nd phosphor and have observed Cu \longrightarrow Nd radiationless energy transfer process in electroluminescent emission. But a Ce \longrightarrow Nd energy transfer process in CaS has not been reported. So an attempt has been made here to prepare an electroluminescent CaS:Nd employing the Ce \longrightarrow Nd energy transfer process which can effectively and efficiently excite the Nd centres. The details of the preparation and the results of the various investigations are presented below.

To a weighed amount of CaS a certain amount of Nd acetate was added along with 5 wt percent of $\text{Na}_2\text{S}_2\text{O}_3$. A slurry of the mixture was then prepared in water. It was then slowly dried and the resulted mass was crushed and fired at 1050°C for 90 minutes with an added amount of sulphur. The emission from the sample was feeble. Three CaS:Ce,Nd phosphor samples were prepared as explained, but added with fixed amount (2.5 wt percent) of Ce and containing Nd in the ratio 1:3:6 as Nd acetate in the mixture taken before firing. It is seen that the emission efficiency is increased considerably compared to the CaS:Nd phosphor and a complete quenching of cerium emission is observed. The phosphor was then treated with fixed quantity of cupric acetate to form Cu_xS coating which further enhanced the emission.

The emission spectra of the phosphor were recorded with the set up described earlier. The EL spectrum of CaS:Nd

is found to have three bands (Fig.4.7). This is the type of emission observed by Shramer et al. [25]. They have attributed it to the transition from the band excitation to the ${}^4F_{3/2}$ level of the Nd^{3+} ion.

The spectra of the $CaS:Ce,Nd$ phosphors which contain different concentrations of Nd are shown in Fig.4.7. It can be seen that at lower concentration of Nd there occur small cerium emission bands. But as the Nd concentration is increased it is completely suppressed. The resulting EL emission consists of broad emission band on which two groups of sharp emission lines are superposed.

From the discussion on the general characteristics of the RE^{2+} and RE^{3+} ion it can be concluded that these emissions are due to the Nd^{2+} centres.

It was not possible to record any I.R. lines. This could be due to the drawback of the cell which was quite unsuitable for IR emission studies and to the poor sensitivity of the detection system at this wave length range.

The two sharp line emissions occurring at 550 nm and 600 nm can be attributed to ${}^2G_{7/2} \rightarrow {}^4I_{9/2}$ and ${}^4G_{5/2} \rightarrow {}^4I_{9/2}$ respectively [26]. The fine structure is due to the splitting of the energy levels involved in the transition.

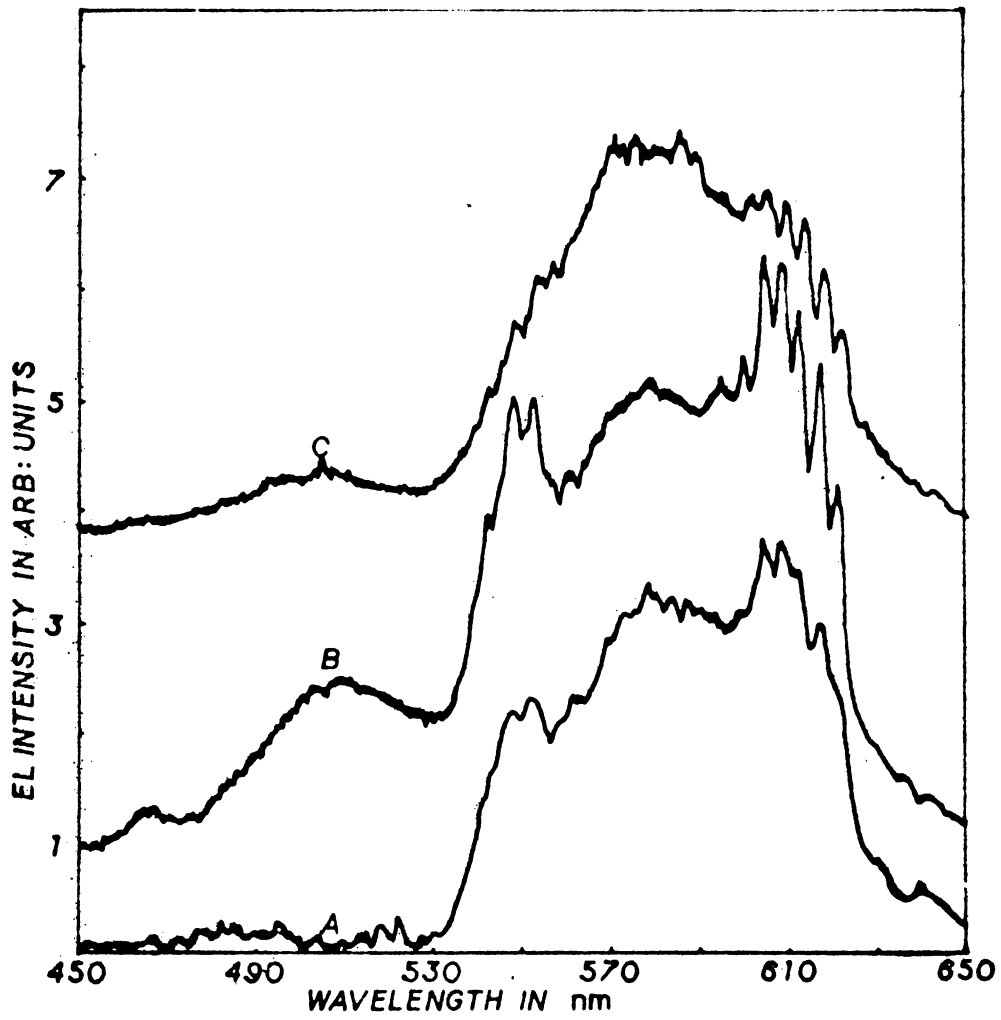


Fig.4.7. Curve A gives the EL spectrum of CaS:Nd, curve B and C are the EL spectra of CaS:Ce,Nd phosphor containing Nd in the ratio 1:6.

The log B vs log V plot of emission from this phosphor is a straight line. The frequency-brightness characteristic curve shows a behaviour similar to that described in the case of CaS:Ce.

The complete suppression of the cerium emission on introducing the Nd ions in CaS and the enhancement of the Nd²⁺ emission can be attributed to the Ce \longrightarrow Nd resonant radiationless energy transfer as explained by Brewer and Nicol [24].

In conclusion, it is observed that the EL emission from the CaS:Ce,Nd phosphor prepared in the laboratory consists of a broad band on which two groups of sharp lines are superposed. The emissions are attributed to Nd²⁺ luminescent centres. Cerium emission is completely suppressed in this phosphor due to the energy transfer process occurring in the phosphor.

4.6 Summary

An outline of the methodology adopted by Lehmann [5] for the preparation of highly efficient alkaline earth phosphors is presented along with the advantages of this class of phosphors over the conventional CL phosphors. The procedure adopted to prepare an alkaline earth phosphor viz. CaS:Ce is then presented. The EL emission spectra and their B-V and B-f characteristics are recorded. The techniques used to enhance the emission of this phosphor are also described. A brief description of the various

energy transfer processes occurring in luminescent crystals and the procedure of preparation of a set of CaS:Ce,Nd EL phosphors is presented. The observed quenching of the Ce emission in the CaS:Ce,Nd EL phosphor is explained as due to energy transfer from Ce to Nd ion. Various level transitions giving rise to different emission bands and lines are identified. The experimental B-f characteristic exhibits an anomalous behaviour and is explained by assuming that there exists a finite detrapping time for charge carriers which excite the luminescent centres.

References

1. P. Lenard; Fluorescence and phosphorescence, Ed. Pringseim (Interscience, NY, 1949).
2. A.J. Watchtel; J. Electrochem. Soc. 107(1960) 199.
3. W. Lehmann; Electrochem. Soc. 104(1957) 45.
4. N. Lehmann; J. of Lumin. 5(1972) 87.
5. B.B. Laud and V.W. Kulkarni; Physica Scripta, 18(1978) 494.
6. B.B. Laud and V.W. Kulkarni; J. Phys. Chem. Solids 39(1978) 555.
7. B.B. Laud and V.W. Kulkarni; Phys. Stat. Sol. (9) 51(1979) 269.
8. B.B. Laud and V.W. Kulkarni; Physica Scripta 22(1980) 415.
9. B.B. Laud and V.W. Kulkarni; Indian J. Pure and Appl. Phys. 19(1981) 4.

10. A.M.Rastogi and S.L.Morr; Indian J. Pure and Appl. Phys. [10] 19(1981) 1019.
11. A.M.Rastogi and S.L.Morr; Phys. Stat. Sol.(a) 63(1981) 75.
12. A.M.Rastogi; Indian J. Pure and Appl. Phys. [11] 19(1981) 1103.
13. A. Vecht, M. Waite, M.A.Higton and R. Ellis; J. Lumin. 24/25 (1981) 917.
14. W. Lehmann; J. Electrochem. Soc. 113(1966) 445.
15. W. Lehmann; J. Electrochem. Soc. 110(1963) 754.
16. W.A.Thornton; J. Electrochem. Soc. 107(1960) 895.
17. Y. Itoh, K. Kotab, K. Hirubayashi and K. Murase; Appl. Phys. A 26(1981) 227.
18. B. Asano, N. Yamashita, Y. Ogawa; Phys. Stat. Sol.(b) [1] 118 (1983) 89.
19. A.S. Marfunin; Spectroscopy, Luminescence and Radiation Centres in Minerals. Translated by V.V.Shiffer (Springer Verlag, New York 1979).
20. G. Destriau and H.F. Ivey; Proc. IRE, 43(1955) 1911.
21. P.Zalm; Philips Research Report (1956) 11, 353, 417.
22. W.A. Thornton; Phys. Rev. 102(1956) 38, 103(1956) 1585.
23. D. Curie; Luminescence in Crystals (Methuen, London 1963)
24. R.M. Brewer and M. Nicol; J. Lumin. 23(1981) 269.
25. E.G.Shramer, M. Leib and G. Huber; J. Limin, 24/25 (1981) 751.
26. G.Z. Zhong and F.J. Bryant; J. Phys. C. Solid State Phys. 13(1980) 4797.

CHAPTER V

A STUDY OF ELECTROLUMINESCENCE SPECTRUM OF CaS:Er PHOSPHOR
AND ENERGY LEVEL SPLITTING IN Er³⁺ ION

5.1 Introduction

Efficient electroluminescent (EL) materials having rare earth elements as activators are of great significance in many practical applications like narrow band emitters and EL lasers [1,2]. These materials are also suitable for producing a variety of colours in EL displays. Alkaline earth ions have relatively large size and consequently, chemical doping of these materials by rare earth ions can be accomplished easily. This makes them excellent host materials for the development of efficient rare earth doped EL phosphors emitting lines and bands in the entire range of the visible spectrum. Moreover spectroscopic analysis of emission from doped ions in these **materials** is relatively easy due to the simple crystal structure of the host lattice. However being of recent origin very little work has so far been done on this class of phosphors. In this chapter, the method of preparation and the EL emission spectrum of such a phosphor viz. CaS:Er are presented. The EL spectrum of this phosphor is found to have essentially nine emission bands covering ultraviolet, visible and near infrared regions. Most emission bands show well resolved line structure and the bands at 550 nm and 530 nm contain as many

as seven well resolved sharp lines. A comparison of the experimentally observed emission line splitting of the 550 nm band with energy splitting calculated on the basis of the point charge crystal field model shows that Er^{3+} ion can occupy Ca^{2+} substitutional sites as well as sulphur vacancy positions.

5.2 Phosphor preparation and study of EL

The Er doped calcium sulphide phosphor samples were prepared by firing a mixture of CaS(Riedel), 0.5 wt percent Er acetate (99.9 percent) and 5 wt percent Analar grade $\text{Na}_2\text{S}_2\text{O}_3$ (added as flux). The mixture with excess amount of sulphur was taken in a quartz test tube with a close fitting cap. Firing was done at 1000°C for 90 minutes in a stagnant sulphur atmosphere. The resulting powder gave a greenish yellow EL emission. It was found that a Cu_xS over coating on the phosphor particle boundaries considerably improved the emission efficiency of the phosphor.

The EL properties of this phosphor were studied by constructing an experimental cell with the sample. The cell was excited with a high voltage power supply and the spectrum was recorded with the set up described in detail in Chapter II.

5.3 Experimental results

A plot of the $\log B$ versus $\log V$ (Fig.5.1) is found to be a straight line which yields the brightness voltage

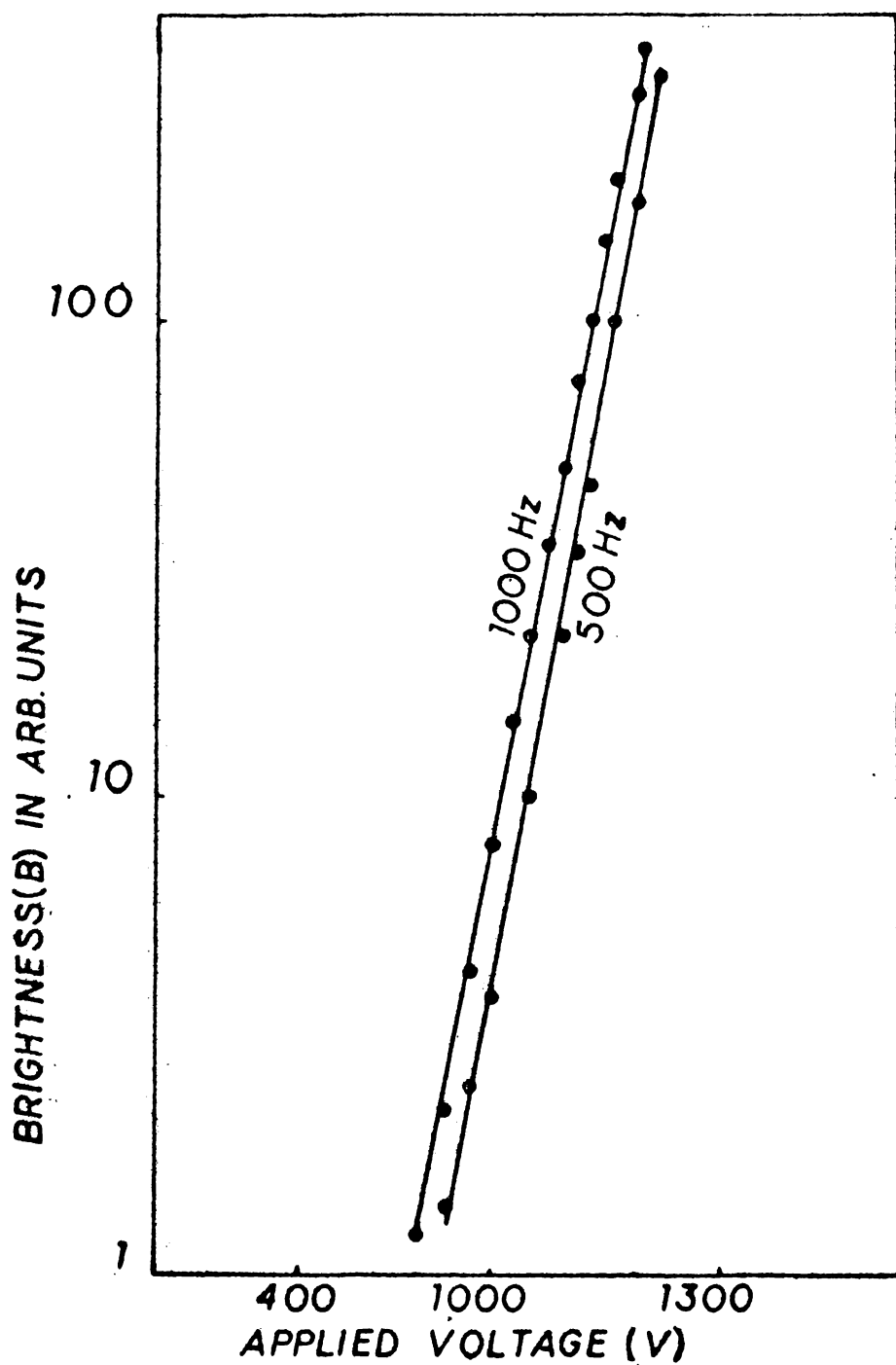


Fig.5.1. A plot of the $\log B$ vs $\log V$ of the EL CaS:Er phosphor at (A) 1000 and (B) 500 Hz.

relation

$$B = b V^n$$

where 'b' and 'n' are constants. This expression can be considered as a special case of Destriau relation [3].

$$B = B_0 \exp - \frac{b}{V}$$

which implies that carrier acceleration is occurring at a Mott-Schottky type barrier.

The decay time of the emission is found to be 370 μ s which compares well with the results obtained by Lehmann [4] in cathode ray excitation studies.

The emission spectrum of CaS:Er is shown in Fig.5.2. It can be seen that the emission spectrum consists of nine emission bands each consisting of several lines. The emission band occurring at the 530 nm and 550 nm is found to have maximum intensity. These emissions are due to the various transitions in the Er^{3+} ions introduced into the CaS lattice involving the f electrons. The wave lengths and the probable energy level transitions [5,6] giving rise to these emission groups are given in Table 5.1.

5.4 Energy level splitting in crystal fields

When an atom or ion is introduced into a crystal it is subjected to an inhomogeneous electric field produced by the ligands which destroy the isotropy of the free space. This results in the splitting of the free atom or

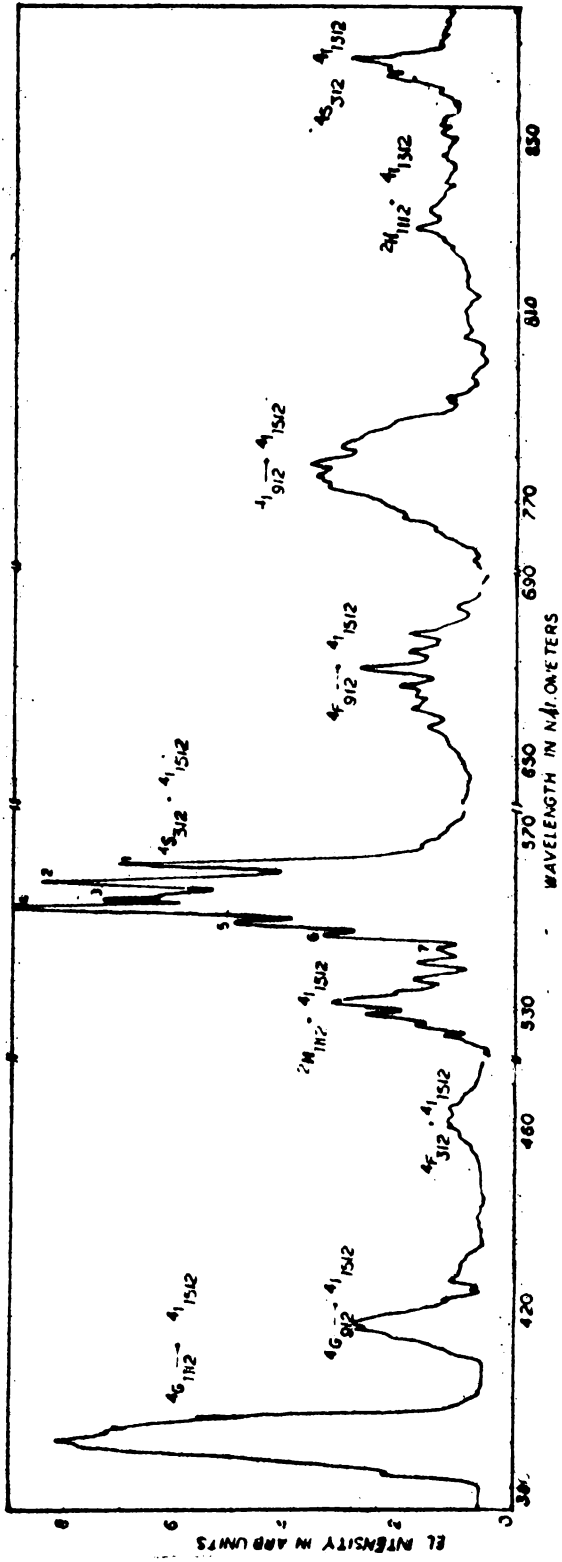


Fig. 5.2. The EL spectrum of CaS:Er phosphor.
 (The UV and the near IR regions are
 recorded at a higher gain)

Table-5.1. Wavelength and assignment of EL emission bands in CaS:Er phosphors.

| Band No | Emission | | Level transition |
|---------|-------------------|---------------------------------|---|
| | wave length nm | Wave number cm^{-1} | |
| 1 | 387.5 | 25806 | ${}^4G_{11/2} \longrightarrow {}^4I_{15/2}$ |
| 2 | 425.0 | 24096 | ${}^2G_{9/2} \longrightarrow {}^4I_{15/2}$ |
| 3 | 460.0 | 21739 | ${}^4F_{3/2} \longrightarrow {}^4I_{15/2}$ |
| 4 | 530.0 | 18868 | ${}^2H_{11/2} \longrightarrow {}^4I_{15/2}$ |
| 5 | 550.0 | 18182 | ${}^4S_{3/2} \longrightarrow {}^4I_{15/2}$ |
| 6 | 670.0 | 14925 | ${}^4F_{9/2} \longrightarrow {}^4I_{15/2}$ |
| 7 | 775.0 | 12903 | ${}^4I_{9/2} \longrightarrow {}^4I_{15/2}$ |
| 8 | 835.0 | 11976 | ${}^2H_{11/2} \longrightarrow {}^4I_{13/2}$ |
| 9 | 865.0 | 11561 | ${}^4S_{3/2} \longrightarrow {}^4I_{13/2}$ |

ion energy levels or in their modification. This effect is essentially due to the perturbation caused by the interactions between ligands and impurity ions. The problem of the influence of the surrounding ion on the energy levels of the central ion in a crystal field was first studied by Bethe [7]. He assumed the point charge crystal field model and used a group theoretical method to predict the multiplicities of the various degenerate levels from a knowledge of the symmetry of the environment of the ion.

The effect of the ligands is most pronounced for the elemental impurities of the three transition series. The effect is smaller by two orders of magnitude for lanthanide ion than for the 'd' electrons of the transition series ions. This is due to the fact that the 'f' electrons of the lanthanide ions are shielded from the surrounding environment by the filled s and p shells. For the actinide series the effect is intermediate between the transition element ions and the lanthanide ions [8,9].

In the present case where an Er^{3+} ion is introduced into a CaS lattice, we are encountering a situation in which a lanthanide ion is placed in a cubic crystal field of octahedral co-ordination. A detailed study [10] reveals that in such a crystal field the ground state ${}^4I_{15/2}$ of the Er^{3+} ion will be split into 5 sublevels viz. $\Gamma_8^{(3)}$, $\Gamma_8^{(2)}$, Γ_6 , $\Gamma_8^{(1)}$ and Γ_7 . So it can be expected that any band arising

from transitions to the ground state $^4I_{15/2}$ will consist of relatively closely spaced emission lines. If the upper level of the transition does not split then the possible number of lines can be five.

It is found that in the above spectra shown in Fig.5.2 the most intense band occurring at 550 nm consists of seven well resolved sharp lines. This, presumably, arises from the $^4S_{3/2} \rightarrow ^4I_{15/2}$ transition in the Er^{3+} ion in which the ground state will be split into five sub levels. In this case the upper state will not be split, and so this transition can give a maximum of only five emission lines. But the observed number of lines is **larger**. Hence, in order to explain this larger observed number of lines, the assumption was made that these emission lines fall into two emission groups arising from Er^{3+} centres occupying two different lattice sites. The lines in the two groups are numbered and the probable transitions are given in Table 5.2.

These groups of lines were then analysed, and from the energy level separations of the lines in the group the crystal field parameters were calculated employing a method suggested by Lea et al. [10] and later used by Bryant et al. [11,12]. The values of the parameters thus obtained were then compared with those calculated from the expression obtained from the point charge crystal field

Table 5.2. The ${}^4S_{3/2} \rightarrow {}^4I_{15/2}$ electroluminescent emission spectrum for Er doped CaS due to Er^{3+} luminescent centres occupying two different sites.

| Line No. | Group | Transition | Emission | | Ground state splittings (cm ⁻¹) | Relative intensities | Classification of Er^{3+} site |
|----------|-------|--|------------------|------------------------------|---|----------------------|--------------------------------------|
| | | | Wave length (nm) | Wave No. (cm ⁻¹) | | | |
| 5 | | ${}^4S_{3/2} \rightarrow \Gamma_8^{(1)}$ | 550.4 | 18169 | 19 | 53.2 | |
| 4 | | ${}^4S_{3/2} \rightarrow \Gamma_8^{(2)}$ | 553.4 | 18070 | 65 | 100 | Ca ²⁺ Substitutional site |
| 3 | A | ${}^4S_{3/2} \rightarrow \Gamma_7$ | 555.4 | 18005 | 237 | 76.5 | |
| 1 | | ${}^4S_{3/2} \rightarrow \Gamma_8^{(3)}$ | 562.8 | 17768 | | 74.5 | |
| 7 | | ${}^4S_{3/2} \rightarrow \Gamma_8^{(1)}$ | 544.2 | 18375 | 110 | 14.99 | |
| 6 | | ${}^4S_{3/2} \rightarrow \Gamma_8^{(2)}$ | 547.5 | 18265 | 96 | 36.2 | Er^{3+} occupying $S2^-$ vacancy |
| 5 | B | ${}^4S_{3/2} \rightarrow \Gamma_7$ | 550.4 | 18169 | 274 | 53.2 | |
| 2 | | ${}^4S_{3/2} \rightarrow \Gamma_8^{(3)}$ | 558.8 | 17895 | | 90.4 | |

model by assuming that the Er^{3+} impurity ion is occupying Ca^{2+} site and S^- vacancy positions. The details of the method of calculation are given below.

5.5 Theoretical calculation

According to Lea et al. [10] for the 4f states of the rare earth ions, within the manifold of angular momentum J composed of f-electron wave functions the most general operator equivalent potential with cubic point symmetry may be written as

$$H = B_4(O_4^0 + 5.O_4^4) + B_6(O_6^0 - 21.O_6^4) \quad \dots \quad 5.1$$

where,

$$\begin{aligned} O_4^0 &= 35J_z^4 - [30J(J+1)-25] J_z^2 - 6J(J+1) + 3J^2(J+1)^2 \\ O_4^4 &= \frac{1}{2} (J_+^4 + J_-^4) \\ O_6^0 &= 231 J_z^6 - 105[3J(J+1)-7]J_z^4 + [105J^2(J+1)^2 - 525J(J+1) \\ &\quad + 294]J_z^2 - 5J^3(J+1)^3 + 40J^2(J+1)^2 - 60J(J+1) \\ O_6^4 &= \frac{1}{4}[11J_z^2 - J(J+1)-38] [J_+^4 + J_-^4) + \\ &\quad \frac{1}{4}(J_+^4 + J_-^4) [11J_z^2 - J(J+1) - 38]. \end{aligned}$$

with x, y, z axes chosen along the $\langle 100 \rangle$, $\langle 010 \rangle$, and $\langle 001 \rangle$ directions. The coefficients B_4 and B_6 are factors which determine the scale of the crystal field splittings.

They are linear functions of $\langle r^4 \rangle$ and $\langle r^6 \rangle$, the mean fourth and sixth powers of the radii of the magnetic electrons and thus depend on the detailed nature of the magnetic ion wave functions. Since these are very difficult to calculate quantitatively it is customary to regard the coefficients B_4 and B_6 as parameters to be determined empirically.

For the numerical calculation of the eigen values, for each J manifold the $(2J+1) \times (2J+1)$ matrix is written down using the operator equivalent matrix element tabulated by Stevens [13] and Elliott and Steven [14]. These tables contain factors common to all the matrix elements, $F(4)$ and $F(6)$, and these are separated out in the calculation in order to keep the eigen values in the same numerical range for all ratios of the fourth and sixth degree terms. Then the Hamiltonian can be written as

$$H = B_4 F(4) \frac{O_4}{F(4)} + B_6 F(6) \frac{O_6}{F(6)} \quad \dots 5.2$$

where $O_4 = [O_4^0 + 5.O_4^4]$ and $O_6 = [O_6^0 - 21.O_6^4]$

In order to cover all possible values of the ratio between the fourth and sixth degree terms, we take

$$B_4 F(4) = Wx \quad \dots 5.3$$

$$B_6 F(6) = W(1 - |x|) \quad \dots 5.4$$

where x is a dimensionless parameter which can have values between -1 and $+1$. It follows that

$$\frac{B_4}{B_6} = \frac{x}{1-|x|} \frac{F(6)}{F(4)} \quad \dots 5.5$$

so that $B_4/B_6 = 0$ for $x = 0$, while $B_4/B_6 = \pm \alpha$ for $x = \pm 1$.

Rewriting equation (5.2),

$$\mathcal{H} = W \left[x \left(\frac{O_4}{F(4)} \right) + (1-|x|) \left(\frac{O_6}{F(6)} \right) \right] \quad \dots 5.6$$

The term expressed in the square bracket represents a matrix whose eigen vectors correspond to the most general combination of fourth and sixth degree crystal fields, and whose eigen values are related to the crystal field energy levels by a scale factor W defined by equation 5.3 and 5.4. The diagonalization of this matrix was performed and for each J manifold x was allowed to take values $0, \pm 0.2, \pm 0.4, \pm 0.6, \pm 0.8, \pm 1.0$. The results thus obtained for the eigen values of Er^{3+} ion which is of interest with $J=15/2$ are summarised in the diagram shown in Fig.5.3. This corresponds to the ground level splitting pattern of Er^{3+} ion in a cubic crystal field and also shows that it splits into 5 sub levels viz. $\Gamma_8^{(3)}, \Gamma_6, \Gamma_8^{(2)}, \Gamma_8^{(1)}$ and Γ_7 .

One can find the sign of the scale factor W and that of the parameter x directly from the signs of B_4 and B_6 as follows:

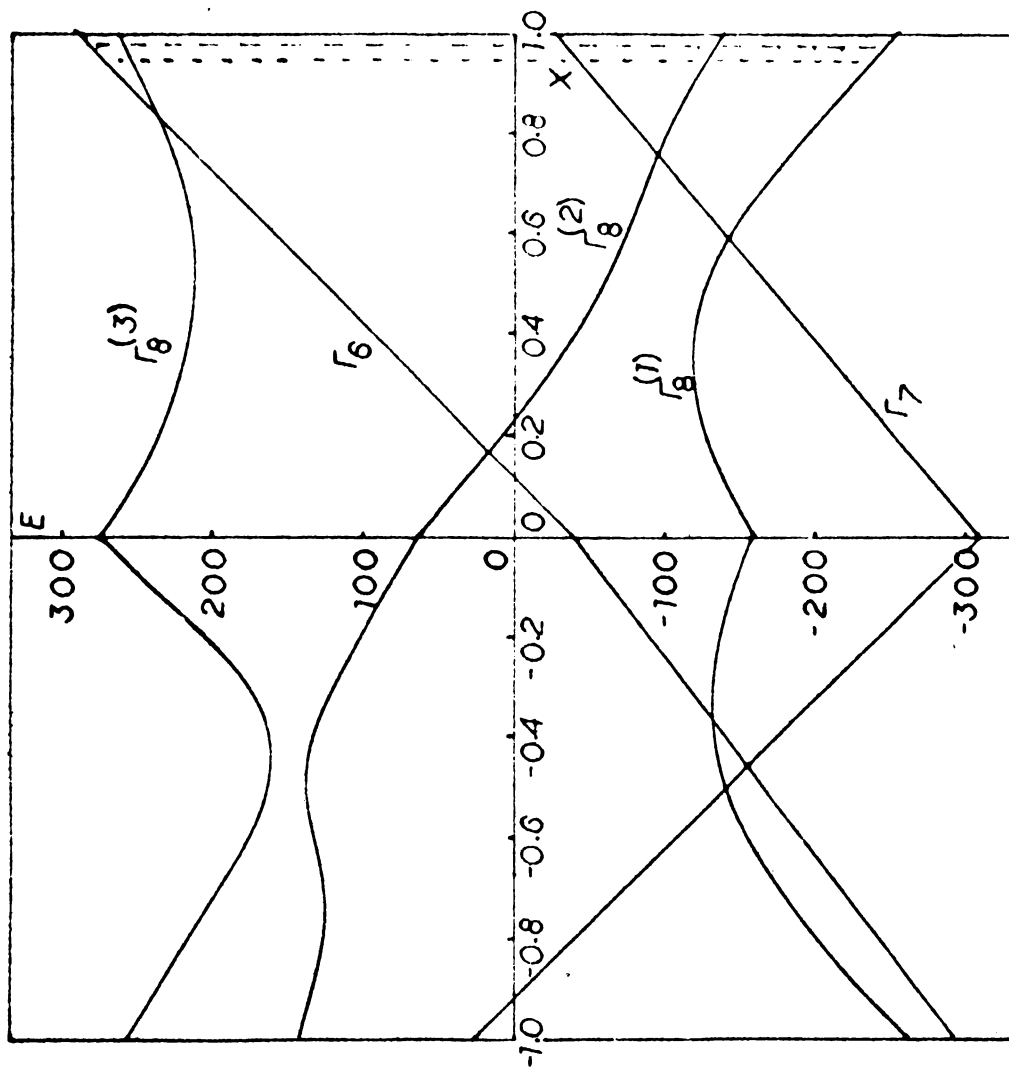


Fig. 5.3. The splitting pattern of the $4I_{15/2}$ manifold of the Er^{3+} ion in the CaS lattice. E is in cm^{-1} ; x is a diameter parameter defined in the text, the broken lines indicate the values of x used to evaluate the scale factor \tilde{w} (in cm^{-1}) required for the experimental determination of crystal field parameters.

(1) From equation 5.4, from which the sign of W is determined by the sign of B_6 since $(1-|x|)$ is always positive for $-1 < x < +1$.

(2) From equation 5.5 which shows the sign of x is determined by the sign of B_4/B_6 , since $F(6)$ and $F(4)$ are both +ve for all J 's. The sign of B_4 and B_6 can be found out from the point charge crystal field model for the geometrical co-ordination factors A_4 and A_6 . There are three types of cubic co-ordination corresponding to 4, 6 or 8 equidistant charges Ze . For each of these, the point charge model gives the following results.

Table 5.3. Point-charge model parameters

| Type of co-ordination | $B_4=A_4 \langle r^4 \rangle \beta$ | $B_6=A_6 \langle r^6 \rangle \gamma$ |
|-----------------------|--|--|
| Tetrahedral (4) | $\frac{-7}{36} \frac{Ze^2}{R^5} \langle r^4 \rangle \beta$ | $+ \frac{1}{18} \frac{Ze^2}{R^7} \langle r^6 \rangle \gamma$ |
| Octahedral (6) | $\frac{+7}{16} \frac{Ze^2}{R^5} \langle r^4 \rangle \beta$ | $+ \frac{3}{64} \frac{Ze^2}{R^7} \langle r^6 \rangle \gamma$ |
| Cubic (8) | $\frac{-7}{18} \frac{Re^2}{R^5} \langle r^4 \rangle \beta$ | $+ \frac{1}{9} \frac{Ze^2}{R^7} \langle r^6 \rangle \gamma$ |

Here R is the distance of the co-ordinating charges Ze from the magnetic ions, 'e' is the charge on the electron, γ is

the radius of the ion β and γ are the Steven's multiplication constants. The values of β and γ for an Er^{3+} ion is 0.444×10^{-6} and 2.0699×10^{-6} respectively. Freeman and Watson [15] gave the value of $\langle r^4 \rangle$ and $\langle r^6 \rangle$ for the 4f electrons of Er^{3+} ion as $1.125 A_H^4$ and $3.978 A_H^6$ respectively where A_H is the Bohr radius. The values of W and x are both positive since the Er^{3+} ion in CaS is experiencing an octahedral crystal field.

In order to explain the occurrence of a number of lines in excess of number of sub levels of ${}^4I_{15/2}$ of Er^{3+} ion, the observed number of lines can be classified into two groups viz. Group A and Group B (Table 5.2). Group A comprises lines 5,4,3,1 and group B contains lines 7,6,5,2. These emissions are apparently due to the transition from the ${}^4S_{3/2}$ upper level to the ground state sub levels $\sqrt{8}^{(1)}$, $\sqrt{8}^{(2)}$, $\sqrt{7}$ and $\sqrt{8}^{(3)}$ of the Er^{3+} ion occupying two different lattice sites. The emission arises from transition to the $\sqrt{6}$ level, however, is not evident. The energy level separation of these groups of lines was then compared with the splitting pattern shown in Fig.5.3. The best fit with the observed energy level splitting as given in Table occurs for lines of group A when $x = 0.95$ and $W = 0.797 \text{ cm}^{-1}$. The values of W were computed at intervals of 0.01 for x . Substituting the values of W and x and calculating $A_4 \langle r^4 \rangle$ and $A_6 \langle r^6 \rangle$ from the expression for B_4 and B_6 one get the experimental values

$$A_4 \langle r^4 \rangle = 284.21 \text{ cm}^{-1}, \text{ and}$$

$$A_6 \langle r^6 \rangle = 1.389 \text{ cm}^{-1}$$

For the second group B the best fit occurs when $x = 0.98$ and $W = 0.929 \text{ cm}^{-1}$ giving

$$A_4 \langle r^4 \rangle = 342.18 \text{ cm}^{-1}$$

$$A_6 \langle r^6 \rangle = 0.652 \text{ cm}^{-1}$$

From the value of x it can be seen that the lowest sub level of the ${}^4I_{15/2}$ ground state of Er^{3+} ion in CaS lattice is $\sqrt{8}^{(1)}$.

Calcium sulphide crystallises in sodium chloride structure. So an Er^{3+} ion introduced as an activator in CaS lattice can most readily occupy a Ca^{2+} substitutional site surrounded by 6S^{2-} ions. Calculating the crystal field parameter on the basis of the point charge model and assuming that the ion is in the octahedral crystal field the values obtained are

$A_4 \langle r^4 \rangle = 284.21 \text{ cm}^{-1}$ with 6.48 percent inward relaxation and $A_6 \langle r^6 \rangle = 1.380 \text{ cm}^{-1}$. These values agree very well with those obtained experimentally for the lines of Group A. (284.21 and 1.389 cm^{-1} respectively).

By taking the ionic radii of the ions as given by Pauling it can be seen that the interstitial radius of the CaS lattice, which is the maximum radius of the solid sphere

which could be placed interstitially in the lattice without any deformation of the latter is much smaller than the radius of the Er^{3+} ion. So it can occupy only an anion or a cation site. The calculations described earlier have conclusively shown that there are luminescent centres occupying Ca^{2+} sites. In order to find out the site of the Er^{3+} ion giving rise to the second group of emission lines, the calculations based on point charge crystal field model assuming that the Er^{3+} ion occupy a S^{2-} vacancy position which, however, is not a very stable position for positive ion is made. This assumption is supported by the observation of an analogous defect centre formation in alkali halide crystals where interstitial halogen atoms have been found to be trapped by cation vacancies [16]. The relatively high ionicity of CaS and the observed violation of charge compensation principles of this compound are factors which further support this assumption [4].

The calculation based on this idea of Er^{3+} occupying S^{2-} vacancy yields a value for $A_4 \langle r^4 \rangle = 339.612 \text{ cm}^{-1}$ with 5.8 percent inward relaxation and $A_6 \langle r^6 \rangle = 1.715 \text{ cm}^{-1}$. The excellent agreement of the calculated values and those observed experimentally (342.18 and 0.652 cm^{-1} respectively) supports the possibility of Er^{3+} ion occupying an S^{2-} vacancy position.

5.6 Conclusion

Er^{3+} doped EL CaS phosphors were prepared. It is found that a Cu_xS coating on the phosphor particle boundaries enhances the EL emission. The observed emission has nine groups of lines. The groups at 530 nm and 550 nm contains as many as seven distinct lines. The occurrence of these lines is explained on the basis of the crystal field splitting calculations as put forward by Lea et al. and applied by Bryant et al. It is found that these lines fall into two groups and arise from Er^{3+} luminescent centres occupying Ca^{2+} substitutional sites and S^{2-} vacancies in the CaS lattice.

References

1. G. Zhong and F.J. Bryant; Solid State Commun. 39(1981) 907.
2. J. Benoit, P. Benalloul and B. Blanzat; J. Lumin. 23(1981) 175.
3. G. Destriau and H.F. Ivey; Proc. IRE, 10(1955) 1911.
4. Lehmann (Private Communication)
5. M. Bancie Grilloit and E. Grilloit; 12/13(1976) 681.
6. A. Garcia and C. Fouassion; J. Lumin. 24/25(1981) 743.
7. H. Bethe; Ann. Phys. Lpz. 3(1929) 133.
8. B.N. Figgis; Introduction to Ligand Fields (Wiley Eastern Limited, New Delhi, Bangalore, Bombay, Calcutta, 1971).

9. F. Albert Cotton; Chemical Application of Group Theory, (Wiley, Eastern Limited, New Delhi, Bangalore, Bombay, Calcutta, 1971).
10. K.R. Lea, M.J.M. Leask and W.P. Wolf; J. Phy. Chem. Solids, 23(1962) 1381.
11. G.Z. Zhong and F.J. Bryant; J. Phys. C. Solid. St. Phys. 13(1980) 4797.
12. C.C. Yu and F.J. Bryant; J. Lum. 18/19 (1979) 841.
13. K.W.H. Stevens; Proc. Phys. Soc. London, A 65(1952) 209.
14. R.J. Elliott and K.W.H. Stevens; Proc. Roy. Soc. A 218(1953) 553.
15. A.J. Freeman and R.E. Watson; Phys. Rev. 127(1962) 2058.
16. M.N. Kabler; Point Defects in Solids Vol.1. (Plenum Press, London 1972) 374.

CHAPTER VI

ELECTROLUMINESCENCE IN CaS:Sm, CaS:Dy and CaS:Mn PHOSPHORS

6.1 Introduction

In continuation of the work presented in the previous two chapters here the method of preparation and the results of the various investigations made on CaS phosphors doped with Sm, Dy and Mn are presented. The rare earth element samarium is used as a luminescent activator to get line emission in the yellow, red and IR regions. Dysprosium is found to emit in the blue, green, yellow and IR regions, when introduced into suitable host lattices. Manganese is the most efficient activator in ZnS. Lehmann has prepared CaS:Sm, CaS:Dy and CaS:Mn cathodoluminescent phosphors [1]. He has obtained an efficiency of 12 percent for CaS:Sm and 16 percent for CaS:Mn. Vecht et al. [2] have prepared a few CaS EL phosphors. Since these compounds form a new class of phosphors, no detailed work has so far been carried out on them. Sm and Dy are used as activators in ZnO and ZnS hosts [3-6]. An energy transfer process occurring from Cu \longrightarrow Sm in ZnS:Cu,Sm has been reported earlier in PL experiments [7]. In the present chapter, the EL emission spectra of these phosphors are presented together with the probable level transitions giving rise to the various emissions. Results of the calculation made to locate the lattice site of the luminescent Sm ion in CaS are also presented.

6.2 Phosphor preparation and experimental set up

The method used for the preparation of CaS:Ce and CaS:Er are used here also to synthesise the phosphors viz. CaS:Sm, CaS:Dy and CaS:Mn. The details of the method are given in Chapter IV. In these samples, the activators were added in the prefired mixture as their acetates. The slurry preparation and the firing process are as described previously.

The experimental set up used for recording the EL spectrum and that for the B-V and B-f characteristics are described in detail in Chapter II.

6.3 EL of Samarium doped calcium sulphide

The EL emission spectrum of CaS:Sm recorded with the experimental cell is shown in Fig.6.1. It can be seen that the spectrum consists of a broad emission band on which two groups of sharp lines are superposed along with a weak unresolved band. The groups of sharp lines occur at 560 and 600 nm while the weak band appears at 650 nm. The broad emission band can be attributed to the d-f transition in the Sm impurity [8]. From the discussion given in Chapter IV regarding the features of the RE²⁺ and RE³⁺ ions and from the spectrum shown in Fig.6.1 it becomes quite plausible to assume that the Sm impurity is existing in the CaS lattice as a Sm²⁺ ion. The observed sharp lines are due to the electronic level transitions occurring in the shielded 4f electron states. The transition giving rise to the lines 560 and 600 nm and

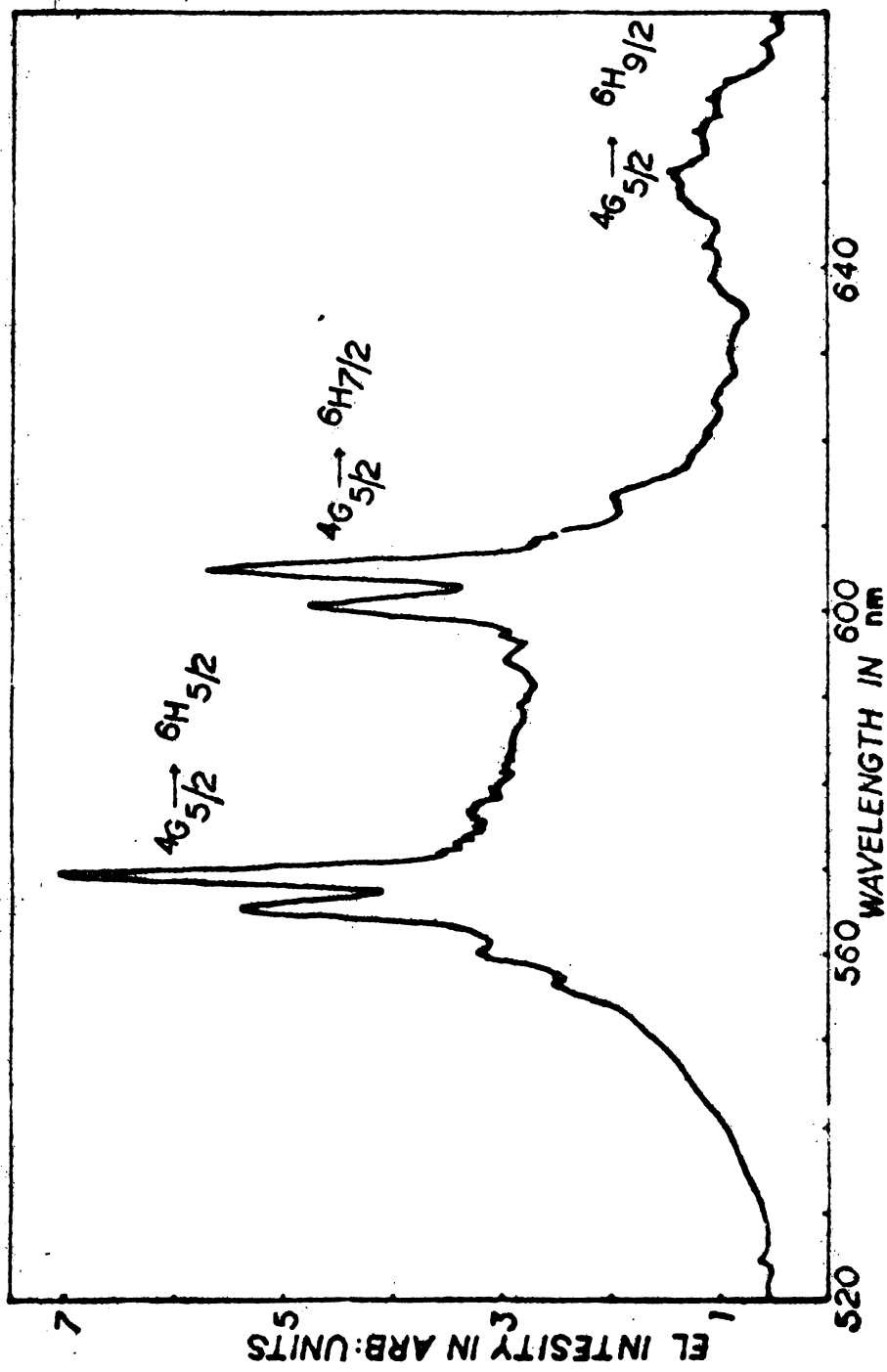


Fig.6.1. EL spectrum of CaS:Sm phosphor

the band at 650 nm can be assigned to ${}^4G_{5/2} \rightarrow {}^6H_{5/2}$; ${}^4G_{5/2} \rightarrow {}^6H_{7/2}$ and ${}^4G_{5/2} \rightarrow {}^6H_{9/2}$ [8]. The occurrence of the sub levels is due to the splitting of the free ion term of the Sm^{3+} under the influence of the ligands of the surrounding ions. In the present case, since CaS crystallises in NaCl structure, an impurity ion occupying a Ca^{2+} site will experience a cubic crystal field with octahedral co-ordination. In such an environment [9] the free ion terms with $J=5/2$ and $J=7/2$ will split into two and three sub levels respectively. So evidently, the first group emission will consist of four lines while the second will comprise of six lines.

In order to identify the various sub levels giving rise to the six lines occurring in the ${}^4G_{5/2} \rightarrow {}^6H_{7/2}$ level and also to find out the level separation between these sub levels an analysis of the spectrum has been carried out. It is found that these six lines can be grouped into two sets consisting of three lines. Each group is separated by an average of 325 cm^{-1} . The lines in each group are found to be separated by 126 cm^{-1} and 78 cm^{-1} . The wave lengths of the emission lines, the probable levels involved and the actual values of the level separations are given in Table 6.1.

TABLE-6.1

| GROUP I | | | | GROUP II | | | | |
|-----------------------------|----------------|----------------|------------------------------------|--|-----------------------------|----------------|----------------|------------------------------------|
| Probable Transi- tion | Wave length | Wave number | $\Delta\nu$ in cm ⁻¹ | $\Delta\nu$ in cm ⁻¹ be- tween groups | Probable Transi- tion | Wave length | Wave Number | $\Delta\nu$ in cm ⁻¹ |
| $4G_{5/2}$ to $6H_{7/2}$ | λ | ν | | | $4G_{5/2}$ to $6H_{7/2}$ | λ | ν | |
| $\Gamma_5 - \Gamma_8$ | 6010 | 16638 | | 331 | $\Gamma_7 - \Gamma_8$ | 6132 | 16307 | |
| | | | 120 | | | | | 134 |
| $\Gamma_5 - \Gamma_6$ | 5967 | 16578 | | 316 | $\Gamma_7 - \Gamma_6$ | 6082 | 16442 | |
| | | | 71 | | | | | 87 |
| $\Gamma_5 - \Gamma_7$ | 5942 | 16829 | | 300 | $\Gamma_7 - \Gamma_7$ | 6050 | 16528 | |

It is to be noted that the difference in values of the level separations obtained from the two series is within the limit of experimental error which is $\sim 25 \text{ cm}^{-1}$.

The method put forward in Chapter V to identify the site of the Er^{3+} ion in CaS giving rise to the emission lines has been used in this case also to identify the site of the luminescent Sm^{2+} ion in the CaS lattice.

The splitting pattern of the $6H_{7/2}$ level of the Sm^{2+} ion in a cubic field is given in Fig.6.2. An exact fit with the observed energy level separation with the above pattern occurs for the scale factor $W = 8.306$ and $x = 0.43$.

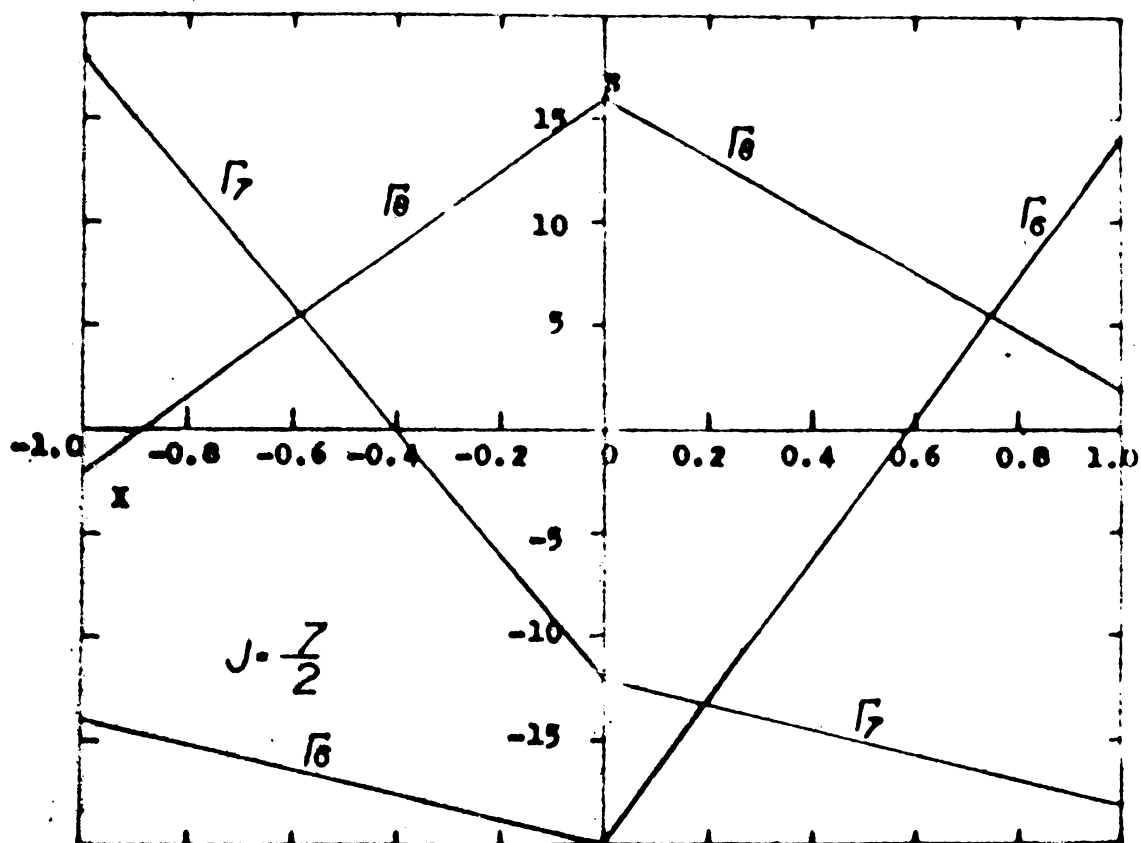


Fig.6.2. The splitting pattern of the ${}^6H_{7/2}$ manifold of the Sm^{3+} ion in the CaS lattice.

From Chapter V it can be seen that

$$B_4 = A_4 \langle r^4 \rangle \beta = \frac{Wx}{F(4)} \quad \dots (1)$$

and

$$B_6 = A_6 \langle r^6 \rangle \gamma = \frac{W(1-|x|)}{F(6)} \quad \dots (2)$$

where β and γ are the Steven's multiplication constants and have values $\beta = 25.012 \times 10^{-4}$ and $\gamma = 0$ for Sm^{3+} . Since $\gamma = 0$, we can compute the parameter $A_4 \langle r^4 \rangle$ only. From equation (1) and from the value of W and x we get

$$A_4 \langle r^4 \rangle = 24 \text{ cm}^{-1}$$

From the point charge crystal field model the parameter $A_4 \langle r^4 \rangle$ can be calculated from the equation

$$A_4 \langle r^4 \rangle = \frac{7}{16} \frac{Ze^2}{R^5} \langle r^4 \rangle \beta$$

where R is the distance of the co-ordinating charges Ze from the impurity ion and 'e' is the charge on the electron. The value of $\langle r^4 \rangle$ has been given by Freeman and Watson [10] as $1.897 (A_H^4)$ where A_H is the Bohr radius of the f electrons. The calculated value of the parameter is found to be 24 cm^{-1} with an inward relaxation of 14 percent.

Thus there is fairly good agreement between the experimental and theoretical values and hence it can be concluded that the Sm ion introduced into the CaS lattice occupies a Ca^{2+} substitutional site.

Figure 6.3 shows the log B versus log V plot of the EL emission from this phosphor. The B-f plot is as shown in Figure 6.4 and have the same characteristics as reported in the case of CaS:Ce phosphor. It appears that the reasons suggested for the occurrence of such a characteristic in the case of CaS:Ce can be extended to this phosphor sample also.

6.4 EL of CaS:Dy

The EL spectrum of the CaS:Dy is shown in Fig.6.5. It consists of five emission bands. The band with the maximum intensity occurs at 580 nm. The emission wave length and the probable level transitions giving rise to these emissions are given in Table 6.2 [11]

TABLE 6.2. The wave lengths and the probable level transitions giving rise to these emissions in CaS:Dy.

| Wave length(nm), | Level Assignment |
|------------------|--|
| 457.5 | ${}^4G_{9/2} \rightarrow {}^6H_{15/2}$ |
| 485.0 | ${}^4I_{5/2} \rightarrow {}^6H_{15/2}$ |
| 580.0 | ${}^4G_{9/2} \rightarrow {}^6H_{13/2}$ |
| 670.0 | ${}^4G_{9/2} \rightarrow {}^6H_{11/2}$ |
| 760.0 | ${}^4G_{9/2} \rightarrow {}^6H_{9/2}$ |

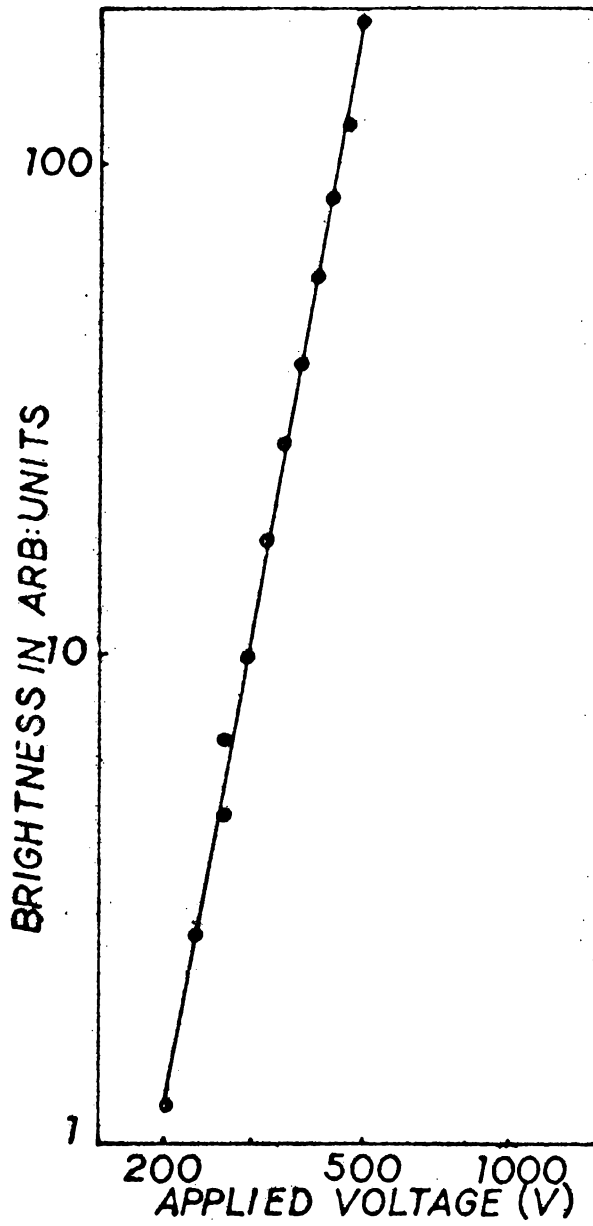


Fig.6.3. log B vs log V plot of a CaS:Sm EL cell.

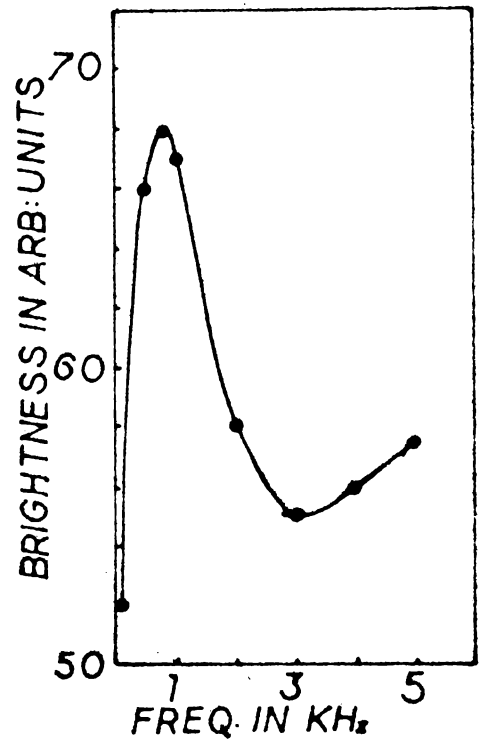


Fig.6.4. B vs f plot of a CaS:Sm EL cell.

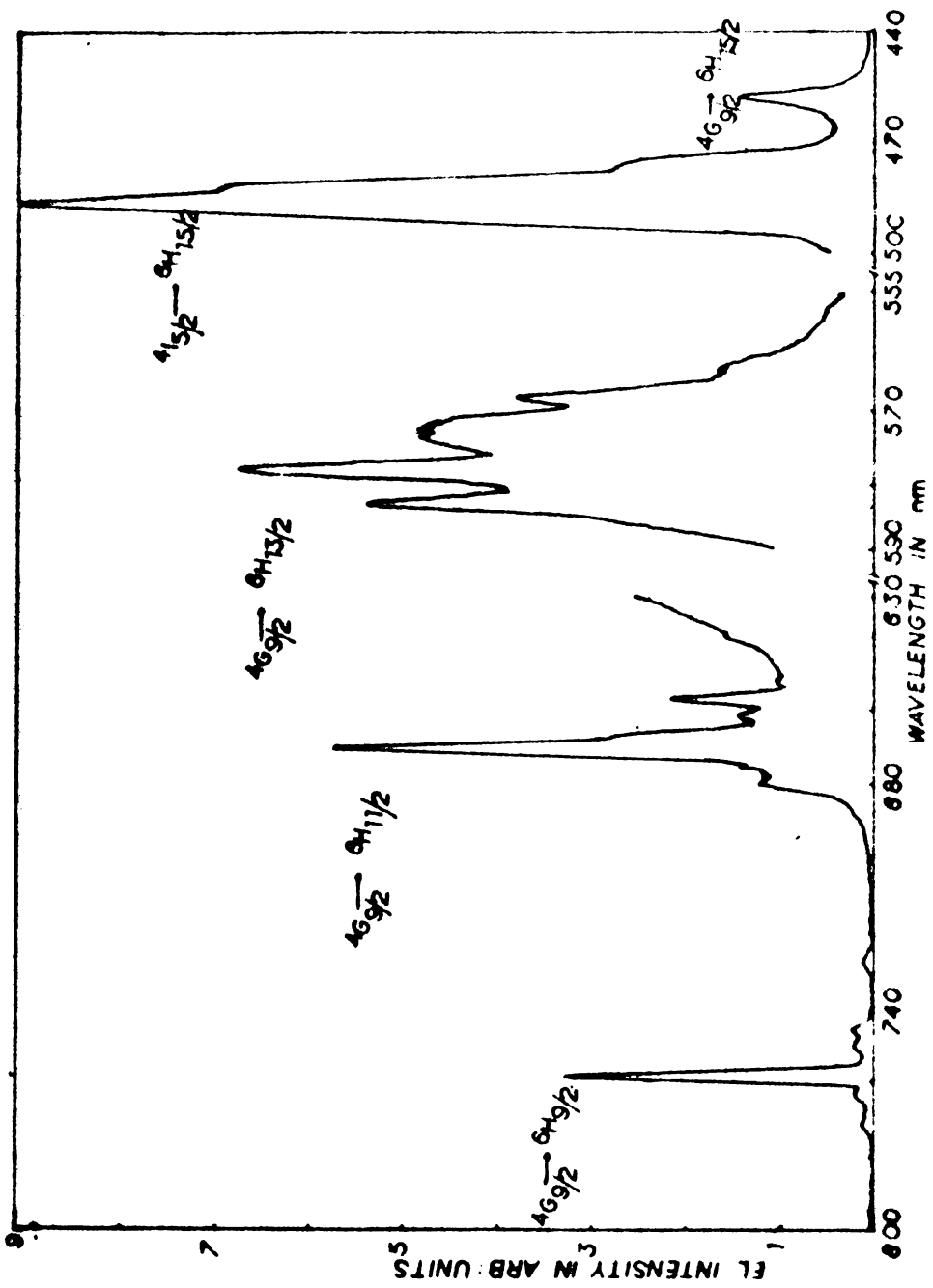


Fig. 6.5. EL spectrum of CaS:Dy phosphor.
 (The regions other than 500 nm are
 recorded at a much higher gain).

The most intense band occurring at 580 nm originates from ${}^4G_{9/2} \rightarrow {}^6H_{13/2}$ and consists of five well resolved lines. But it can have a maximum of 18 lines, since the upper and lower levels can split into 3 and 6 levels in a cubic crystal field [9]. So it can be assumed that some of the lines have merged together to give somewhat broader peaks. So for this spectrum the type of analysis put forward in the previous case becomes difficult. An important feature of the spectrum is that the maximum intensity occurs for a transition for which the lower level is not the ground state of the ion.

Such effect has been observed in this ${}^4G_{9/2} \rightarrow {}^6H_{13/2}$ transition in the Dy^{3+} ion previously [11] and is explained as due to the hyper sensitive nature of this transition.

It is observed that one or two transitions of each lanthanide is extremely sensitive to the environment. They exhibit a normal intensity, for example, in aquo ions but have a marked increase in intensity relative to all other observed transitions in certain environment. These are termed as hypersensitive transitions. This has been explained as due to the effect of the polarization of the ligand by the f-electrons of the Ln^{2+} which extends the sphere of influence of the f-electrons. So as long as there is no centre of inversion, the induced dipoles can interact and yield a non-vanishing dipole moment. This, then interacts with the radiation field, and the result is that a normally forbidden electric dipole transition becomes allowed [11].

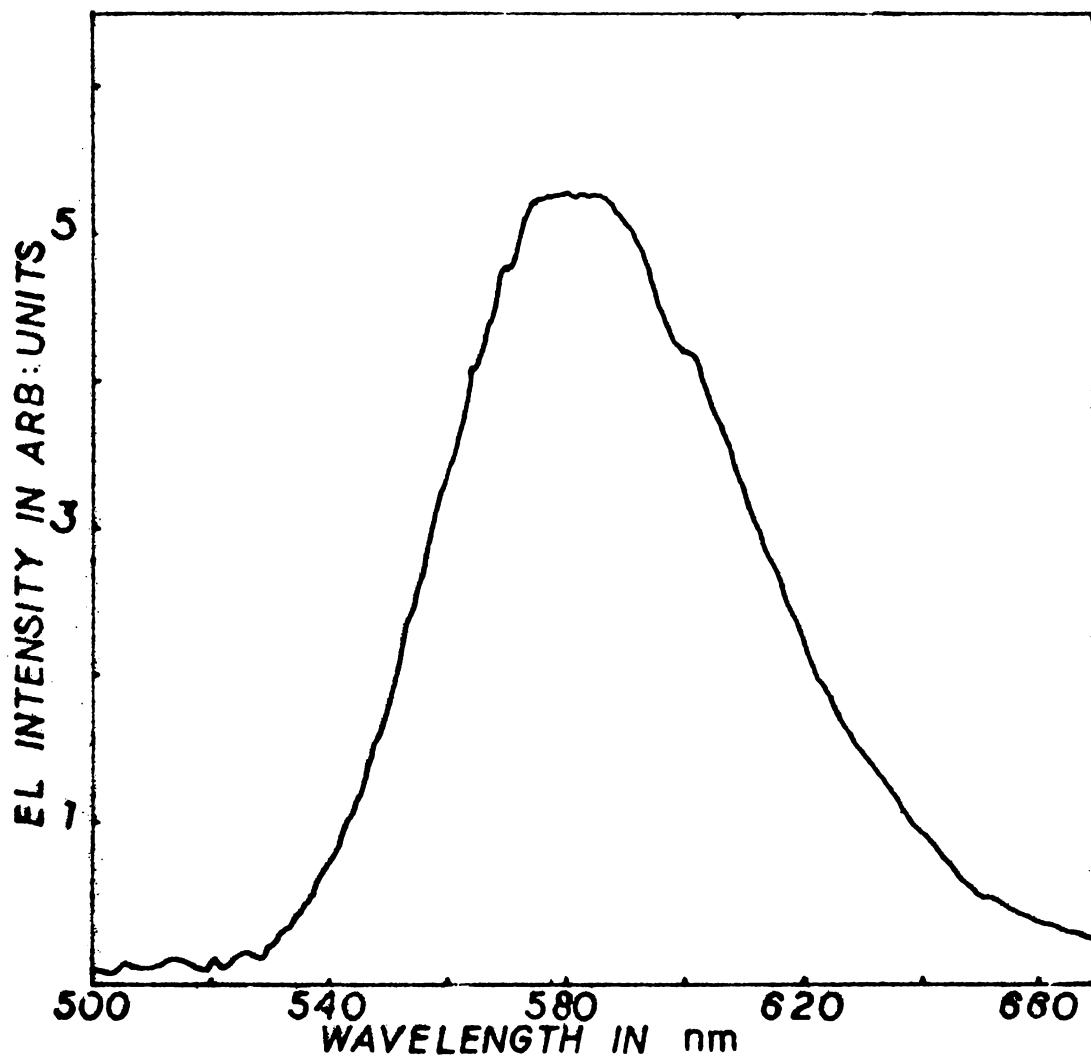


Fig.6.6. EL spectrum of CaS:Mn phosphor.

In the present case it can be speculated that such an effect is taking place in the case of Dy^{3+} ion in CaS lattice also. However, the hypersensitive nature of this transition can be established only after doing some more detailed experiments.

The brightness voltage characteristics and frequency dependence of these phosphors are also found to show the same characteristics as observed in the case of other CaS phosphors.

6.5 CaS:Mn EL phosphor

The EL spectrum of CaS:Mn is given in Fig.6.6. It consists of a single broad band with its maxima at 580 nm. This is due to the well known $4T_1 \rightarrow 6A_1$ [12] transition in the Mn^{2+} ion. The phosphor prepared is found to be less efficient than the CaS:Ce and far inferior to ZnS:Mn.

6.6 Conclusion

The EL spectra of CaS:Sm, CaS:Dy and CaS:Mn are presented. The CaS:Sm gives rise to three groups of emission lines while the CaS:Dy exhibits five emission groups. The probable level transitions giving rise to these emission bands are identified. An analysis of the CaS:Sm spectrum is carried out and the level separations of the sub levels of the $4G_{5/2}$ and $6H_{7/2}$ of the Sm^{2+} ion are estimated. On the basis of a crystal field parameter calculation the site of the Sm^{2+} in CaS is identified. The larger intensity **due to the**

${}^4G_{9/2} \rightarrow {}^6H_{13/2}$ in **CaS:Dy** is assumed to be due to hypersensitive nature of the transition. The brightness-voltage characteristic and the frequency dependence of brightness are also presented.

References

1. W. Lehmann; J. Lumin. 5(1972) 87.
2. A. Vecht, M. Waite, M.A. Higton and R.Ellis;
J. Lumin. 24/25 (1981) 917.
3. S. Bhushan, A.N. Pandey, B. Raokaza;
Phys. Status Sol. (a) [1] 53(1979) K57.
4. S. Bhushan, A. Pandey and B. Raokaza;
J. Lumin. [1] 20(1979) 29.
5. M. Frankowick; J. Krieszyna, W. Smigeelska;
Bull. Acad. Pol. Sci. Ser. Sci. Maths.
Astron. and Phys. [6] 23(1975) 717.
6. J. Benoit, P. Benalloul and B. Blanzat; J. Lumin.,
23(1981) 190.
7. W.W.Anderson, S. Razi and D.J.Walsh;
J. Chem. Phys. 43(1965) 1153.
8. A.N. Tarashchan; Luminescence of materials,
Kiev Nankova dumka 1978.
9. K.R.Lea, M.J.M. Leask and W.P.Wolf;
J. Phys. Chem. Solids 23(1962) 1381.
10. A.J.Freeman and R.E. Watson; Phys. Rev. 127(1962) 2058.
11. Shyama P. Sinha; Systematics and the properties of
the lanthanide, Ed. S.P.Sinha (D. Reidel
Publishing Co. Dordrecht, Boslan, Lanchaster,
1983).
12. T. Skolnick; J. Phys. D. Appl. Phys. 14(1981) 301.

CHAPTER VII

A STUDY ON DC POWDER EL DEVICES

7.1 Introduction

Presently available powder EL devices are of two types: (1) AC Powder EL cell and (2) DC Powder EL cell, [1]. The AC powder cells are the earliest and the most common. These are essentially Destriau type cells which consist of the electroluminescent phosphor suspended in a dielectric sandwiched between two electrodes. An efficient DC powder EL device, which is the subject of discussion in this Chapter was first reported by Vecht et al. [2]. Their results triggered the interest of many workers in this field. Vecht et al. have developed information display panels using ZnS:Cu,Mn [3] and, recently, CaS:Ce [4] phosphors. Yashiyama et al. [5,6] have successfully fabricated a TV display panel based on DC powder technology. Hiroshi Kawarada et al. have fabricated a TV display panel of 50176 picture elements [7]. It is reported that, compared to the AC powder panels, DC devices can be excited to higher (excitation) levels in the pulsed excitation mode thus producing higher brightness level. Cross talk effect is less in this type of panels because of their highly non-linear brightness-voltage characteristics. Moreover, the scanning circuit of these devices will be simpler due to the DC mode of operation. The green emitting CaS:Ce system is

very significant in this context due to its fairly broad band emission ranging from 450 nm to 650 nm, which when used with appropriate filters can produce red, yellow, green and blue displays [4]. So, some attempts were made to fabricate a few such devices using ZnS:Cu,Mn and CaS:Ce. Eventhough the conventional ZnS:Cu,Mn cells have been prepared, no detailed investigations on these devices are presented here, since their characteristics are quite well known [2,8]. This chapter essentially contains the preparation details of a ZnS:Cu,Mn device and of CaS:Ce device together with the results of some investigations made on the latter. In addition a brief outline of the DC powder EL device fabrication technology, the DC forming process and an analysis of the various electrical characteristics of such devices are also given.

7.2 DC powder cell fabrication

The phosphors for the preparation of DC powder EL cells of ZnS:Cu,Mn can be prepared either by the conventional slurring technique or by the simultaneous activation; i.e. by precipitating the phosphor from solution containing appropriate amounts of Cu and Mn. The latter method is found to be more suitable for DCEL cells. This is because the phosphors thus obtained have virtually no particle size distribution unlike those obtained from the slurry technique [9]. Moreover, these samples will have an even spreading of Cu and Mn, which will improve the visual appearance of the

device. The doped samples obtained by (any one of) the above methods were then treated with cuprous or cupric salt solution to form a high conductive skin of Cu_xS . The most suitable method found was to treat it with a cupric salt solution rather than with a cuprous salt solution since phosphors obtained from this technique showed better reproducibility. The Cu_xS coating thus obtained is a p-type semiconducting layer. So, a heterojunction will be developed between the doped ZnS and Cu_xS suitable for the formation of high field region for the injection of charge carriers [7].

These Cu_xS coated phosphor particles were then dispersed in a suitable binder with appropriate phosphor-binder ratio. It was then spread on a suitably etched transparent electrode by one of the following methods, viz. silk screen printing, doctor blading or spraying. Because of variation in the thickness of large area glass substrates, doctor blading has been used only for test areas and small display panels. The phosphor-binder mixture is diluted with large volumes of solvents to obtain a solution useful for spraying. Silk screen printing gives controlled thickness layers of high packing density with little waste, provided a suitable binder and solvent mixture to give screen stability can be compounded. It is observed that devices of thickness in range 30-100 μm have the same electrical characteristics and brightness [3]. The back electrode is usually provided with an evaporated aluminium or with a graphite paint. The binder

is used to hold the phosphor particles in contact with each other and to the glass substrate. It occupies less than 5 percent of the total volume of the layer [9].

7.3 DC forming of the cell

Two essential features of any DC EL panel are that the phosphor particles are in contact with each other and with the electrodes. On the initial application of a DC voltage, a high current flows and no light emission is observed. This is because the high conductivity of the phosphor surface and the interparticle contacts precludes any current flow through the ZnS particles themselves. At a critical power density the current falls and light emission appears at the positive electrode. An increase in applied voltage produces a temporary rise in current density but this falls rapidly and the panel brightness increases. This is termed as the 'forming process'. A study of the EL cells with a planar electrode configuration gap cell: showed that virtually all the applied voltage appears across the light emitting region. The remaining phosphor retains its high surface conductivity and acts as an extension of the electrode [9]. The forming process does not occur simultaneously over the whole of the panel area but usually begins where the shortest current path exists between the electrodes. This represents the region of highest current density. When forming takes place, the resistance of the phosphor increases and the current density falls. This increases the current

density in adjacent unformed areas and forming will take place at this region. Thus the formed region will spread across the panel area until a complete plane of high resistance phosphor develops between the electrodes. These devices, except when pulsed, are invariably operated at a final forming voltage. The forming process results from the diffusion of copper from the copper sulphide surface coating into the bulk of the zinc sulphide particle. Considerable heating of the panel takes place during the forming process and a phase change in the copper sulphide coating seems to contribute to the development of a high resistance region [10]. Since the EL brightness is field dependent, the localization of the applied field in the formed layer gives an important advantage in these devices. High fields can be generated at relatively small applied voltage provided the applied voltage has reached a value where the current has dropped by an order of magnitude or more. The forming process is irreversible, as the high resistance of the phosphor permanently reduces the power density.

7.4 Structure of a typical cell and its analysis

Figure 7.1 shows the cross sectional view of a typical DCEL powder cell. Details of the fabrication are given by Alder et al. [10]. It consists of a tin oxide coated glass substrate which acts as the positive electrode. The active layer is $\sim 25 \mu\text{m}$ thick and of area $4 \times 7 \text{ cm}^2$, spread on the transparent electrode. The structure is completed with

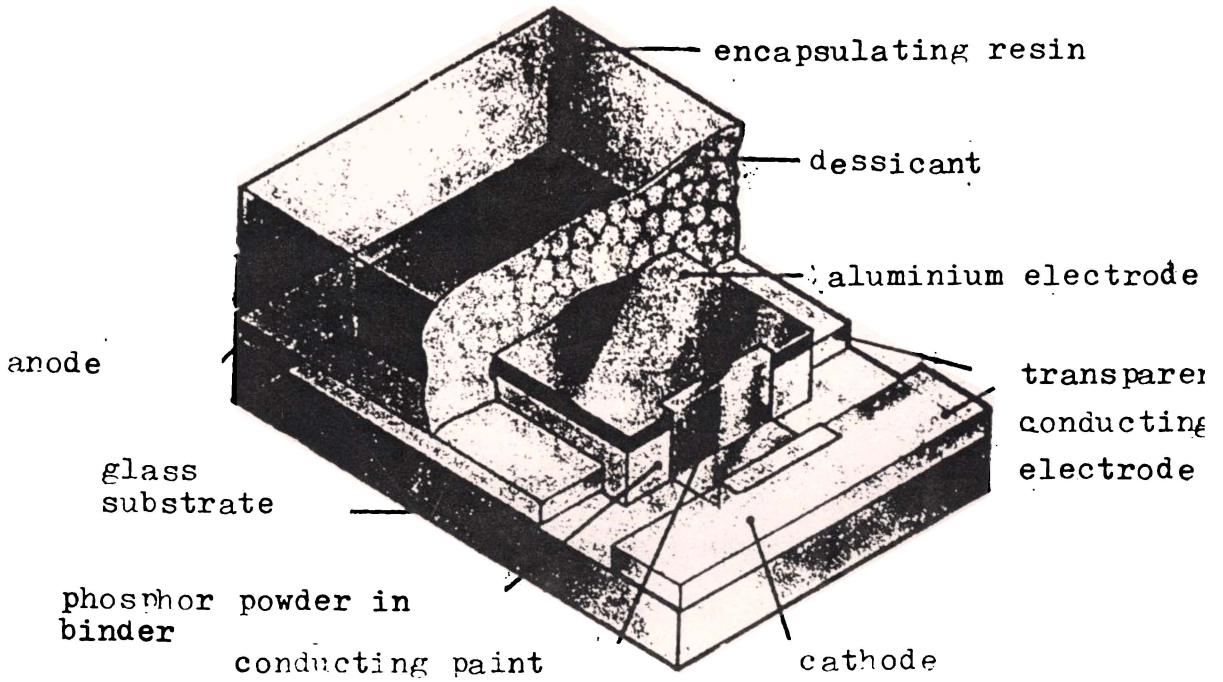


Fig.7.1. Structure of a DCPEL cell

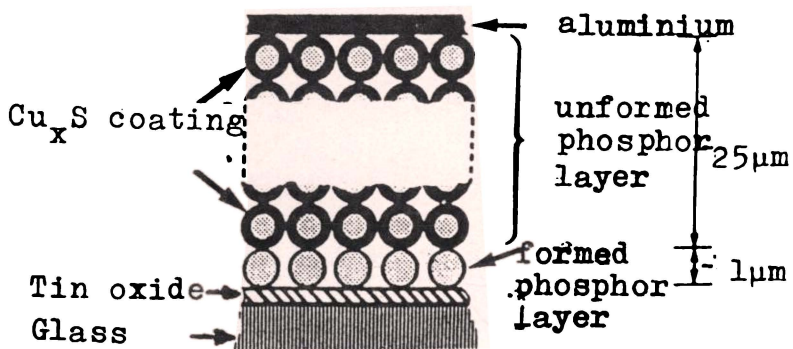
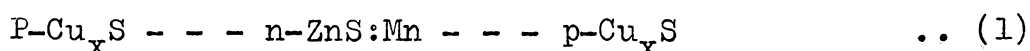


Fig.7.2. Depicts the formed and unformed regions

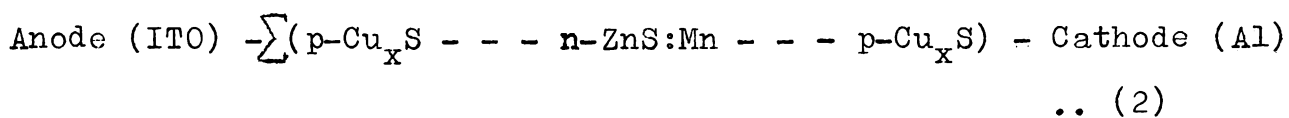
the rear Al electrode. The whole assembly is then encapsulated with a proper dessicant to exclude water vapour from the atmosphere.

Physically, the phosphor layer in the formed device consists of atleast two regions, the formed and the unformed (Fig.7.2). It has been shown that the unformed layer is quite conducting while the formed region is far more resistive [9].

Abdalla et al. [12] have assumed that a concentric multi-hetero structure exists for each powder particle with the configuration



where the n-ZnS:Mn is known to be an insulator. For the assembled device this configuration then becomes,



When voltage is applied to the device, a high current defined as the forming current is found to pass through the device. This current has been attributed to the high surface conductivity of Cu_xS surrounding each powder particle. The current voltage characteristics of the device during the initial forming stage resemble that of pure resistance. The configuration of the luminescing device has been proposed as [13]

Anode-doped ZnS- \sum (p-Cu_xS --- n-ZnS:Mn --- p-Cu_xS)-Cathode .. (3)

Thin luminescing
active region

Extended cathode
(globally p-type)

which shows that the luminescing device can always be regarded as reverse-biased. The current voltage characteristics of such a luminescing device is similar to that of a leaky diode [13].

Reversal of the device polarity results in another forming process, which is terminated by the appearance of luminescence localized at the new as well as the old anode. The current-voltage characteristics of the device then resemble that of two diodes connected back to back. But the brightness in this case is lower since the applied voltage has to be divided between the two localized regions.

7.4.1 Current voltage characteristics of freshly prepared devices and the conduction mechanism

A freshly prepared device which has not undergone any detailed life tests shows two conduction process. The first one occurs in the voltage range extending approximately to a value corresponding to the emergence of EL while the other at a voltage beyond this value. The logarithm of the current is found to increase in proportion to the square root of the applied electric field in the first range. Such a behaviour can be interpreted as either due to the Poole-Frenkel effect or the Schottky effect [14]. Both effects are characterised

by the reduction of the height of the potential barrier due to the applied electric field. In order to distinguish between these two effects, the current at constant voltage is recorded at different temperatures. It is observed that a plot of the $\log I$ versus $1/T$ is a straight line. This confirms that in this voltage range the conduction process is dominated by Poole-Frenkel effect since the Schottky effect is described by a $1/T^2$ dependence of $\log I/T$ [13].

Another type of conduction process occurs at applied voltages beyond the first region. In their studies on reverse biased heterojunction devices, Riben and Fenchel [15] showed that the current density can be explained by means of Zener tunnelling model where the current is expressed as

$$I \propto AV \exp BV^{-\frac{1}{2}}$$

where A and B are constants. In the present case it is observed that in the second range a plot of $\log I/V$ versus $1/\sqrt{V}$ is a straight line which means that such a relationship exists in this region. So it can be assumed that the heterojunction occurs between the thin luminescing active region (n-type) and the extended cathode (globally p-type) region. Furthermore, measurements at different temperatures gives straight lines with almost similar slopes, which is characteristic of the tunnelling process [14]. So, it can be concluded that, in freshly prepared devices, there exists a reverse biased heterojunction, as given by the configuration depicted by equation (3) which is responsible for the conduction mechanism.

7.4.2 Current-voltage characteristic of degraded devices

The degraded device shows ohmic conductivity at lower voltages. At higher voltages space charge limited conductivity ($\log I \propto V^2$) predominates which indicates that the electrical conduction mechanism seems to have undergone modification due to degradation.

7.4.3 The electrical equivalent circuit of the device and the effect of degradation on the circuit parameters

The evaluation of the equivalent circuit consists of applying a unidirectional voltage pulse of amplitude V and analysing the corresponding current wave form. A typical current wave form for a square wave applied voltage is shown in Fig.7.3. The instant voltage is applied, current decreases exponentially from a maximum value I_0 to reach a constant value I_R . Therefore, current at any instant t can be expressed as

$$i(t) = I_R + (I_0 - I_R) \exp - t/\tau$$

The first term in the above equation can be regarded as due to a resistance of value R_p given by

$$R_p = V/I_R$$

The second term is due to a charging current in a capacitor of value C in series with a resistance of value R_s given by

$$R_s = V/(I_0 - I_R)$$

with a time constant $T = R_s C$. The equivalent circuit of the device is shown in Fig.7.4.

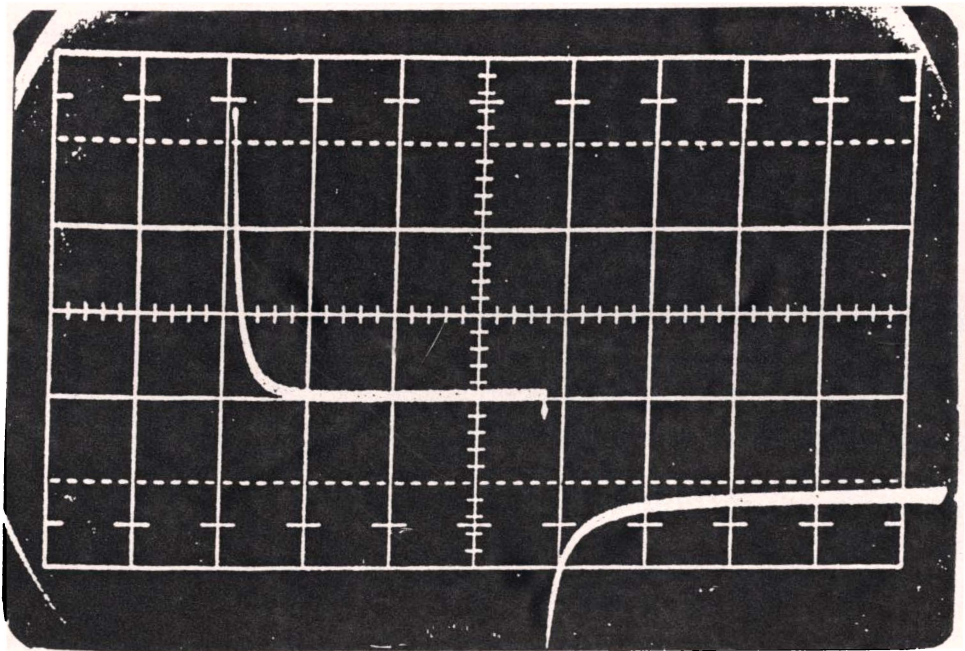


Fig.7.3. Typical current wave form of a DC FEL cell.

In order to study the effect of degradation on the equivalent circuit parameter a plot of the R_s , R_p and C_s as a function of time is usually drawn. A typical plot is shown in Fig.7.4. It is seen that for a fresh device the value of R_p is higher than R_s . But when the device is operated for extended periods R_s is found to increase more rapidly than R_p and it even assumes values greater than R_p . The value of C_s is found to decrease due to degradation [14]. A detailed analysis of these parameters shows that for DC EL powder devices to operate at reasonable brightness levels for extended periods of time, the R_s , R_p and C_s values must be stabilized. This can be achieved only by stabilizing the thickness of the localized region by keeping Cu ion migration to a minimum.

7.5 Preparation of ZnS:Cu,Mn DCPEL cells

In the present case powder phosphors required for the fabrication of DCPEL cells of ZnS:Cu,Mn were prepared by the slurring technique. For this, a weighed amount of luminescent grade ZnS (BDH Poole, England) was mixed with cupric acetate containing 0.5 wt percent copper and Manganese acetate containing 1 wt percent of Mn. A slurry of the mixture was then prepared in aqueous solution. It was then slowly dried and then fired at 1000°C for 90 minutes at 10^{-2} torr, by introducing the phosphors into the high temperature zone of a horizontal furnace. The fired phosphor was then treated with cupric acetate solution containing 2 wt percent copper.

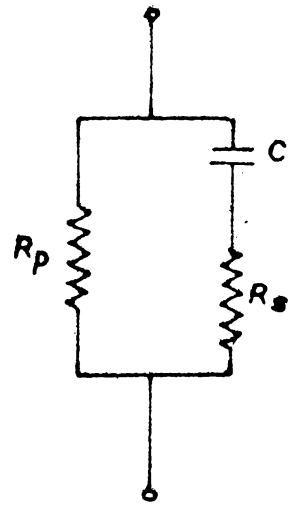
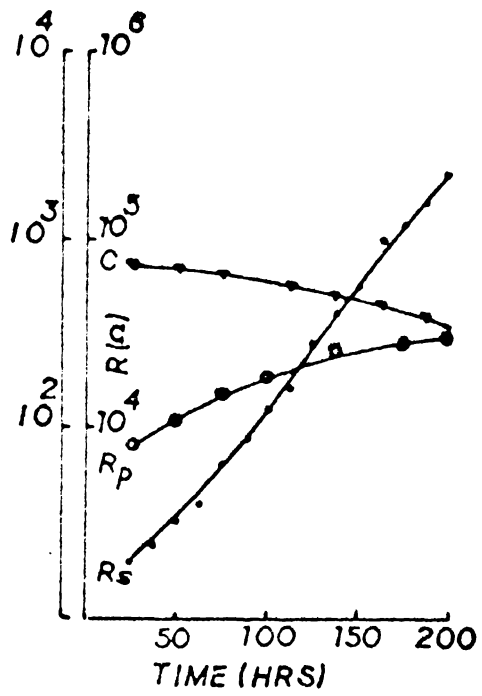


Fig. 7.4(A). Variation of R_s , R_p and C as a function of time of operation.

(B). The equivalent circuit.

The treated phosphor was black in colour indicating the formation of black copper sulphide layer on the phosphor particles. The powder thus obtained was then mixed with a polymethyl methacrylate solution prepared in chloroform. The mixture was then agitated ultrasonically by suspending the mixture container in an ultrasonic cleaning tank. This uniformly dispersed the powder particles in the binder.

Phosphor binder mixture thus obtained was spread on a suitably etched transparent conducting electrode. For this a mica mask 100 μm thick with a groove of size 4 x 2 cm^2 was cut, and placed on the transparent electrode. Then the phosphor mixture was poured in the groove, carefully filling it with a flat glass or metal strip. Then the solvent was allowed to evaporate from the mixture. When the solidification was complete the mask was removed, and a thin phosphor layer embedded in the polymer matrix resulted. The thickness of the layer could be changed by altering the binder solvent ratio. It was observed that a fast evaporation rate of the mixture resulted in a foggy phosphor layer. So the whole preparation procedure was done in an atmosphere which favoured slow evaporation of the solvent. After evaporation of all the solvent the device was introduced into a vacuum chamber and an aluminium metal electrode was deposited as the rear electrode through proper mask. The device thus fabricated is of the type as shown in Fig.7.1.

7.6 Preparation and study of CaS:Ce DCPEL Cells

The CaS:Ce phosphor used for the fabrication of the cell was prepared by the slurring technique. For this, to a weighed amount of CaS, 2.5 wt percent of Ce in the form of ammonium ceric sulphate and 5 wt. percent $\text{Na}_2\text{S}_2\text{O}_3$ was added. A slurry of the mixture was then prepared in aqueous solution. It was then slowly heated and dried. The resulting mass was then crushed and mixed with equal amount of sulphur. The mixture, taken in a quartz test tube with close fitting cap, was introduced into the high temperature zone of a horizontal furnace kept at 1000°C . The firing was done for 90 minutes. This resulted in a pale yellow powder which was then suspended in a cupric acetate solution containing 2.5 wt. percent of copper. The solution was boiled until the phosphor particles turned black in colour. It was then dried and mixed with methyl methacrylate solution prepared in trichloroethylene. The rest of the fabrication procedure was the same as that adopted for the fabrication of ZnS:Cu,Mn cells.

On the first application of the electric field, it is observed that a large current flows through the device. As the voltage is increased, the current increases and after attaining a certain value the current drops with the simultaneous appearance of the EL emission. For a cell of area $0.5 \times 2 \text{ cm}^2$ this transition occurred at 100 mA. On further increasing the voltage the current increases but levels off again with increase in brightness. The B-V characteristic

of the device measured with a current limiting resistance of 47 K ohm included in the circuit is shown in Fig. 7.5. The brightness wave of the cell under square wave excitation is found to have two brightness peaks, corresponding to the rise and fall of the square pulse. This can be easily understood on the basis of the equivalent circuit as shown in Fig.7.4. Under very low excitation frequency, in addition to the brightness peaks, a flat portion of low amplitude is also observed corresponding to the flat portion of the excitation pulse (Fig.7.6).

Eventhough the cell can be excited to a moderately high brightness level it consists of large bright spots as well as small feeble emitting points. This, evidently, is due to the variation in size of the phosphor particles. Moreover, it is observed that the metal electrode at the back of the most intense spots gets destroyed in course of time. So it is not possible to improve the brightness level beyond a limit. It is felt that the most serious drawback of the cells thus prepared arises from the lack of control of the particle size. Since the performance of the cell was not very satisfactory, no detailed investigation on their electrical characteristics was carried out.

7.7 Conclusion

This chapter consists of a brief discussion of the DC powder electroluminescent devices and their DC forming process. An analysis of the DC electrical

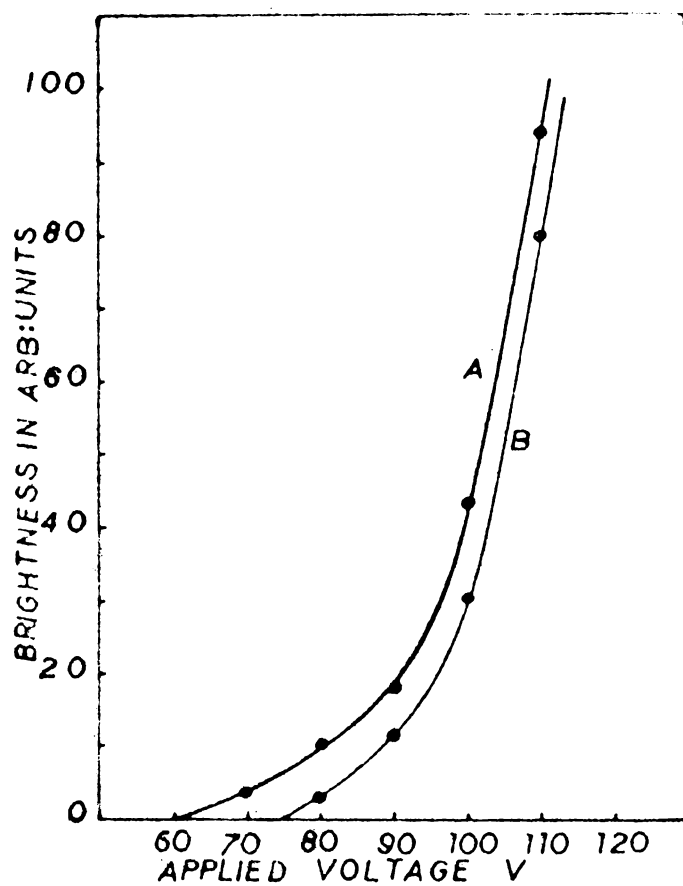


Fig.7.6. B-V characteristic of the CaS:Ce DCPFL cell drawn (A) with initial reading (B) with readings taken after 30 minutes of continued operation.

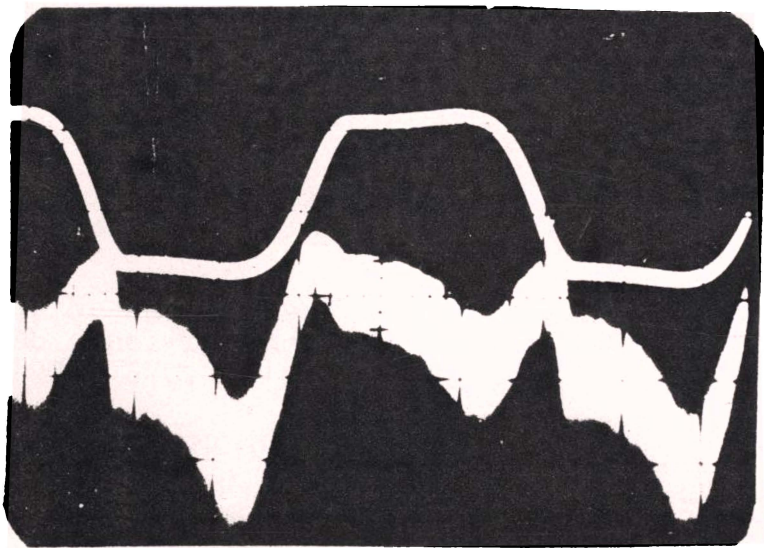
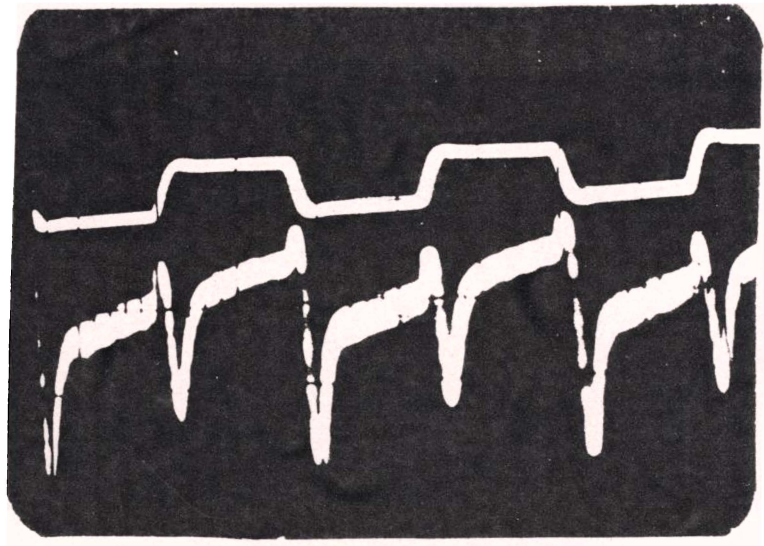


Fig.7.6. The brightness waves of a CaS:Ce DC cell under square wave excitation of different amplitudes.

conductivity is also included. Attempts made to fabricate DC powder cells using ZnS:Cu,Mn and CaS:Ce are outlined. The characteristics of the ZnS:Cu,Mn cells are found to be almost the same as those described extensively in the literature. The CaS:Ce cells prepared are found to be of poor quality mainly due to the lack of control of the particle size. However, some of the results of the investigations made on this new type of cells are presented.

References

1. A. Vecht; J. Cryst. Growth 59(1982) 81.
2. A. Vecht, N.J. Werring and P.J.F. Smith;
Brit. J. Appl. Phys. (J. Phys. D) Ser.2
1(1968) 134.
3. A. Vecht, N.J. Werring, A. Ellis and P.J.F. Smith;
Proc. IEEE [7] 61(1973) 902.
4. A. Vecht, M. Waite, M.H. Highton and R. Ellis;
J. Lumin. 24/25 (1981) 917.
5. M. Yoshiyama, N. Ohshima and R. Yamamoto;
DC-EL panel TV display, Nat. Tech. Rep.
17(1971) 670.
6. M. Yoshiyama; Electron 42(1969) 114.
7. Hiroshi Kawada and Nobumasa Ohshima;
Proc. IEEE [7] 61 (1973) 907.
8. A. Vecht and N.J. Werring; J. Phys. D: Appl. Phys.
[2] 3(1970) 105.

9. A. Vecht, N.J. Werring, R. Ellis and P.J.F. Smith;
Brit. J. Appl. Phys. (J. Phys. D) Ser. 2
2(1969) 953.
10. D. May; In Electronic Displays 1981 Session 1.
11. C.J. Alder, A.F. Cattell, K.F. Dexter, M. Dixon,
J. Kirton and M.S. Skolnick; IEEE Trans.
on Electron Devices, ED-28(1981) 680.
12. M.I. Abdalla, A. Godin and J.D. Noblane;
J. Lumin. 18/19 (1979) 473.
13. M.I. Abdalla, Annick Godin, Alain Brenac and
Jean-Pierre Noblane; IEEE Trans.
ED-28(1981) 689.
14. J.G. Simmons; DC Conduction in Thin Films,
(M and B monographs, London, 1971).
15. A.R. Riben and D.L. Feucht; Sol. State. Electronics
9(1966) 1055.

CHAPTER VIII

FABRICATION OF THIN FILM EL DEVICES: EXPERIMENTAL SET-UP8.1 Introduction

Thin film EL devices can be classified mainly into two categories: DC thin film and AC thin film EL devices. The former consists of an active layer of thin film phosphor in between two electrodes one of which is transparent. The other is a metal electrode. The active layer (eg. ZnS:Cu,Mn) of these devices is prepared either by direct evaporation of the EL phosphor or by co-evaporation technique [1,2]. The devices fabricated by the co-evaporation technique are required to undergo a current forming process as discussed previously in the case of DC powder EL devices. Very high quality devices with long life have been developed (eg. Sigmatron Nova (USA) and Sharp Corporation (Japan) though they are not freely available commercially. These devices consist of active layer ZnS:Mn in between two insulating films of high dielectric constant and of high breakdown strength. The typical structure of such a device first reported by Inoguchi et al. [3] of Sharp Corporation laboratories is shown in Fig.8.1. The materials and fabrication techniques of the various layers are as given below:

(1) Transparent electrode - It is made of SnO_2 or In_2O_3 using conventional thermal decomposition - oxidation method

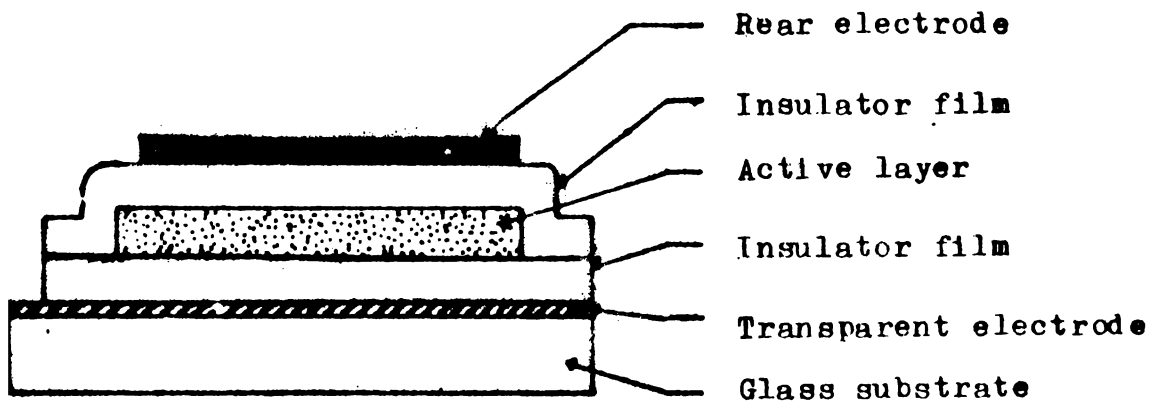


Fig.8.1. Typical thin film EL device structure.

(SnO₂) or vacuum evaporation method (In₂O₃) on glass substrate.

(2) Insulating layers - High dielectric strength and high dielectric constant materials like Y₂O₃, Si₃N₄, Al₂O₃ lead titanate [4], lead zirconate titanate [5] etc. also can be used. Y₂O₃ can be vacuum evaporated from an electron beam bombarded Y₂O₃ pellet; Si₃N₄ is usually reactively sputtered from Si cathode or RF sputtered from Si₃N₄ cathode in (Ar+N₂) atmosphere. Al₂O₃ is vacuum evaporated from an electron bombarded Al₂O₃ pellet or reactively sputtered from Al cathode in (Ar+O₂) atmosphere. Lead titanate and lead zirconate titanate are prepared by sputtering technique.

(3) Active layer - High purity ZnS pellet doped with Mn upto 5 wt percent is used as the source material for the deposition of EL films by means of electron bombardment. During the deposition of ZnS:Mn films, the substrate temperature is maintained around 250°C and a post deposition annealing is done around 550°C for one hour in vacuum for stabilization.

(4) Rear electrode - Usually formed by vacuum evaporated aluminium film.

(5) Protection layer - The device is protected from humidity usually with a Si₃N₄ overlayer.

The devices of the various manufacturers have essentially the same structure as described above but differ in the method of deposition of successive layers and in the technique adopted to improve the visibility under ambient

illumination. For example devices made by Sharp Corporation make use of metallic specular reflectors as the rear electrode but the ambient light reflection is eliminated by providing a circular polarizing filter at the front surface. Devices of Sigmatron Nova make use of a black absorbing layer in between the rear dielectric layer and the back electrode which is a composite of As_2S_3 and $BaTiO_3$. Oy Lohja Corporation devices have transparent rear electrodes which make the whole device transparent. A non critical black pigment layer may also be applied to the rear surface [6]. For devices with long operating life time, different kinds of passivation layers are applied in between the successive films [7]. In view of the various requirements for the fabrication of such a device appropriate systems were built in the laboratory. They are described in this chapter.

8.2 Vacuum system for the deposition of electrodes

The metal electrodes for the devices were deposited by the vacuum evaporation technique [8,9,10]. The deposition system used was fabricated in the laboratory. It consisted of a 6" oil diffusion pump, liquid nitrogen trap and Baffle valve connected in series to a chrome plated base plate suspended on a 1m x 0.75m x 1.75m MS frame. A 550 litre/min. rotary vacuum pump was used as the backing pump. The base plate used had provision for 14 side feed throughs. A 12" glass bell jar placed over this base plate provided the vacuum chamber. Within the vacuum chamber the filament holders,

substrate holder, substrate heater, etc. were mounted on the base plate. All the high current and high voltage feed throughs needed were designed and constructed in the laboratory. The system can produce a pressure of 10^{-5} torr in the chamber within 45 minutes. Pressure down to 10^{-3} torr was measured with a Pirani gauge. The pressure below this range was monitored with a Penning gauge. A 100A transformer was used for the resistive heating of the vapour source. The various controls, gauges, high voltage and high current meters and the indicators were fitted on the front panel. A photograph of the system is shown in Fig.8.2. This system has provided trouble free operation for the last four years and still continues to work satisfactorily.

8.3 Deposition system for insulator and active layer films

A separate vacuum coating unit specially suited for the deposition of insulator films and the active ZnS:Mn films was fabricated. It was built using a 200 litre/minute rotary vacuum pump and a 4" oil diffusion pump. The deposition chamber consisted of a base plate covered with an SS dome with viewing windows. The diffusion pump was connected to the chamber through a liquid nitrogen trap and a baffle valve which reduced the back streaming of the oil and provided vacuum isolation between the pump and the chamber.

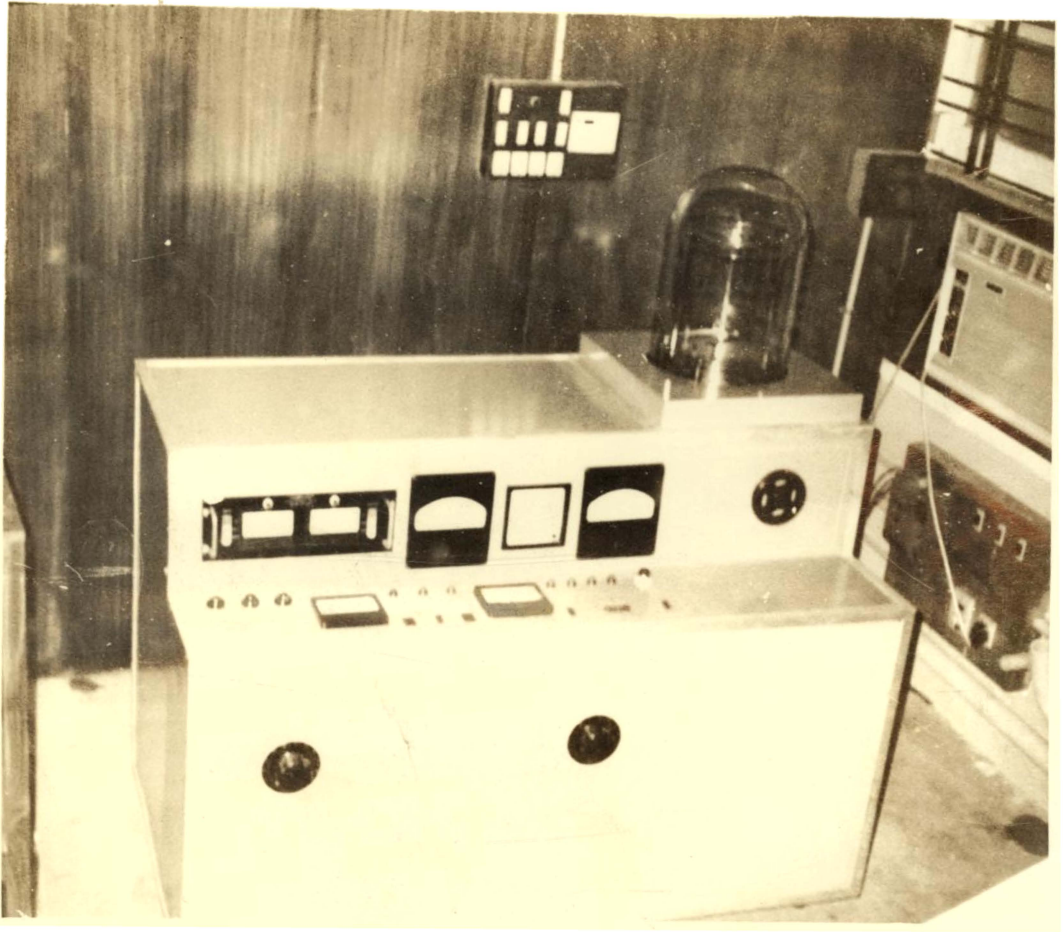


Fig.8.2. Photograph of the vacuum coating unit fabricated for the deposition of metal films

Conventional thermal evaporation of the doped ZnS:Mn layer was attempted as follows: An evaporation source was designed which consists of a small quartz crucible in between two molybdenum strip heaters which fully cover the crucible. By passing a high current through the strip, the crucible is uniformly heated and fairly high evaporation rate was obtained without any spattering problem. As the heater is unshielded it heats the chamber walls also and hence a metallic dome is necessary which also facilitated the deposition of the films at elevated temperatures.

Electron beam evaporation system

Even though the electroluminescent material of interest ZnS:Mn can be evaporated from such thermally heated evaporation sources, attempts made to evaporate good dielectric materials like Y_2O_3 , Al_2O_3 , SiO_2 were not successful. To achieve this, the most logical approach is to use an electron beam evaporation system specially suited for the deposition of highly pure, stoichiometric films. Moreover, materials with extremely high evaporation temperature can be easily deposited by this technique.

The simplest electron-bombardment/heating arrangement consists of a heated tungsten filament to supply electrons which are accelerated by applying a positive potential to the material for evaporation. The electrons lose their energy in the material very rapidly, their range being determined by their energy and the atomic number of the material. Thus

the surface of the material becomes molten and evaporation takes place. By the use of electron optics the beams can be focussed or can be directed onto the material for evaporation.

In the present investigation a 3 kW electron beam evaporation unit supplied by M/s. Hind High Vacuum Company is used. The schematic circuit diagram is shown in Fig.8.3.

It has a bent beam (180°) water cooled electron beam gun with 4 crucibles suitable for the deposition of four different materials, sequentially on a single substrate in one vacuum cycle. The filament heating is provided by a 10V, 30A LT transformer. The filament is kept at -6 KV, and it can be varied from -5 KV to -7 KV which facilitates a 2 mm shift in the striking point of the beam. The maximum beam current is 500 mA at 6 KV which corresponds to a maximum beam power of 3 KW. The filament voltage and the beam current can be measured on the front panel meters on the power supply unit. The evaporation rate can be controlled by adjusting the beam current. With the remote control facility this can be done by visually monitoring the source. The current and voltage stabilization in the circuit maintain the beam current and voltage irrespective of the line and load fluctuations.

8.4 Substrate heater

The active layers are usually deposited at elevated temperatures and a post deposition annealing is also required at a temperature of about 550°C . So a suitable substrate

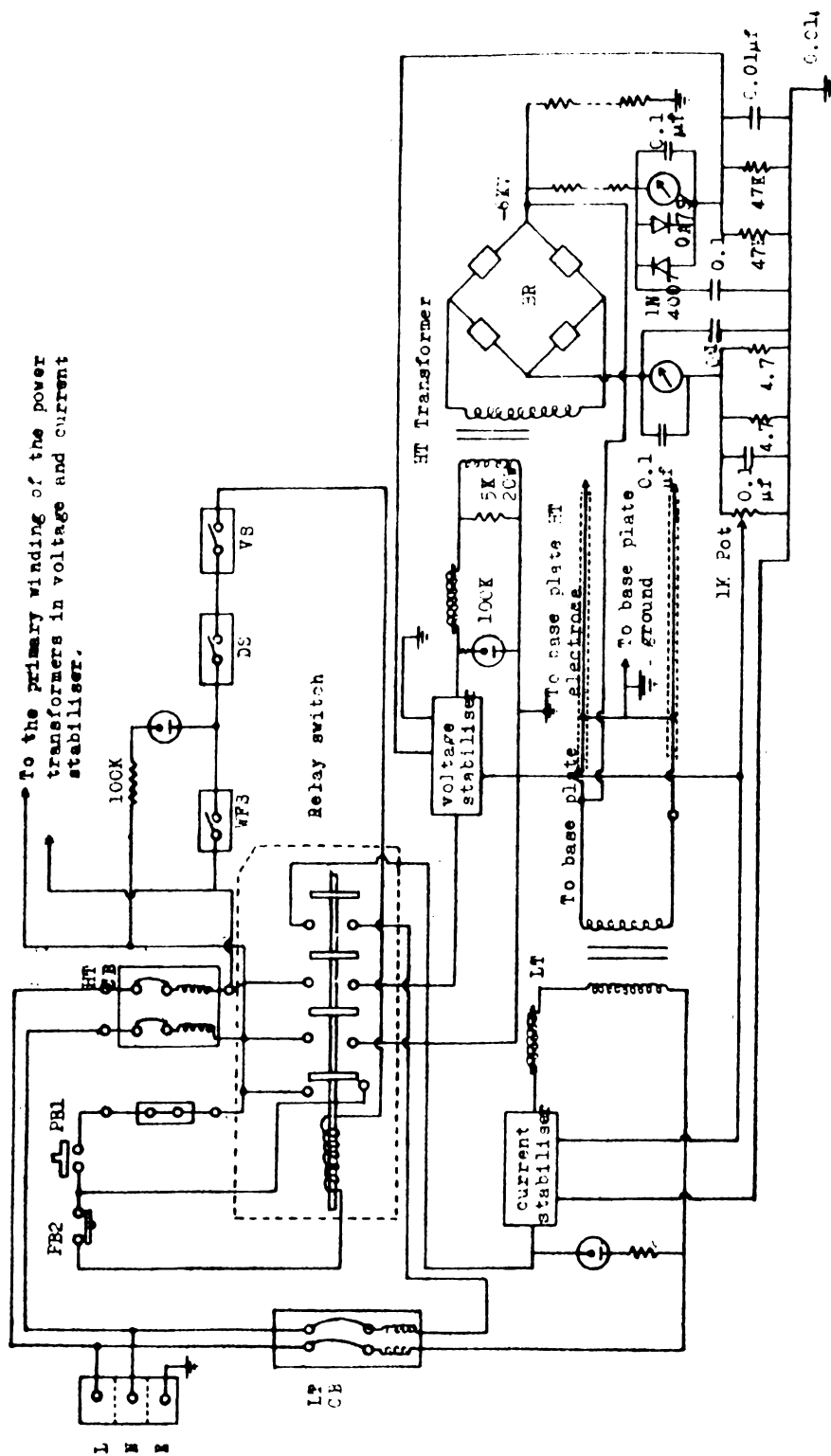


Fig.8.3. Schematic circuit diagram of the EBE system.

heater is needed for the fabrication of the device which can uniformly heat the substrate. A substrate heater suited for this purpose was constructed. It consists of two flat polished SS plates of 7.5 cm x 7.5 cm between which a flat kanthal wire (22 gauge) filament insulated from the metal sheet with two mica sheets is placed. The filament connections were taken through two ceramic insulation feed throughs. The glass substrates were placed on the polished surface of the heater plate and fitted firmly to it with two SS clamps. The substrate heater is positioned in the chamber such that the substrate faces the vapour source. The heater is fixed in position with ceramic insulators so that the heater support does not get heated. It is found that with a current of 3A through the heater it can reach a temperature 550°C within 90 minutes.

8.5 Thickness measurements

8.5.1 Determination from the evaporated mass

During trials it was not necessary to measure the thickness accurately. But an idea about the thickness of the film deposited is obtained by knowing the mass evaporated from the source and applying the formula

$$t = \frac{m}{2\pi\rho R^2} \quad \text{for a strip source, where}$$

m is the mass evaporated, ρ the density of the film, R the distance between the source and the substrate and t the thickness of the film. For filament sources the thickness

will be half of this value [11].

8.5.2. Multiple beam interferometry

Whenever the film thickness is to be measured accurately, it is done with the help of a multiple interferometric technique.

The principle of this method is based on the fact that when a partially reflecting surface is placed on a totally reflecting surface forming an airwedge and a monochromatic parallel beam of light falls on it, interference fringes are produced. The optical path difference between successive minima is λ which is the wavelength of the monochromatic light. If a step is formed by the thin film whose thickness is to be measured, the interference fringe pattern will be shifted as shown in Fig.8.4. The thickness of the film can now be measured from the fringe shift x and fringe separation y as

$$t = \frac{x}{y} \cdot \frac{\lambda}{2}$$

This method was first used by Wiener [12] and further developed by Tolansky [13]. The experimental setup as described by Chopra [11] is used for the measurement. A travelling microscope of least count .001 mm is used to measure the fringe shift.

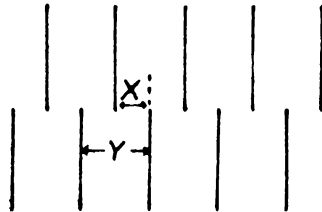


Fig.8.4. The illustration of fringe shift: X is the fringe shift and Y is the fringe separation.

Quartz crystal

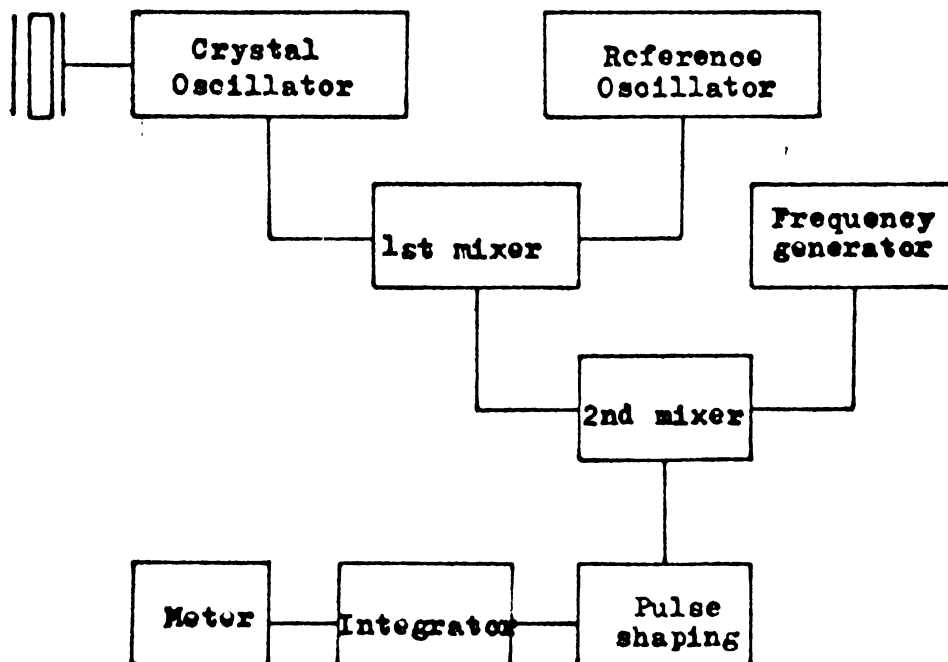


Fig.8.5. Block diagram for Quartz-crystal oscillator instrumentation.

8.5.3. Crystal film thickness monitor

A quartz-crystal thickness monitor for monitoring the rates of both deposition and evaporation of metals, non metals and multicomponent films is the single most important monitoring device for thin film technology. Moreover it has the combined advantage of simplicity as well as high sensitivity.

The monitor utilizes the thickness shear mode of a piezo electric quartz crystal. Here the major crystal surfaces are antinodal and the mass added on either one or both sides shift the resonance frequency irrespective of the thickness, density, elastic constants or stiffness of the added material. AT cut ($35^{\circ}20'$ cut) quartz crystal is used for this purpose because of its low temperature coefficient of resonant frequency [11]. The fundamental resonance frequency for an AT cut crystal is given by

$$f = \frac{1}{2d} \left(\frac{c}{\rho}\right)^{\frac{1}{2}} = \frac{N(\text{mm H}_z)}{d}$$

where d is the crystal thickness ρ_q its density, c its elastic constant and $N = \left(\frac{c}{4\rho}\right)^{\frac{1}{2}} = 1670 \text{ mm H}_z$. The change in frequency Δf produced by deposited mass m , added to the area A of the antinodal surface of mechanical resonator can be written as [11]

$$\Delta f = \frac{f^2 Km}{N\rho A} = - C_f \frac{m}{A} = - C_f t_{\text{film}}$$

where $C = f^2 K / N \rho$ is a constant of the crystal, and $m = A t \rho_{\text{film}}$ assuming a uniform film of thickness 't' and a constant density ρ_{film} . From the above relation it can be seen that higher sensitivity can be obtained for high frequency crystal i.e. of crystals with smaller thickness. But the relation between Δf and m is valid only if $t \ll d$. So for higher frequency crystals the non linear region will be reached with smaller film thickness. As a compromise between these two factors, crystals of resonance frequency ~ 6 MHz are usually used.

The sensitivity of the crystal is limited by the variation in crystal frequency due to changes in temperature, oscillator drive level etc. The latter is more severe since the crystals are to be mounted in ~~the deposition chamber~~ so as to see the evaporation source. So they are mounted in water cooled electrically shielded crystal holders. In order to eliminate the possible damage to the control circuit due to electrostatic pick up especially when used with EBE system the crystal electrode facing the source is grounded.

The frequency changes in the quartz crystal oscillator can be directly measured with a frequency counter having an accuracy of 1 Hz in the MHz range. But with a heterodyning technique a less expensive meter readout for this small frequency shift can be obtained. In this method, by beating the frequency of the monitor crystal with that of another quartz crystal of a slightly different frequency a beat

frequency is obtained. This is then mixed with the output from another variable frequency oscillator and a second intermediate frequency is obtained. It is then amplified, rectified and read on a meter. The rate of change of frequency can be obtained by an RC differentiating circuit. The block diagram of such a circuit is shown in Fig.8.5.

In the present case the thickness of the various layers deposited for the fabrication of the device was monitored with a (Hind High vacuum, model CFM-1) quartz film thickness monitor. In this system a 6 MHz monitor crystal is mounted on a water cooled crystal holder and placed inside the vacuum chamber. The reference crystal is of 6.5 MHz and is kept inside the control unit. Here the difference between the crystal frequencies is amplified and fed into another circuit where it is mixed with a variable oscillator so as to produce a final difference frequency between 0 and 100 KHz. As discussed above, the mass of the deposited material causes a reduction in the natural resonant frequency of the monitor crystal, causing an increase in the final difference frequency. This change is converted into a DC signal which actuates both the frequency shift meter and the rate change meter. The frequency shift meter reading can be reset to zero by changing the frequency of the variable oscillator and it can be done with an external reset control .

The meter readout in the thickness monitor provides the film thickness in terms of the frequency shift. So it

has to be translated into thickness value in absolute units using proper calibration procedure . For this the crystal monitor head is fixed in the deposition chamber such that it can see the vapour source and is kept at a distance equal to that of the substrate from the source. A weighed amount of MgF_2 is taken in a molybdenum boat and evaporated at a pressure of 10^{-5} torr, noting the frequency shift in the thickness monitor. The substrate was taken out and the thickness was measured with Fizeau fringe method described in Section 8.5.2. From this the film thickness in terms of the change in frequency is found out, which will remain the same as the relative position of the thickness monitor, substrate and the source are not changed. For example if a frequency shift of 1000 Hz is noted for a film thickness of 200 nm then 2 nm thickness corresponds to frequency shift of 10 Hz for MgF_2 film. For other materials thickness can be found by knowing the frequency shift and their densities. If the relative position of the substrate, the crystal or the source is changed the system is recalibrated for the new configuration. With this system in conjunction with the EBE system, films of Y_2O_3 , ZnS:Mn , SiO_2 , Nb_2O_3 , MgF_2 , etc. have been successfully deposited to required thickness values. Fig.8.6 shows the whole experimental setup used for the fabrication of the device.

8.6. Deposition of transparent conducting electrode of SnO_2 by Spray Pyrolysis method

Non stoichiometric and doped films of oxides of tin, indium, cadmium, zinc and their various alloys, deposited by

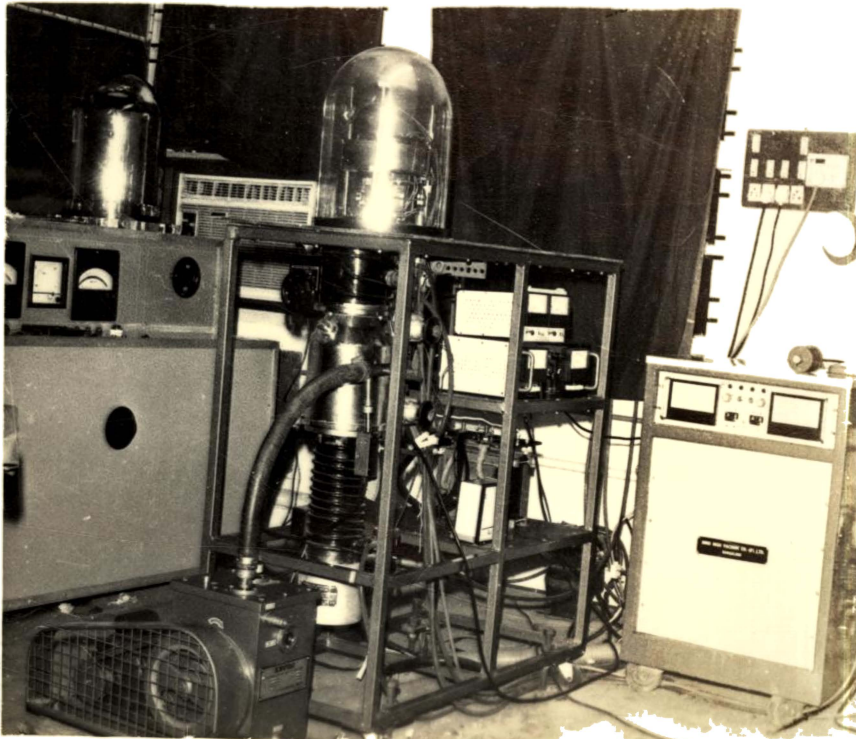


Fig.8.6. Photograph of the setup used for the fabrication of TFEL cells

numerous techniques exhibit high transmittance in the visible region, high reflectance in the IR and nearly metallic conductivity. The electrical as well as the optical properties of these unusual materials can be tailored by controlling the deposition parameters. Among them the most prominent one is that of oxides of Indium and tin doped with appropriate dopants. These transparent coatings find application as transparent electrodes in various electro-optic devices, as resistors, transparent heating elements for aircraft and automobile windows, antistatic coatings for instrument windows, heat reflecting mirrors for glass windows and in incandescent bulbs; anti-reflection coatings, selective absorber interconnections in solar heat collectors, gas sensors, touch sensitive switches etc. [14].

Because of their immense technological importance, extensive investigation is being carried out especially in the preparation and characterisation of these films. It is found that the quality of the film obtained depends largely on the method adopted for the preparation. By almost all thin film deposition techniques such films have been prepared.. They include the post deposition oxidation of metal [15], reactive evaporation [16], direct evaporation by thermal [17] and EBE [18], sputtering [19], reactive ion plating [20], chemical vapour deposition [21], spray pyrolysis [22], Dip technique [23], chemical solution growth [1] etc. The film of best quality was that of indium doped tin oxide obtained by spray pyrolysis. Next is the sputtered film of ITO [1].

As the transparent electrode for the present EL devices tin oxide film obtained by spray pyrolysis method was used. This method was selected because it can yield high quality film with a comparatively simple experimental setup.

In the present case, an aqueous $\text{SnCl}_4 \cdot 5\text{H}_2\text{O}$ solution taken with excess amount of isopropyl alcohol was sprayed on to a heated glass substrate. The spray strikes the substrates at an oblique angle and the entire process is done in a good stream of air or oxygen. The details of the setup in the present case are described below.

The glass substrate to be coated was first cleaned in soap solution and in chromic acid. It was then placed on a hot plate made of stainless steel which could be heated upto 500°C . A good stream of air was made to flow from an electric fan. The spray solution was taken in a special chromatographic sprayer. The spray was produced by blowing compressed air into the sprayer and was controlled by adjusting the air pressure. Spraying was done such that it hits the hot substrate at about 45° . The air stream and the spray from the nozzle of the sprayer carried away the residual gases which mainly consisted of HCl and alcohol vapour.

A number of trials were made with different concentrations of spray solution and with different substrate temperatures. In the present case a saturated solution of $\text{SnCl}_4 \cdot 5\text{H}_2\text{O}$ at room temperature in isopropyl alcohol sprayed on a glass plate

kept at 400°C gave the best films with a sheet resistance of 80 Ω /sq. and transmittance \sim 85 percent.

Selective removal of the SnO₂ films was done by reacting it with nascent hydrogen. The films prepared has good adhesinn to the substrate, and it could be subjected to ordinary cleaning methods which facilitated its repeated use. But a prolonged acid treatment was found to destroy the film.

8.7. Summary

An outline of a typical AC thin film EL device is given together with an account of the deposition techniques for the various films used in them. Different experimental setup developed in the laboratory to fabricate such a device is explained. The method of deposition of transparent conducting electrode of SnO₂ is described at the end of the chapter.

References

1. Z. Porada, E. Schabowska and T. Piech; Acta Physica Polonica, A 57(1980) 267.
2. Mohammed Abdalla, Jaquos Thomas, Alain Brenac and Jeam Pierre Noblanc, IEEE Trans. ED-28 [6] (1981) 694.
3. T. Inoguchi, M. Takeda, Y. Kakihara, Y. Nakala and Y. Yoshida '74 SID Tutorn. Symp. Digest(1974).
4. T. Inoguchi and S. Mito; Electroluminescence Topics in Applied Physics Vol.17, Ed. J.I. Pankove (Springer Verlag, Berlin 1977) 198.

5. Kenji Okamoto, Yasuhiro Nasu, Yoshiro Hamakawa;
IEEE Trans. ED-28[6] (1981) 698.
6. Webster E. Howard; J. Lumin. 24/25 (1981) 835.
7. P.N.R. Panicker; Sigmatron Nova (Private Communication)
8. Leon I. Maissel and Reinhard Glang; Hand Book of Thin
Film Technology (McGraw Hill, New York 1970).
9. L. Holland; Vacuum deposition of Thin Films,
(Chapman and Hall, New Fetter Lane, London, 1970)
10. A. Roth; Vacuum Technology)(North Holland Publishing
Co., Amsterdam, New York, 1976).
11. K.L. Chopra; Thin Film Phenomena (McGraw Hill, New York,
1969) 103.
12. O. Wiencze; Wied. Ann. 31(1887) 629.
13. S. Tolansky; Surface Microtopography (John Wiley and
Sons, New York, 1960).
14. K.L. Chopra, S. Major and D.K. Pandya; Thin Solid Films,
102(1983) 1.
15. T. Nishino and Y. Hamakawa; Jpn. J. Appl. Phys. 9(1970)1085.
16. W. Spence; J. Appl. Phys. 38(1967) 3767.
17. M. Mizuhashi; Thin Solid Films 70(1980) 91.
18. A. Balasubramonian, M. Radhakrishnan and C. Balasubramanian;
Thin Solid Films 91(1982) 71.
19. R.R. Mohta and S.F. Vogel; J. Electrochem. Soc. 121(1974)
394.
20. R.P. Howson, J.N. Avaritsiotis, M.I. Ridge and C.A. Bishop;
Thin Solid Films 63(1979) 163.
21. T. Muranoi and M. Furunkoshi; Thin Solid Films 48(1978)309.
22. H.S. Soni, S.D. Sathaya and A.P.B. Sinha; Indian J.
Pure and Appl. Phys. 21[4] (1983) 197.
23. H. Dislich and E. Hussmann; Thin Solid Films 77(1981) 129.

CHAPTER IX

FABRICATION AND STUDY OF AC THIN FILM EL DEVICES OF

MgF₂ AND Y₂O₃ INSULATING LAYERS

9.1 Introduction

AC thin film EL (ACTFEL) devices of the type pioneered by Inoguchi et al. [1] which consist of the active layer ZnS:Mn sandwiched between two insulating layers of Y₂O₃ have now acquired the status of a reliable display element of very high brightness (~ 1500 fL) and long life ($\sim 20,000$ hrs). At present these devices lack the advantage of IC compatibility due to their high operating voltages. Efforts are now being made to reduce the operating voltages for these devices. The various attempts in this direction are essentially based on the conclusion of Howard [2] that in order to obtain high brightness and high efficiency for these devices, the insulator film used must satisfy the condition that the product of its dielectric constant (ϵ) and breakdown voltage (E_b) must be at least three times higher than the corresponding value for the active ZnS:Mn layer. This implies that low voltage operation can be obtained without sacrificing the brightness or efficiency by using insulators of high dielectric constant and, preferably, with high breakdown voltage. Based on this idea Okamoto et al. [3] have prepared a device using piezoelectric PbTiO₃ ($\epsilon \approx 150$) insulating layer and found that they can operate at ~ 50 volts. Attempts are also being made to use SrTiO₃ and BaTa₂O₃ films

in such devices [4]. Another innovative idea on this type of devices is due to Yoshiro Oishi et al. [5] who have very recently fabricated a tunable color EL device.

Quite different from these attempts, the author has prepared an AC thin film EL device of ZnS:Mn whose emission threshold and hence the brightness depends strongly on the frequency of the excitation field. This device makes use of MgF₂ insulator layer instead of Y₂O₃ and has the structure SnO₂-MgF₂-ZnS:Mn-MgF₂-Al. The dielectric loss factor (tan δ) of these films is strongly dependant on the field frequency and hence this property is made use of in the working of such a device. MgF₂ has a dielectric constant of 4.9 [6] and breakdown strength 2 x 10⁶ V/cm [7] which mean that it is more suitable for such applications than SiO and SiO₂ films. Moreover films of MgF₂ can be deposited by the simple evaporation technique. The following sections of this chapter give the complete details of fabrication and study of such a device and also of a conventional SnO₂-Y₂O₃-ZnS:Mn-Y₂O₃-Al EL device fabricated by the electron beam evaporation technique.

9.2 Fabrication of MISIM device

The structure of the EL device fabricated by the author is shown in Fig.9.1. The insulator and active films were deposited sequentially in a single vacuum cycle. The substrate used for the fabrication was ordinary glass slides of 7.5 cm x 2.5 cm size. The detailed procedure for deposition of each film is given below.

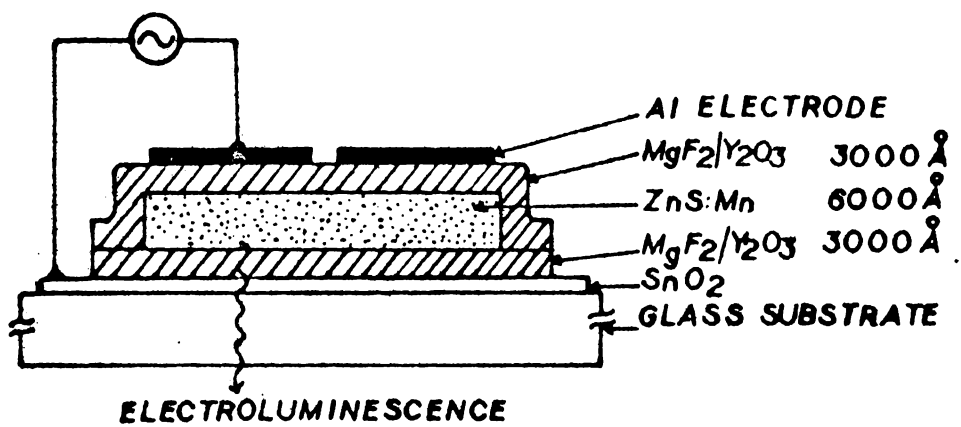


Fig.9.1. Structure of the thin film EL cell fabricated

The SnO_2 transparent conducting films on the glass substrates were deposited by the chemical spray pyrolysis method which is described in detail in chapter VIII. For the fabrication of the thin film devices, films of sheet resistance $80 \Omega/\text{sq.}$ and of transparency 85 percent were used. The deposited electrodes were then suitably etched by a chemical method. These transparent electrodes were then cleaned with soap solution and washed in water, then rinsed in distilled water, xylene and in acetone successively. It was then subjected to an ultrasonic cleaning procedure. The plates were then dried and fitted on to the substrate heater which was mounted in the high vacuum chamber.

Before commencing the actual fabrication procedure, trial experiments were done for the calibration of the thickness monitor for each film material to be deposited with fixed substrate-monitor head-source positions. The details of this procedure are discussed in chapter VIII. In the present case the substrate and the monitor head were kept at the same level relative to the source.

For the deposition of the layers in the device of the type $\text{SnO}_2\text{-MgF}_2\text{-ZnS:Mn-MgF}_2\text{-Al}$, weighed amounts of MgF_2 and ZnS:Mn which are slightly in excess needed for the deposition of required thicknesses were taken in the respective sources. For MgF_2 , a molybdenum boat was used as the source heater which was powered by a 200 A, 10 V transformer. The ZnS:Mn was taken in the form of pressed pellets and the source used

was a quartz crucible kept surrounded by a molybdenum strip heater. On SS dome with view ports and water cooling facility was used instead of glass dome for the vacuum chamber. The chamber was then pumped down to a pressure of 2×10^{-5} torr. During evacuation the substrates were finally cleaned by subjecting it to ion bombardment which was done at 10^{-2} torr for 15 minutes. The films of MgF_2 , ZnS:Mn and MgF_2 were then deposited sequentially to desired thickness with the help of the thickness monitor.

The conventional EL cell of the structure SnO_2 - Y_2O_3 - ZnS:Mn - Y_2O_3 -Al was fabricated with a 3 KW electron beam evaporation (EBE) system. The details of the EBE system are discussed in detail in chapter VIII. The weighed amounts of Y_2O_3 and ZnS:Mn were taken in separate crucibles of the four crucible gun source. The thickness was controlled with the help of the quartz film thickness monitor. It was found that for the evaporation of Y_2O_3 , beam power of 2.5 KW was required. While for ZnS:Mn a power of 600 W was sufficient. During the deposition of ZnS:Mn the substrate temperature was kept at 200°C and after the deposition the film was annealed at 450°C for one hour.

Hot pressed pellets of MgF_2 supplied by Balzers, Liechtenstein, were used for the deposition of MgF_2 dielectric film. Y_2O_3 powder was supplied by Fluka, Germany. ZnS:Mn phosphor samples were prepared in the laboratory by a slurry-ing technique; the details of which are discussed in chapter III. For the present studies ZnS:Mn phosphors were

prepared from the slurry containing 3 wt. percent of manganese.

The device fabrication was completed by the deposition of the final aluminium back electrode. This was done by the usual vacuum evaporation method. The Al film was deposited through a mica mask suitably prepared so that on each substrate 7 aluminium electrode strips of size 2 cm x 0.3 cm were formed. This resulted in seven identical cells each of emitting area 0.4 cm².

Even though the deposition of the ZnS:Mn film at elevated temperature and the subsequent annealing at about 450°C improve the EL emission of Y₂O₃ insulator device, it is not the case with MgF₂ insulator device. In the latter device such a procedure actually diminishes the emission. This observation is supported by the recent studies on Y₂O₃ insulator devices by Theis et al. [8] with the aid of transmission electron microscopy (TEM) technique. They have found that annealing actually changes the crystallinity of the insulator layer and not that of the ZnS:Mn active layer. However, during the thermal deposition of ZnS:Mn film the substrate temperature is found to increase upto 85°C. Hence until the completion of the entire deposition process, the substrate temperature was maintained at 85°C for the SnO₂-MgF₂-ZnS:Mn-MgF₂-Al device.

Since the unbaked MgF₂ is highly sensitive to moisture, adequate measures were taken to reduce the humidity in the laboratory and immediately on removal from the chamber the device was transferred to a dessicator. While in use these

devices were covered with a glass plate and the sides were sealed with cellophane tape. Thus protected devices can operate for weeks without any sign of deterioration. For the Y_2O_3 insulator device also, such protection measures was adopted.

On the first application of electric field to a newly built cell, there occur spurious arcing and momentary rupturing of the metal electrodes followed by the emission of light. This is due to the self healing pin-hole burn-out occurring in small isolated regions. Eventhough there exist burn-out portions, they are not visible on illumination and the entire area is uniformly illuminated. The cells were then operated for several hours continuously (for about 50 hours) without any observable deterioration. To ensure reliability, devices tested for long time operation only have been subjected to detailed investigation.

The EL spectrum of the TF cell was recorded with the setup described in Chapter II. The excitation setup and the arrangement used for the voltage brightness measurements were also the same as used for the study of powder cells described in Section 2.6 of that chapter. The devices were operated at voltages around 150 V AC.

9.3 Results and discussion

The EL emission spectrum recorded for the two types of the cells are almost the same and a typical spectrum is

shown in Fig.9.2. The emission has its maximum at 585 nm and the width at half maximum is 40 nm. This is due to the well known intra-atomic transition of the Mn^{2+} ion from the 4T_1 to 6A_1 state [9].

Figure 9.3 a and b shows the Brightness (B) versus Voltage (V) characteristic of the two devices having the MgF_2 insulator and Y_2O_3 insulator respectively. It can be seen from the figure that the two cells have almost the same features. Upto a threshold voltage (V_{th}) the brightness is zero. Beyond this value of the applied voltage the brightness increases steeply and after attaining a certain brightness value it levels off indicating a saturation. Such a saturation phenomena has been observed for all type of AC thin film EL devices as well as in some DC powder devices [10]. Tornquist [11] has attributed this apparent brightness saturation to two causes: (1) Due to the dissipative current in the $ZnS:Mn$ layer that is directly related to the excitation of the Mn^{2+} ion. (This is because at higher fields the conductivity of the $ZnS:Mn$ layer will increase and hence the internal field will be limited by the capacitance of the insulating layers), (2) Due to the internal quenching of the Mn^{2+} emission.

The main difference between these two devices is in the frequency dependence of the threshold voltage. Fig.9.4 shows B-V characteristic of device of structure $SnO_2-MgF_2-ZnS:Mn-MgF_2-Al$ for different frequency of excitation. It can

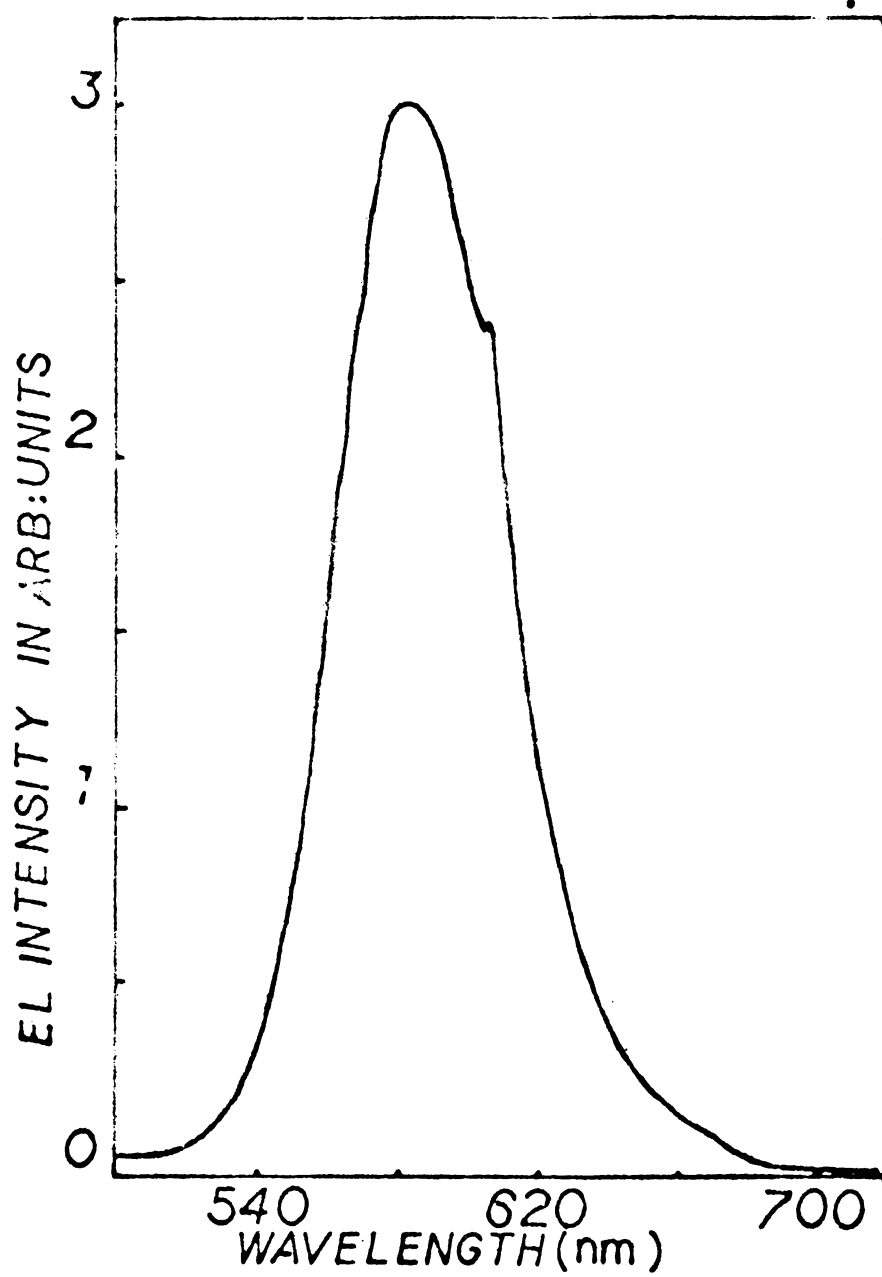


Fig.9.2. EL emission spectrum of the thin film device.

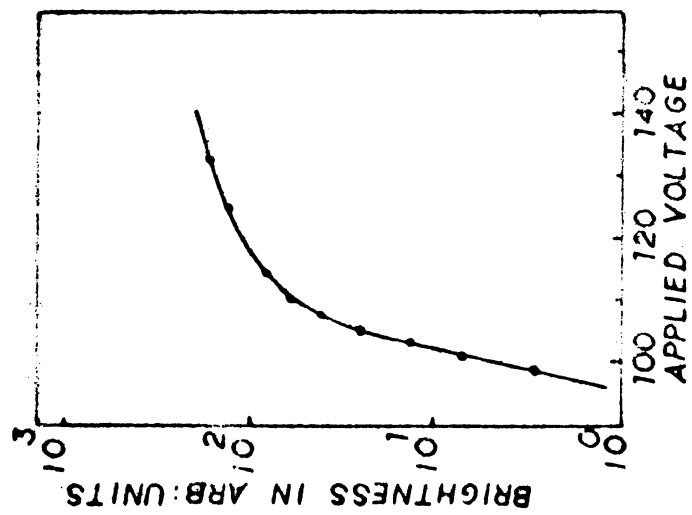


Fig. 9.3(b). B-V characteristic of Y_2O_3 insulator device.

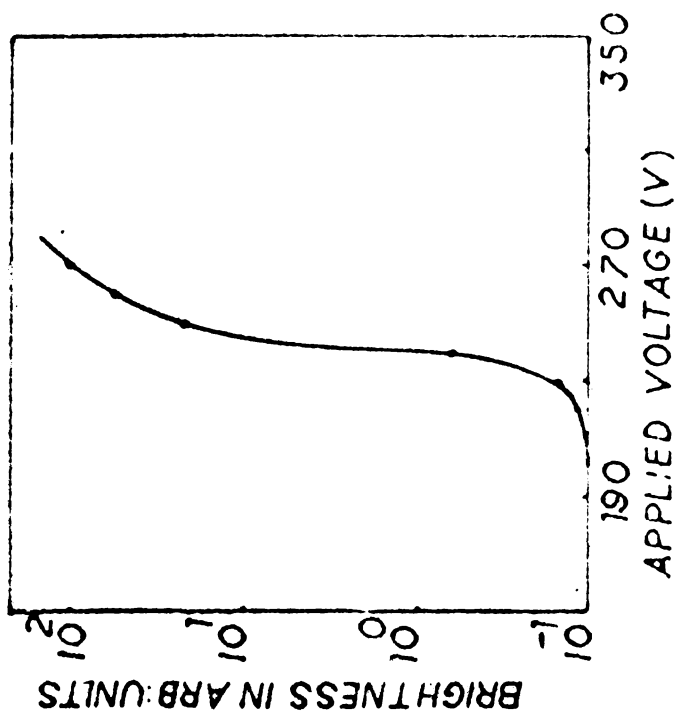


Fig. 9.3(a). B-V characteristic of MgF_2 insulator device.

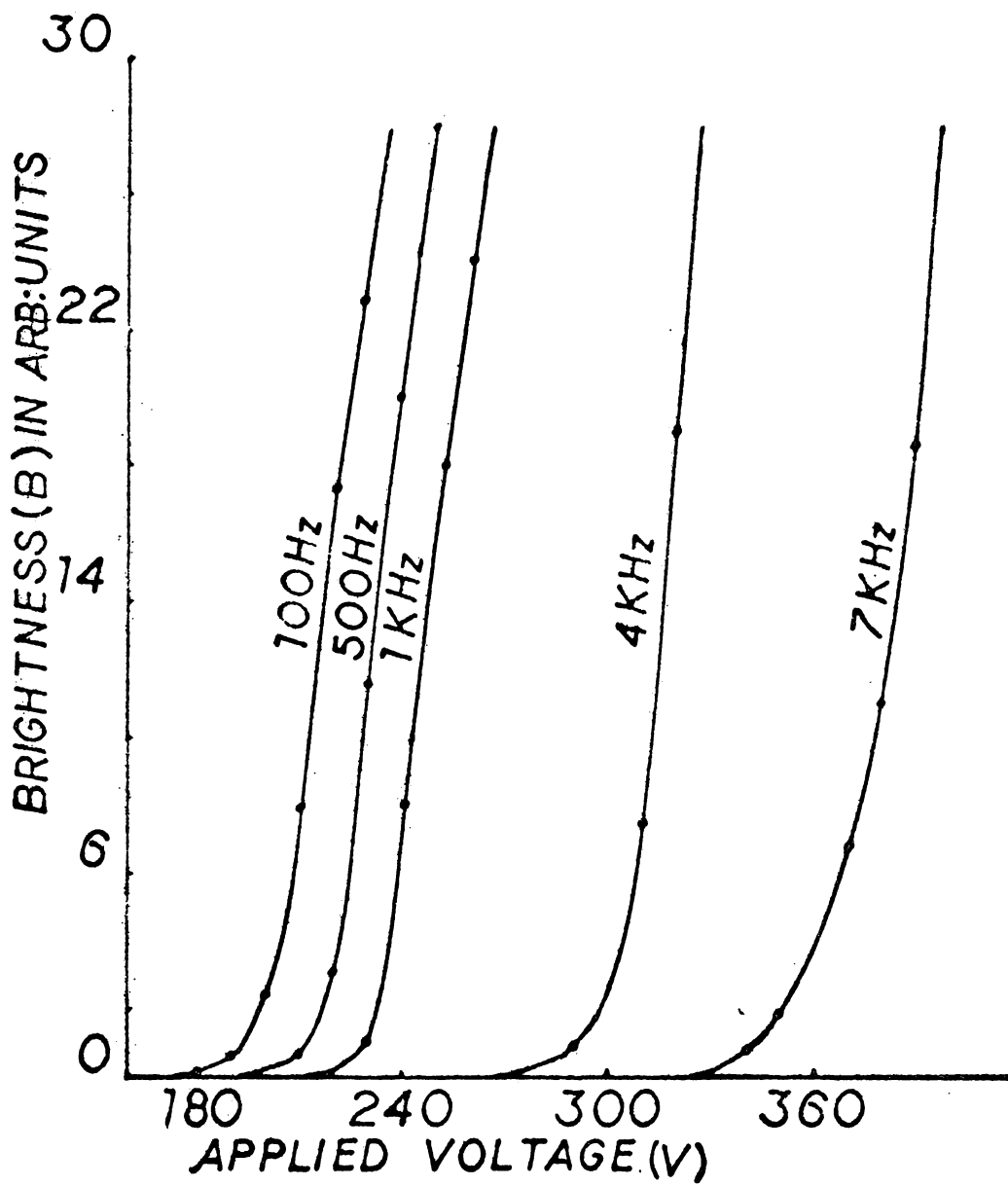


Fig.9.4. B-V characteristics of MgF₂ insulator device for different frequencies of excitation.

be seen that the higher the excitation frequency, higher is the threshold voltage. No such phenomenon has been reported so far and it is observed here for the first time in these types of ACTFEL cells. This observations can be explained as follows:

In order to understand the usual B-V characteristics in this type of devices (Fig.9.3) an equivalent circuit as shown in Fig.9.5, but without the parallel resistance R_i , is made use of [11]. In the present case, the resistance R_i is included, in the equivalent circuit parallel to the insulator layer (MgF_2) capacitance, to account for all leakage paths. From Fig.9.5 it can be seen that if V is the applied voltage and U the voltage appearing across the active layer then

$$U = \frac{Z_s(\omega)}{Z_i(\omega) + Z_s(\omega)} V \quad \dots (1)$$

Here C_i is the capacitance of the MgF_2 layers and C_3 that of the phosphor film. $Z_s(\omega)$ is the impedance of the phosphor film and $Z_i(\omega)$ that of the insulator layer. If U_{th} is the threshold voltage to be applied across the active layer for the onset of light emission and V_{th} the corresponding applied voltage. For a particular frequency of excitation we can write

$$U_{th} = \frac{Z_s(\omega)}{Z_i(\omega) + Z_s(\omega)} V_{th} \quad \dots (2)$$

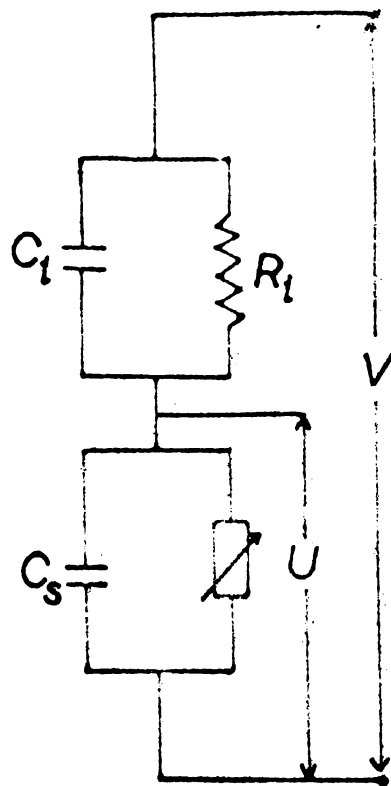


Fig.9.5. Equivalent circuit.

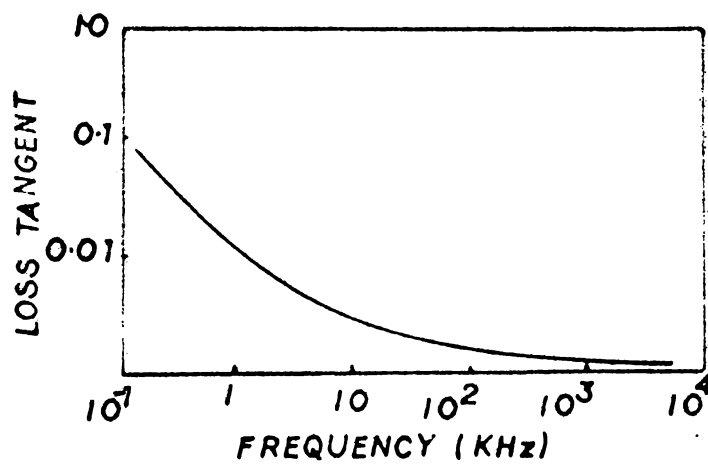


Fig.9.6. Typical frequency - $\tan \delta$ plot of MgF_2 thin film.

$$\text{But } Z_i(\omega) = \frac{R_i}{\sqrt{1 - \tan^2 \delta}} \quad \dots (3)$$

which means that the voltage drop across the insulator layer is a function of $\tan \delta$ and higher the $\tan \delta$ value the lower the $Z_i(\omega)$ value or the drop across the insulator. So for higher $\tan \delta$ value the U_{th} can be attained for a much lower applied voltage as is evident from equation (2). In case of MgF_2 its $\tan \delta$ value is a strongly dependent function of frequency and it goes on decreasing as the frequency is increased [12]. A typical plot is given in Fig.9.6. This leads to the result that by increasing the excitation frequency the $\tan \delta$ value is decreased thereby increasing the value of the applied voltage required to produce emission from ZnS:Mn. Thus one can conclude that the threshold voltage should depend on the excitation frequency and the nature of this dependence must be as shown in Fig.9.6.

9.4. Conclusion

AC thin film devices of $SnO_2-Y_2O_3-ZnS:Mn-Y_2O_3-Al$ and $SnO_2-MgF_2-ZnS:Mn-MgF_2-Al$ were successfully fabricated by EBE and thermal evaporation techniques respectively. The two types of devices have the same emission spectrum and brightness voltage characteristics. But for the MgF_2 insulator devices, the threshold voltage of emission is found to be a strongly dependent function of the frequency of the applied voltage. It is explained as due to the change of loss factor $\tan \delta$ of the MgF_2 film with frequency. Also it is observed that no annealing process is needed for the MgF_2 insulator device.

References

1. T. Inoguchi and S. Mito in Electroluminescence;
Topics in Applied Physics, Vol.17
Ed. J.I. Pankove(Springer Verlag, Berlin,1977).
2. W.E. Howard; Proc. SID, 18(1977) 119.
3. K. Okamoto, Y. Nasu and Y. Hamakawa;
IEEE Trans. ED-28 [6] 698.
4. Y. Fujita, J. Kuwata, M. Nishikawa, T. Tohda;
T. Matsuoka, A. Abe, T. Nitta; Japan Display '83.
Paper 4.1, October 3-5, Kobe Japan.
5. Yoshiro Oishi, Takatoshi Kato, Yoshihiro Hamakawa;
Japan Display '83, p 3.2, October 3-5, Kobe
Japan.
6. K.L. Chopra; Thin Film Phenomena, (McGraw Hill Book
Company, New York, 1969) 472.
7. Leon I Maissel and Reinhard Glang; Hand Book of Thin
Film Technology (McGraw Hill, New York, 1970)
16-31.
8. D. Theis, H. Venghaus, H. Oppolzer and S. Schild;
Proc. First Europ. Display Res. Conf. SID/NTG
(1981) 152.
9. H.E. Gumlich; J. Lumin. 23(1981) 73.
10. P.J. Dean; J. Lumin. 23(1981) 17.
11. R. Tornquist; J. Cryst. Growth 59(1982) 399.
12. K.L. Chopra; Thin Film Phenomena (McGraw Hill Book
Company, New York 1969) 475.

CHAPTER X

SUMMARY AND CONCLUSIONS10.1 Summary of the work

The first chapter of the thesis is a concise review on the subject of EL giving special importance to high field EL. In the initial part, the importance of II-VI semiconducting materials as the phosphors for the development of large area format display systems is brought out and then an account of the various activators and co-activators used in some important EL materials and their method of preparation is given. This is followed by a description of the various physical mechanisms involved in both high field (intrinsic) and injection electroluminescence phenomena. The second part of this chapter gives a comprehensive report of the state of art ACFEL devices along with the essential physics of memory and non memory EL devices. The empirical requirements for the preparation of ACFEL cells showing memory phenomenon are also noted.

In the second chapter, the details of the experimental setup used for the various investigations by the author are described. It contains an account of the procedure for preparation of the EL phosphors, the vacuum furnace used for their preparation, the setup for recording the spectrum of the EL emission etc. It also gives the details of a PMT.

preamplifier used for recording the spectrum of weak EL emission. Towards the end of the chapter, the method adopted to estimate the brightness of the EL cells in foot-lamberts is described.

The third chapter describes the details of a series of experiments done on ZnS:Cu,Cl phosphor with different concentration of chlorine added to the premixture. It is found that all the experimentally observed facts can be explained on the basis of a new energy level scheme which includes levels corresponding to Cu^{2+} , Cu^+ and Cl^- in the forbidden gap of ZnS. In contrast to the previous models this scheme is found to explain satisfactorily the occurrence of the red emission as well. Here this particular emission is attributed to transition from the donor (Cl^-) to the acceptor (Cu^+) centre. Another important investigation presented here is on the preparation and study of ZnS:Cu,Mn,Cl and ZnS:Cu,Dy,Cl phosphors. However, these phosphors are found to be less efficient. The EL spectrum of ZnO which is discussed at the end of the chapter gives a new ultraviolet band, in addition to the previously reported green band.

The method of preparation of an efficient CaS:Ce EL phosphor together with the detailed description of their electrical and spectral characteristics are the main topic of discussion in chapter IV. Here it is concluded that the luminescent centre giving rise to the EL emission is the Ce^{2+} ion. The brightness-frequency characteristics of

these phosphors are found to exhibit an anomalous behaviour. It is explained on the basis of the field controlled trapping and detrapping of charge carriers. Such a characteristic is observed in the case of all CaS phosphors. Another important result presented in this chapter is the quenching of the emission from Ce in the CaS:Ce,Nd phosphor. This is explained as due to the resonance radiationless energy transfer from Ce to Nd. The various emission lines and bands observed in the spectrum of this phosphor are identified. It is concluded that they are essentially due to the Nd²⁺ luminescent centres.

Chapters V and VI report the EL emission spectra of CaS:Er, CaS:Sm, CaS:Dy and CaS:Mn. The emission groups occurring in the spectra of each phosphor are identified. On the basis of a group theoretical calculation the sites of the Er and Sm luminescent centres in CaS host material are found out. An interesting observation on the EL spectra of the CaS:Dy is that its most intense band occurs as a result of a transition from an excited state to a level next to the ground state. It is speculated that this may be due to the hypersensitive nature of this transition. CaS:Mn phosphor shows a single band in its emission spectrum but it is found to be of very low intensity.

Chapter VII presents a detailed account of the fabrication of DC powder EL cells. It contains a brief discussion of the phosphor preparation, DC forming, the equivalent circuit for the DCPEL cells and the dependence

of the circuit parameters on the degradation. Here a detailed description of the preparation of ZnS:Mn and CaS:Ce, DCPEL cell and some of the experimental results obtained on CaS:Ce DCPEL cells are given.

In chapter VIII a description of the experimental setup used for the fabrication of an ACTFEL cell is given. It starts with an outline of a typical device fabrication method followed by a brief description of the various experimental setup used. It includes the fabrication details of two vacuum coating units, the evaporation system (both resistive and EBE), substrate heater and film thickness measurements. It also describes the method by which films of predetermined thickness values were deposited with the help of a quartz film thickness monitor. At the end of the chapter a detailed account of the spray pyrolysis method used for the deposition of transparent conducting electrodes of SnO₂ is given.

A concise report of the detailed experimental procedure for the fabrication of an SnO₂-MgF₂-ZnS:Mn-MgF₂-Al device by resistive heating, and an SnO₂-Y₂O₃-ZnS:Mn-Y₂O₃-Al devices by EBE technique is given in chapter IX. The latter device has the same characteristics as reported by various workers. But the former, apart from the brightness saturation at high excitation fields, shows a strong dependence of the threshold voltage (for the onset of light emission) on the frequency of the excitation.

10.2 Scope for further work

The thesis contains the procedures for preparation and studies of a number of EL phosphors. Emission spectra, B-V characteristics, B-f characteristics and brightness waves are the important aspects studied here in the case of these materials. However, many other aspects like temperature dependence of emission, time resolved spectrum etc. still remain to be investigated.

In the investigations presented here no attempt is made to find out the optimum condition for the preparation of different phosphors except in the case of CaS:Ce. The method adopted to optimise the CaS:Ce can be extended to the other phosphor systems as well. The proposed energy level scheme put forward to explain the EL emission from ZnS:Cu,Cl is formulated mainly on the basis of the emission spectra observed for phosphors containing different concentrations of chlorine and on the chemical method used for its preparation. This model can be ascertained further by studying the time resolved EL spectrum of this material. It is also possible to extend the work on ACTFEL by using insulator materials other than MgF_2 and Y_2O_3 .

It is hoped that, the studies described in the thesis have been able to shed some light on certain aspects of the phenomenon of EL. It also reports some new EL phosphor

materials which will be of interest to physicists as well as to display technologists. Obviously, there exists immense scope for further work directed towards the development of new phosphor materials and EL devices.

APPENDIX

ELECTROLUMINESCENCE OF ELECTRO-POLYMERISED CASTOR OIL AND LIQUID PARAFFIN

1. Introduction

The most widely used type of experimental electro-luminescent cell consists of the powder phosphor in the form of a thin layer dispersed in a suitable dielectric liquid. This dielectric is chosen such that at the operating voltages of the cell it does not produce luminescence. The dielectric commonly used for this purpose is castor oil. In most of the studies on powder phosphors presented in the thesis, locally available castor oil (IP grade) is made use of. But it was necessary to ascertain its suitability for the above purpose before using it in the EL cells. So a dummy EL cell was fabricated without the phosphor powder. An AC voltage of amplitude normally used to excite the EL cells was applied. It was found that at this voltages the cell does not produce any luminescence. This ensures that castor oil is suitable for normal application in the EL cells. But during testing it was found that if an excessive field was applied to the cell (~ 2 kV between the electrodes) at 1 kHz some small bright emission spots appear on the cell which is white in color. These spots gradually spread and cover the entire area in between the electrodes producing very good emission. The changes produced in the cell are permanent. It is found that the oil is converted into a solid material during this process. This evident solidification of the oil could be due

to the occurrence of electropolymerisation of the liquid during the application of intense electric field [1]. This observation prompted the author to try two more materials viz. coconut oil and liquid paraffin. The castor oil and coconut oil are esters while the liquid paraffin is a long chain hydrocarbon with the formula $\text{CH}_3-(\text{CH}_2)_n-\text{CH}_3$. Light emission under similar circumstances has been observed from transformer oil, castor oil and from paraffin by some earlier workers [3,4]. But they were not able to record the emission spectra. Here the EL emission spectra and the N_2 laser induced fluorescence spectra of electropolymerized materials and those of the pure oils are presented.

2. Fabrication of the cells and the electro-polymerisation process

The cell was fabricated by placing a thin mica sheet $\sim 100 \mu\text{m}$ thick dipped in the oil (for instance in castor oil) in between two electrodes one of which is a polished aluminium plate and the other a transparent conducting electrode. The electrodes were then pressed gently with the help of insulating clamps. The cell thus formed consists of two thin liquid layers on either side of the mica sheet. The mica insulator is essential; otherwise, on applying the field, direct arcing will take place between the electrodes which will burn the oil and also destroy the conducting transparent electrode. A sine wave voltage generator capable of delivering $\sim 2 \text{ kV}$ at 1 kHz was connected to the cell (details are described in

chapter II). A low voltage was applied initially and was slowly increased. When it reaches about 2 kV small bright spots begin to appear on the cell. On further increasing the voltage number of spots appearing is found to increase. If the voltage level is maintained these bright spots spread slowly and cover the entire area in between the two electrodes. If the power is now switched off and started again the light emission appears from the entire area even for a low applied voltage. As voltage is increased further, brightness also increases. Repeated application of the field does not produce any change in this behaviour of the cell. This indicates that the first application of very intense electric field has produced some irreversible change in the cell which makes it luminescent. Another cell with a polypropylene sheet as the insulator instead of the mica sheet was prepared. The same effects were observed which indicate that the electroforming and light emission are actually taking place in the oil film. On the mica sheet and on the electrode surface a thin layer of a white solid material is deposited. This deposit was scraped out and its IR and UV spectra were recorded and compared with that of the original oils. No new information was available regarding the electrical forming process occurring in the cell. The polymerized and un-polymerized materials showed same characteristic peaks in the IR spectra. Since spectra of the deposited solid mass have the same features as the spectra of the original oil, it can be concluded that the oil has undergone a

polymerisation process thereby increasing its molecular weight by several fold. The UV spectrum has not provided any useful information either. The earlier workers believed that the emission may be due to some impurities present in the oil which act as the luminescent centres [3]. This can be proved only by using very sensitive analytical tools like mass spectrometry or neutron activation analysis. We have however used oils supplied by different manufacturers and all of them showed the same effect which points that the oil itself is responsible for emission.

The EL spectra of these cells were recorded with the setup described in chapter II. The spectrum in the case of castor oil consists of a broad band on which a series of sharp lines were superposed (Fig.A.1). These lines could be grouped into four series and each series was found to be separated by 1030 cm^{-1} and lines in each group are separated by 1430 cm^{-1} . So it follows that these emission lines are due to transitions occurring between vibrational levels in the excited and ground state of a molecular group acting as the luminescent centres in the electropolymerised material. The emission wave lengths and the probable level transitions giving rise to these emissions are given in Table 1.

The result of the above analysis alone is not sufficient to identify the luminescent centres involved in the EL emission. It is reported that the EL emission from organic polymers are due to the functional groups acting as

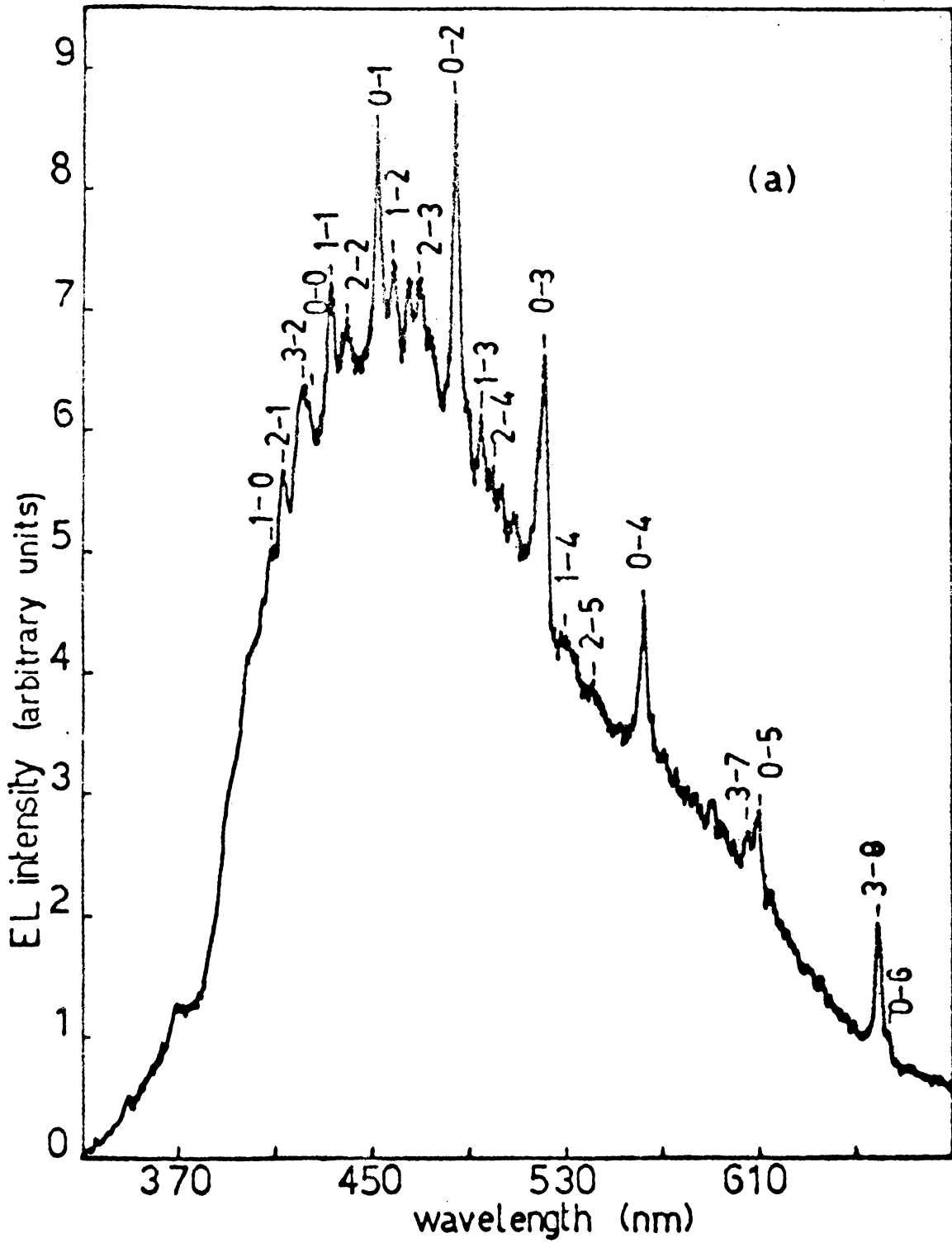


Fig.A.1. EL spectrum of electro-polymerised castor oil

luminescent centres [5]. If it is valid here also then, another material having the same functional group should show the same spectrum. So an attempt has been made to produce EL in coconut oil which is also a long chain molecule having an ester group similar to castor oil. As expected, the EL spectrum of this oil is found to give the same type of emission spectrum as observed in the case of electro polymerised castor oil which is an indication that some feature common to both of them are responsible for the emission. To pursue the matter further, another material which does not contain the ester group is tried, namely, liquid paraffin which has the formula $[\text{CH}_3-(\text{CH}_2)_n-\text{CH}_3]$.

The same procedure adopted for the preparation of electropolymerised castor oil is used for the preparation of the electropolymerised liquid paraffin also. But in this case the forming takes place at a lower voltage and the emission spots are green in color. These spots then spread in a spectacular manner. It is found that, if the applied field is maintained the bright spots initially formed spread but the boundaries of these emitting regions continue to emit green light though the interior begins to emit yellow light. If the field is applied continuously for a few hours the entire area becomes covered by the yellow glow except for some green emitting spots. If the power is switched off and switched on again after some time (~ 30 minutes) it is found that some of the initially formed regions show further forming. This repeated application of the field was continued

till no more forming occurs. If the mica sheet is taken out from the cell it can be seen that a thin layer of an yellow solid material is deposited on the insulating sheet. The IR spectrum of this solid mass was recorded. It shows the same characteristics as those observed in the case of liquid paraffin. Since the solidification of the liquid can be taken as an indication that its molecular weight is increased, it can be assumed that for the present case also an electropolymerisation process has taken place.

The EL spectra of the electropolymerized liquid paraffin cell is shown in Fig.A.2. It consists of two broad bands with the maxima at 560 nm and 480 nm without any significant sharp line features. This observation actually supports the earlier assumption that the functional groups are responsible for the emission **lines** in the esters.

It is found that during the first application of the field a good amount of gas was found to evolve from the cell. So there are good chances for some of the gases to be trapped in the cell and subsequently excited on the application of the field. To check this, the cell was introduced into a vacuum chamber and evacuated to a pressure of 2×10^{-5} torr and was then excited. The cell was found to work for hours together in this pressure. This experiment was done for both of the castor oil and liquid paraffin cells

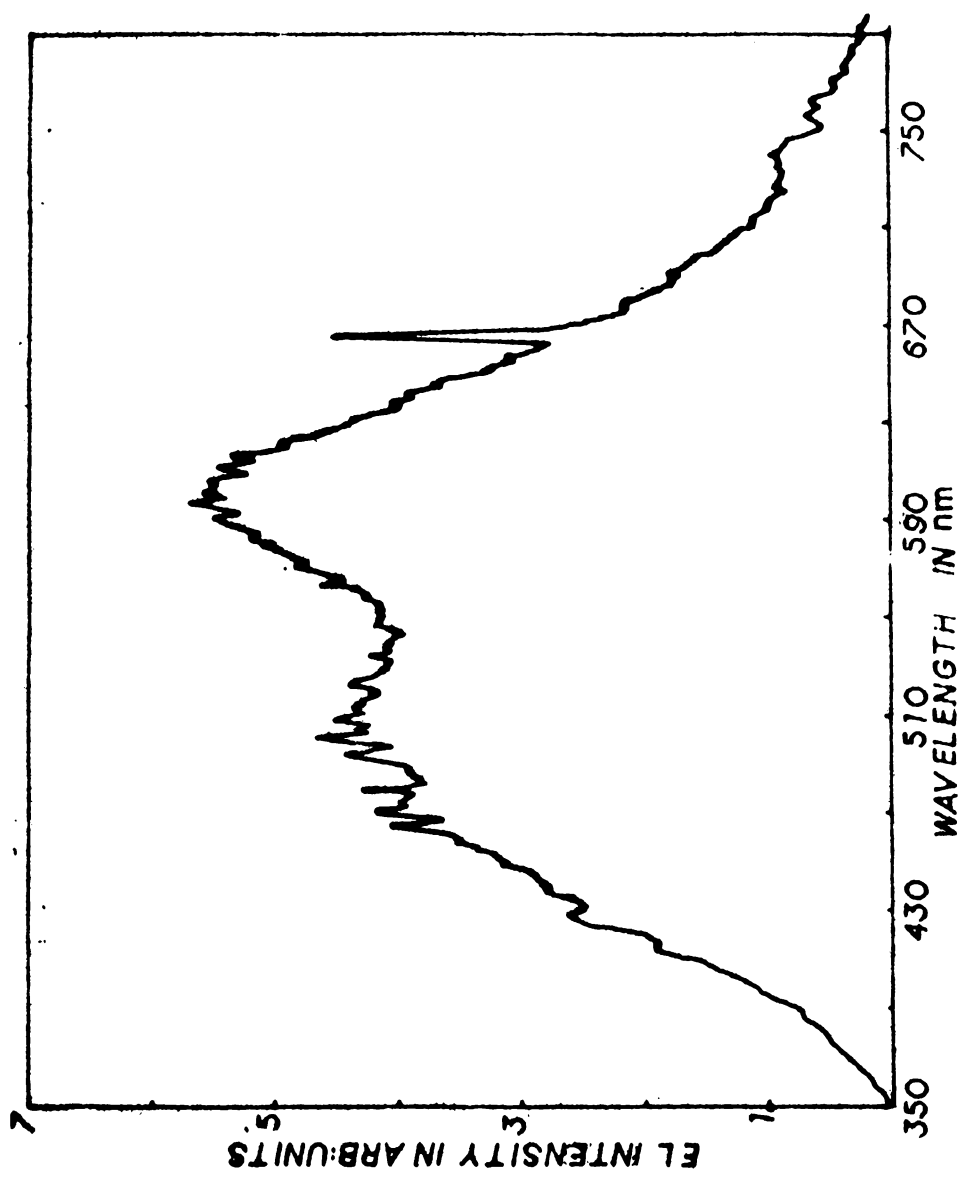


Fig. .2. EL spectrum of electro-polymerised liquid paraffin.

The PL spectra of the polymerised and unpolymerised samples were recorded by exciting them with pulsed nitrogen laser of peak power 150 KW. The detection and recording setup is as described earlier. The spectra of the polymerised and unpolymerised castor oil are shown in Fig.A.3 curves A and B. It can be seen that the spectrum of the oil consists of two bands at 450 nm and 485 nm. But the polymerised specimen is having a single band emission spectrum with the maximum at 450 nm. The non gaussian nature of the spectra indicates that the band at 485 nm still exists but has a reduced intensity. The fluorescence spectrum of liquid paraffin Fig.A.4 curve A consists of smaller peaks with 50 nm half width and occurs respectively at 460, 435, 360 and 355 nm. But the polymer spectrum Fig.A.4 curve B has only one broad band with the maximum at 450 nm. From these spectra it can be seen that there are notable difference in the fluorescence spectrum of the oil and polymerised products which suggests that the electric field has caused some substantial changes in the original material. But this data is insufficient to give information on the exact nature of the changes that have taken place.

The brightness wave of the electropolymerized castor oil consists of two brightness peaks per cycle but slightly asymmetric in nature, which may be due to the asymmetric structure of the cell. These type of brightness waves are observed for other organic EL materials as well [6].

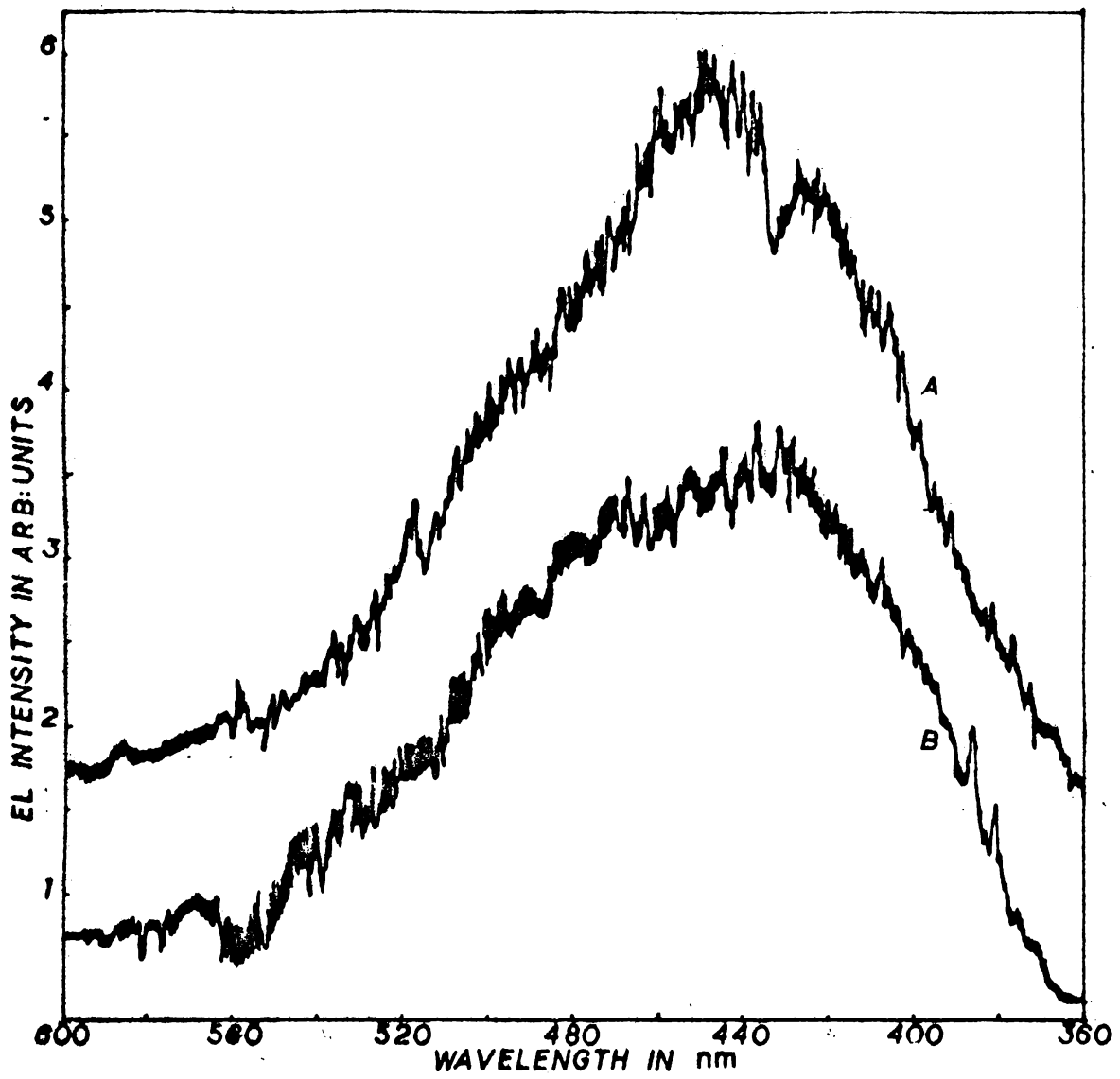


Fig.A.3. Curve A, N_2 laser excited fluorescence spectrum of castor oil. Curve B, N_2 laser excited fluorescence spectrum of electro-polymerised castor oil.

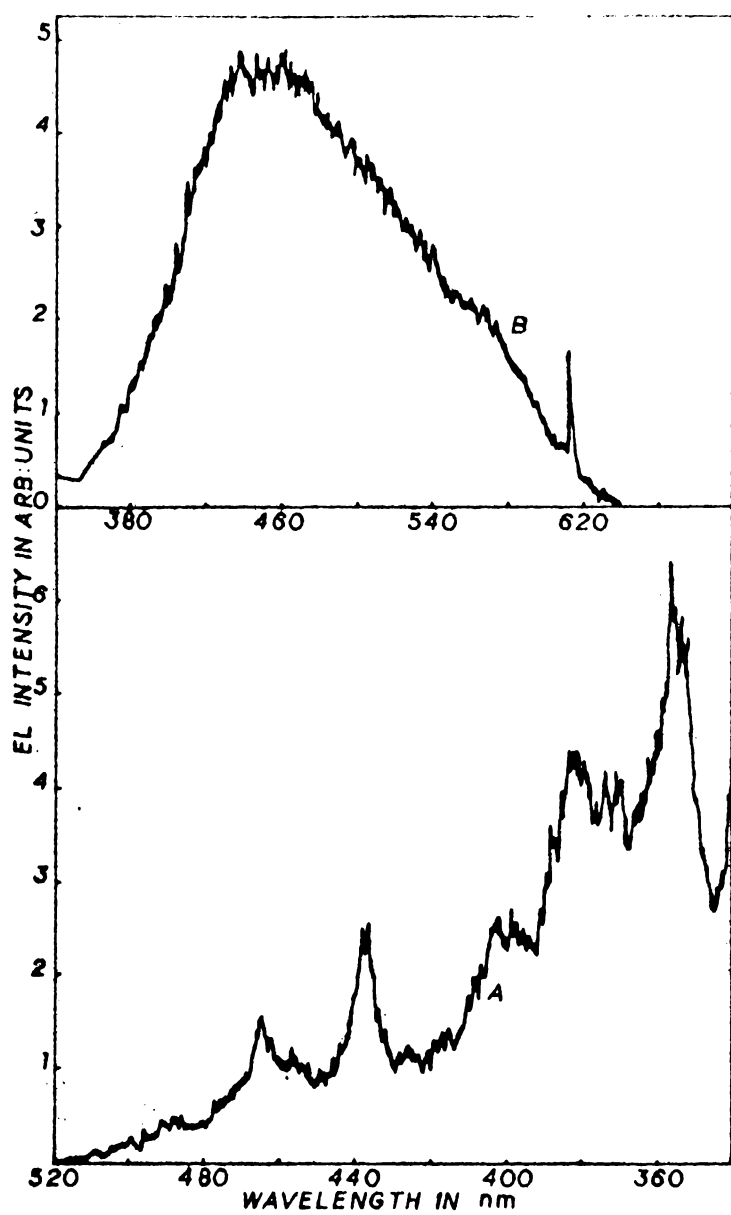


Fig. A.4. Curve A, N_2 laser excited fluorescence spectrum of liquid paraffin. Curve B, N_2 laser excited fluorescence of electro-polymerised liquid paraffin.

In order to get some insight into the excitation mechanism, the brightness-voltage characteristics were studied. A plot of the $\log B \propto \frac{1}{V}$ for different excitation frequencies are shown in Fig.A.5. At low voltage regions the plot shows very large rate of increase of brightness with voltage. This is because at low voltage, the emitting area is very small. On increasing the applied voltage the brightness as well as the emitting area increases. But it can be seen from the figure that after attaining a certain voltage level the brightness steadily increases with the applied voltage and obeys the relation,

$$B = A \exp\left(\frac{-b}{V}\right) \quad \dots (1)$$

where B is the brightness, V the voltage and A and b are constants. This indicates that the EL process involves a carrier acceleration and collision process.

The log-log plot of B-f characteristics is found to be a straight line which indicates that

$$B = m f^n \quad \dots (2)$$

where n and m are constants which can be estimated from the B-f plot. Equations (1) and (2) can be combined and written as

$$B = B_0 f^n \exp\left(\frac{-b}{V}\right)$$

The cells thus formed have been operated for days together by plugging it into the mains. They did not show any substantial decrease in intensity or deterioration of any sort.

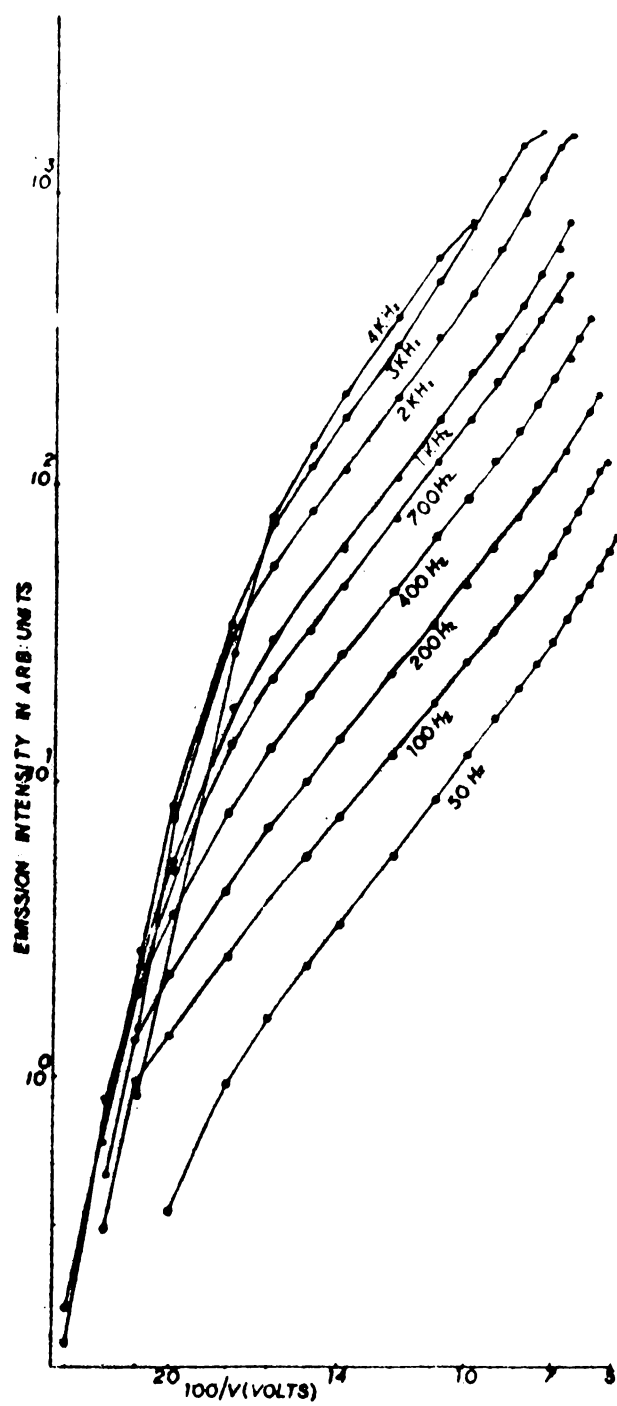


Fig.A.5. $\log B$ vs $\frac{1}{V}$ plot of an electro-polymerised castor oil EL cell.

3. Conclusion

Electroluminescent cells from castor oil and liquid paraffin have been prepared by an electroforming process. It is assumed that during the electroforming the oils get polymerised. The EL spectrum of the cell thus obtained from castor oil is found to exhibit a large number of sharp lines which can be grouped into four series. The N_2 laser excited fluorescence spectrum of the polymerised materials and that of the pure liquids are also presented.

References

1. Manuel M. Baizer Ed. Organic Electro Chemistry (Marcel Dekken Inc. New York)
2. M.I. Eidelberg; Optics and Spectrosc. 14[2] (1963) 155.
3. T.W. Dakin and D. Berg; Nature 184(1954) 120.
4. H.L. Armstrong and J. Hancoch; Can. J. Phys. 42[4] (1964) 824.
5. W.A. Hartman and H.L. Armstrong; J. Appl. Phys. 38[5] (1967) 2393.
6. A. Bernanose; Brit. J. of Appl. Phys. Suppl. 4(1955) 54.

